# AN OVERVIEW OF JOINT DETERIORATION IN CONCRETE PAVEMENT

Mechanisms, Solution Properties, and Sealers

Wesley Jones, Yaghoob Farnam, Paul Imbrock, Jeffrey Spiro, Chiara Villani, Mike Golias, Jan Olek, and W. Jason Weiss

PURDUE UNIVERSITY

INDIANA DEPARTMENT OF TRANSPORTATION

JOINT TRANSPORTATION RESEARCH PROGRAM — Discovery with Delivery — Since 1937 — JTRP

National Concrete Pavement Technology Center — CP Tech Center

AN OVERVIEW OF JOINT DETERIORATION IN CONCRETE PAVEMENT

Mechanisms, Solution Properties, and Sealers

Wesley Jones, Yaghoob Farnam, Paul Imbrock, Jeffrey Spiro, Chiara Villani, Mike Golias, Jan Olek, and W. Jason Weiss

AUTHORS

Wesley Jones
Graduate Research Assistant
Lyles School of Civil Engineering, Purdue University

Yaghoob Farnam
Graduate Research Assistant
LylesSchool of Civil Engineering, Purdue University

Paul Imbrock
Graduate Research Assistant
LylesSchool of Civil Engineering, Purdue University

Jeffrey Spiro
Graduate Research Assistant
LylesSchool of Civil Engineering, Purdue University

Chiara Villani
Graduate Research Assistant
LylesSchool of Civil Engineering, Purdue University

Mike Golias
Graduate Research Assistant
LylesSchool of Civil Engineering, Purdue University

Jan Olek, PhD, PE
Professor of Civil Engineering
Director of the North Central Superpave Center
Lyles School of Civil Engineering, Purdue University

W. Jason Weiss, PhD
Jack and Kay Hockema Professor of Civil Engineering
Director of the Pankow Materials Laboratory
Lyles School of Civil Engineering, Purdue University
(765) 494-2215
wjweiss@purdue.edu
Corresponding Author

NOTICE

This work was done examining long term joint deterioration in jointed plain concrete pavement where salt may be applied and as such it may not be applicable to other deterioration that occurs in concrete.

EXECUTIVE SUMMARY

AN OVERVIEW OF JOINT DETERIORATION IN CONCRETE PAVEMENT: MECHANISMS, SOLUTION PROPERTIES, AND SEALERS

Concrete pavements represent a large portion of the transportation infrastructure. While the vast majority of concrete pavements provide excellent long-term performance, a portion of these pavements have recently shown premature joint deterioration. Substantial interest has developed in understanding why premature joint deterioration is being observed in jointed portland cement concrete pavements (PCCP). While some have attributed this damage to insufficient air void systems, poor mixture design, or chemical reaction between the salt and the paste, it is the hypothesis of this work that a component of this damage can also be attributed to fluid absorption at the joints.

This report begins by discussing the importance of the level of concrete saturation on freeze-thaw damage. It was determined that damage can occur in samples having a degree of saturation higher than some critical value (approximately 86%) after even one freezing cycle. When deicing salts are used, the freezing temperature is depressed; however, additional damage is observed as compared to just water. Additional damage appears to occur on thawing for systems with higher salt concentrations, presumably due to the phase change in the hydrohalite.

Second, this report describes the influence of deicing salt solutions on drying and wetting of concrete. The presence of deicing salts alters the viscosity, surface tension, and activity of the liquid. Models were presented for the solution properties as a function of temperature, as well as for sorption and drying. Samples containing deicing salts can be expected to have higher degree of saturation. This has practical implication in highway concrete, as the sample containing deicing salt solutions will have a higher degree of saturation and will remain saturated for a longer time.

Third, the report presents the results of laboratory work performed on concrete core samples collected from several locations around the state of Indiana. The samples were collected from both distressed and un-distressed concrete pavement joints as well as from the middle of the panels (for comparative purposes) in an effort to determine the underlying causes of the observed joint distresses.

Fourth, the report discusses soy methyl esters polystyrene blends (SME-PS) as a potential method to seal the concrete surface and to extend the service life of concrete pavements by limiting the ingress of salt solutions. SME-PS has been found to reduce salt ingress and freeze thaw damage. The report also discusses field application of the SME-PS blends for field investigation.

Finally, the report discusses the development of a test to assess chloride solution ingress during temperature cycling. The aim of this work is to provide background on some aspects that can lead to joint deterioration and to provide the pavement community alternatives on how sealers and deicers may be able to be used more efficiently to reduce joint damage. While still preliminary, this approach has the ability to shed light on how these sealers may influence the performance at joints, especially when the temperature is cycled.

CONTENTS

LIST OF TABLES

LIST OF FIGURES

The work performed in this project was also published in the journal papers:

1. Y. Farnam, D. Bentz, A. Sakulich, D. Flynn, and J. Weiss. Measuring Freeze and Thaw Damage in Mortars Containing Deicing Salt Using a Low-Temperature Longitudinal Guarded Comparative Calorimeter and Acoustic Emission, *Advances in Civil Engineering Materials (ASTM),* Vol. 3, No. 1, 2014, pp. 1–22, doi: 10.1520/ACEM20130095.
2. Golias, M. The Use of Soy Methyl Ester-Polystyrene Sealants and Internal Curing to Enhance Concrete Durability. Master's thesis, Purdue University, West Lafayette, Indiana, 2010.
3. Golias, M., J. Castro, A. Peled, T. Nantung, B. Tao, and J. Weiss. Can Soy Methyl Esters Improve Concrete Pavement Joint Durability? In *Transportation Research Record: Journal of the Transportation Research Board*, No. 2290, Transportation Research Board of the National Academies, Washington, D.C., 2012, pp. 60–68.
4. Li, W., M. Pour-Ghaz, J. Castro Sepúlveda, and W. J. Weiss. Water Absorption and Critical Degree of Saturation Relating to Freeze-Thaw Damage in Concrete Pavement Joints. *Journal of Materials in Civil Engineering*, Vol. 24, 2012, pp. 299–307.
5. Villani, C., R. Spragg, M. Pour-Ghaz, and W. J. Weiss. The Influence of Pore Solutions Properties on Drying in Cementitious Materials. *Journal of the American Ceramic Society*, Vol. 97, No. 2, 2014, pp. 386–393. doi 10.1111/jace.12604.

1. INTRODUCTION AND OVERVIEW

Concrete pavements represent a large portion of the transportation infrastructure. While many of these pavements provide excellent long-term performance, a portion of pavements in the Midwestern United States have recently shown premature joint deterioration (*1– 11*). This joint deterioration is problematic because it compromises the performance and potential service life of an otherwise healthy pavement.

Figure 1.1 provides photographs showing the typical pavement joint damage that is being discussed in this report (*12,13*). This type of damage is frequently seen as one of two types of damage. The first type of damage consists of small cracks that progressively spall off; these cracks are parallel to the saw-cut face at fractions of an inch from the saw cut face. The second type of damage consists of the development of cracking parallel to the joint or spalling; the damage begins with a hollowed out region at the bottom of the saw cut, resulting in a crack to the surface of pavement that is typically four to six inches from the edge of the joint. Unfortunately, damage is not frequently observed at the surface of the pavement until a significant amount of damage has occurred inside the joint. During field inspections it has been observed that where the joints are damaged, the sealant is damaged and the joint contains a significant amount of standing water (or fluid), as shown in Figure 1.2. The pavements in Figure 1.2 were examined in 2005. The material in the pavement exhibited a complete destruction of the matrix while the aggregate remained intact. It should be noted that it had not rained for nearly two weeks; however, fluid was standing in the joint. It is important to note that while this damage is more likely to occur in pavements with poor air entrainment, damage occurs in both poorly air entrained and properly air entrained concrete.

Figure 1.3 illustrates a proposed series of mechanisms that appear to be partially responsible for this damage (*1*). In Figure 1.3 (a) D-1 construction joint is illustrated that is typical of that used by the Indiana DOT. The joint is created by saw-cutting the pavement shortly after placement with a single cut that is approximately 1/3 the depth of the pavement. The intention of this saw-cut is to provide stress relief, which can allow cracks to form at these locations. A

Figure 1.1 Field observation showing damage in pavement joints.

Figure 1.2 Field observation showing damage in pavement joints containing water.

previous report provided details on how to best place and time these saw-cuts to minimize the potential for random cracking (*14*). The pavement would then be expected to crack at the joint (though this crack does not always occur, as explained in the following paragraphs). After several days (to weeks) the saw cut is cut again to widen the cut, which provides a notch at the top of the joint for the placement of backer rod and a joint sealant. This second cut also allows minor raveling to be removed and attempts to provide a more uniform joint width since some of the opening has already occurred. The joints are then cleaned, dried, and a non-absorptive backer rod is placed in the joint and a joint sealant is then placed. If ideal, this constructed sealed joint will keep water and deicing salt out of joints; however, invariably the sealer pulls away from one of the walls or cracks as shown in Figure 1.3 (b). It is proposed that this detachment allows water and deicing salt to enter the joint and be absorbed by the faces of the saw cut concrete. While the fluid enters the hollow section created by the saw-cuts, the fluid likely drains through the crack at the base of the saw cut into the open graded base. This will increase the degree of saturation along the walls of the saw-cut and along the walls of the crack. This changes dramatically, however, (i.e., it will not occur) if the crack does not form below the saw-cut (as shown in Figure 1.3 (c)). Without a crack, the fluid pools in the joint is absorbed by the concrete and becomes increasingly concentrated (with respect to deicing salt) over time. This can develop a zone with a high degree of saturation. This high level of saturation can result in freezing damage and/or in chemical reaction in some systems (e.g., the formation of Friedel salt that can infill air voids (*5,7–11*), the production of oxychloride (*15,16*), or the replacement of calcium in calcium silicate hydrate (*3*)). While this mechanism would explain the 'soft zone' frequently observed at the base of the saw-cut, an alternative damage pattern is observed with the side of the saw-cut flaking off in layers that are fractions of an inch thick. At the current time it seems that this may be due in part to freezing and thawing or due to salt crystallization pressure (*17*); however, additional work is needed to examine this type of failure.

The previous section discussed how fluid can sit in the saw-cut if the joint sealant fails and the concrete pavement has not cracked. It has been hypothesized (*2*)
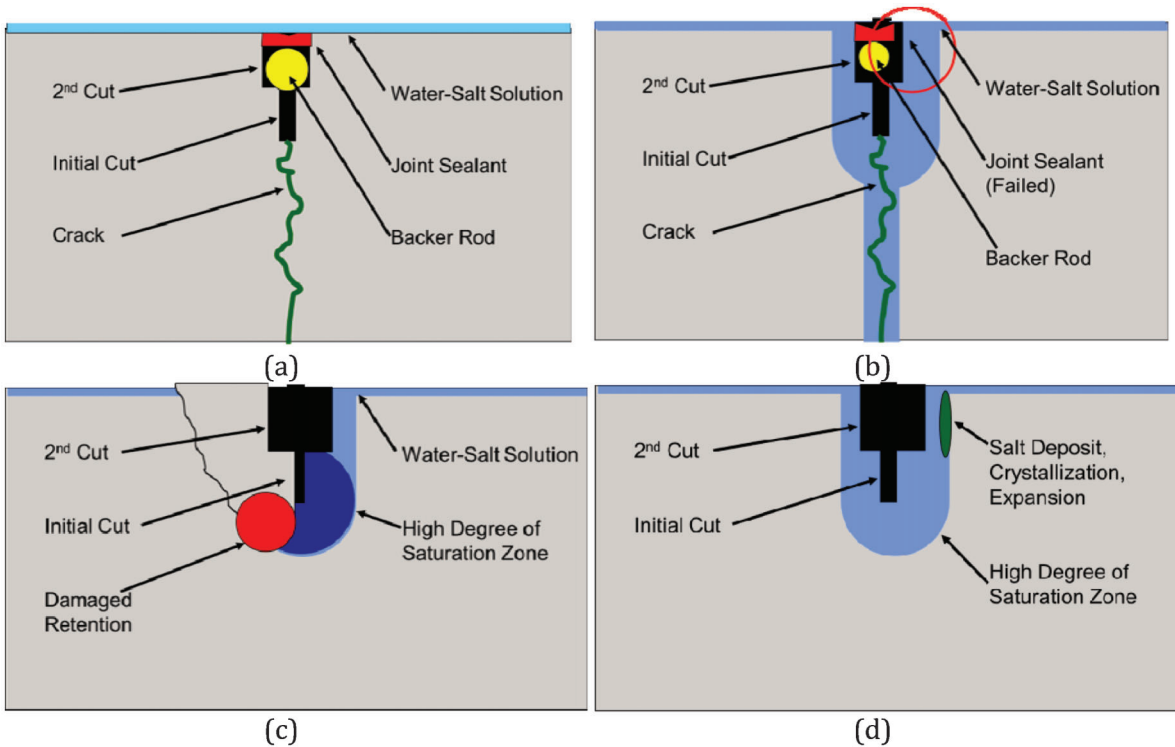
Figure 1.3 Potential degradation hypothesis: (a) an ideal joint; (b) a joint with damaged joint sealant but cracked; (c) a joint with damaged joint sealant that is uncracked; and (d) a joint illustrating potential salt crystallization locations.

that the joints may be less likely to crack if pavements gain strength more rapidly, if the joints become more closely spaced, or if the pavements are thicker. In all these cases, the factors that drive the cracking are reduced. The width of the cracks that form are controlled by the presence and amount of steel tie bars in the longitudinal joint that may hold sections together while the width of the transverse joints is dependent on the number of joints that crack and the alignment of the dowel bars. It should also be noted that if the joints are sawed late micro-cracking can occur at the base of the saw-cut and this micro-cracking (if present) would enable faster water absorption, resulting in a higher degree of saturation (*18*).

It is important in this discussion to remember that the fluid in the joint is not water. It is a solution that contains deicing salts since deicing salts are used to depress the freezing point of the water on the concrete surface. Although the addition of deicing salts on the surface of concrete elements are effective for melting the ice and increasing the safety of infrastructure, it may also be partially responsible for the issues that develop at the joints in the pavement. When concrete that contains a deicing salt is exposed to freezing and thawing, a variety of complex damage mechanisms occur (*17,19–25*). Ice can form inside the concrete pore structure (*24*); osmotic pressure can develop due to partial freezing of solutions in capillaries (*25*); and large-scale migration of unfrozen water from small pores to large cavities filled by frozen water (*21*) and crystallization of salt can occur.

For example, Figure 1.4 illustrates the behavior of salts under only drying and wetting and it can be noticed that even in cases where freezing may not be occurring, damage can develop at the joint. At the current time this appears to be consistent with salt crystallization during drying and wetting or formation of an alternative phase (*16*); however, this mechanism has not been studied in great detail for pavement joints.

It has been proposed (*27,28*) that one way to reduce the increase in the degree of saturation or the ingress of chloride ions is to seal the faces of the cut concrete surface to help repel the fluid that may sit in the joints. While the concept sounds positive, there are some results that suggest that sealers may not be effective to reduce damage (*29*). As a result, field trials may be useful to examine if sealers may have potential to improve joint durability. If sealers are a positive
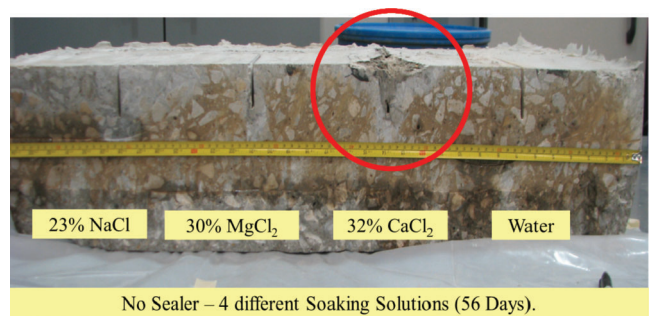
Figure 1.4 Damage development due to drying and wetting with deicing salts.

approach, guidelines would be needed for their use as well as test methods that may evaluate these materials.

This report was developed as a part of a pooled fund (TPF 244) study conducted by the National Concrete Consortium for concrete pavements. There are several publications that contain additional details on the experiments performed; however, many of these details are not included in this document to assist users by providing a document that is shorter and less burdened by testing details. This report has five distinct sections: First, it will discuss the working hypothesis the authors have used to discuss some of the important aspects of freezing damage in concrete with and without deicing salts (12,16,30). Second, the work discusses how salts will alter the physical properties of the solution and how this influences drying and wetting (31,32). Third, results of field studies are presented to provide observations from the field concrete (11). Fourth, the work discusses a potential concrete surface treatment that may help reducing water/salt ingress with the hypothesis that reducing ion ingress can reduce damage (27,28). Fifth, the work discusses a version of the sorption test that is being developed to evaluate sorption with and without thermal changes.

2. MECHANISMS OF FREEZE-THAW DAMAGE

2.1 Effect of Critical Degree of Saturation on Freeze-Thaw Damage

Concrete is susceptible to freeze-thaw damage when it is sufficiently wet (33–35). The degree of saturation (S) is a term that can be used to describe this wetness with a certain level of precision. The degree of saturation can be defined as the ratio of the volume of absorbed water to the total volume of water that can be absorbed by concrete (i.e., total porosity). It has been suggested that there is a critical degree of saturation (S_{cr}) beyond which freeze-thaw damage can begin to initiate. For degrees of saturation below the critical degree of saturation, freeze-thaw damage is not observed to occur even after a large number of freeze-thaw cycles (33–40).

2.1.1 Materials, Mixture Proportions, Sample Preparation and Sample Conditioning

Mortar mixtures have been prepared that are similar to those used in concrete pavements. They have been developed with an ordinary type I portland cement, a water to cement ration of 0.45, and an aggregate volume of 75%. The mixtures were designed to have different air contents (13 and 31% air by volume as measured in paste which would correspond to an approximate air content 4 and 9% by paving concrete volume). Mixing was performed in accordance with ASTM C192-06 (41) and prisms (25 mm × 25 mm × 125 mm) were used to evaluate the freeze-thaw damage.

The prismatic specimens were prepared to have different degrees of saturation before freeze-thaw testing. The specimens were oven dried at 105°C and then placed in desiccators and vacuumed. This emptied the fluid from the pores. After the pores were emptied, water was introduced into the desiccators to saturate the concrete (i.e., 100% degree of saturation). The degree of saturation was reduced for some specimens (i.e., 0.96, 0.92, 0.90, 0.86, 0.82, and 0.78) by short periods of drying at 23 ± 1°C and 50 ± 2% RH. After drying, all the specimens were sealed in plastic bags for a minimum of 3 days to allow moisture to redistribute before freezing and thawing testing.

2.1.2 Testing Procedure

The term acoustic emission (AE) event refers to sound waves generated when a material undergoes cracking. AE can be performed in either a passive or active mode. In the passive mode, AE transducers are attached to samples to capture acoustic waves generated by the formation of cracks during the test. In the active mode, coupled transducers are attached at a known distance from one another on the surface of the samples. One of the coupled transducers generates known pulses and the other transducers record the sent pulses. The changes in pulse properties and its speed through the sample during the experiment indicate damage occurring in the sample.

Figure 2.1 shows the procedure used for preparing the specimens for acoustic emission (AE) testing during freeze-thaw cycles. After saturating the specimens they were wrapped with a thin plastic sheet and then sealed with a loose fitting "heat shrink wrap" to further protect the specimens against moisture exchange with surroundings (prevent them from absorbing or releasing water during the freeze-thaw process keeping the degree of saturation constant). The AE sensors (transducers) were attached on the two ends with a thin layer of vacuum grease. All the specimens were placed on a suspended base in testing to minimize noise/vibration transmission from surrounding environment (Figure 2.1(d)). Each day, one cycle of freezing and thawing was applied. The temperature was controlled to vary from 10 ± 1°C to -18 ± 1°C. The rate of the temperature change was 14°C/h resulting in a 2-h transition period and two 10-h periods at 10 ± 1°C and -18 ± 1°C, respectively.

2.1.3 Results and Discussion

Figure 2.2 (a) and (b) shows the amplitude of the acoustic events as a function of time for a specimen with 96% degree of saturation and 13% air content (in the mortar) during first and second freezing cycle. This figure also shows the temperature at the center of the mortar specimen and the AE events that have occurred. A cluster of AE events is shown in Figure 2.2 (a) using the green ellipsoid during first cycle. This cluster of data is not seen during the second cycle in Figure 2.2 (b). These events can be attributed to micro-cracking of the specimen because of the thermal loading, which may be a result of temperature gradient or a result of thermal
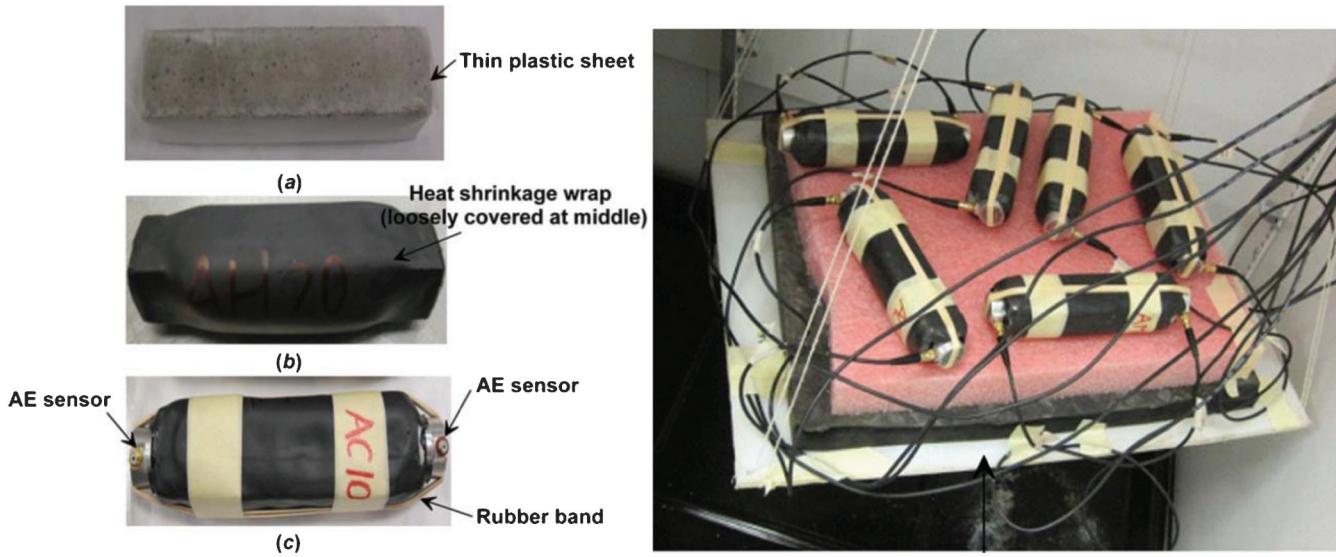
Figure 2.1 Left: preparation of specimens for AE testing during freeze-thaw cycle, and right: specimens placed on a suspended base to eliminate vibration and noise from surrounding environment (inside of freeze-thaw chamber) (*33*).
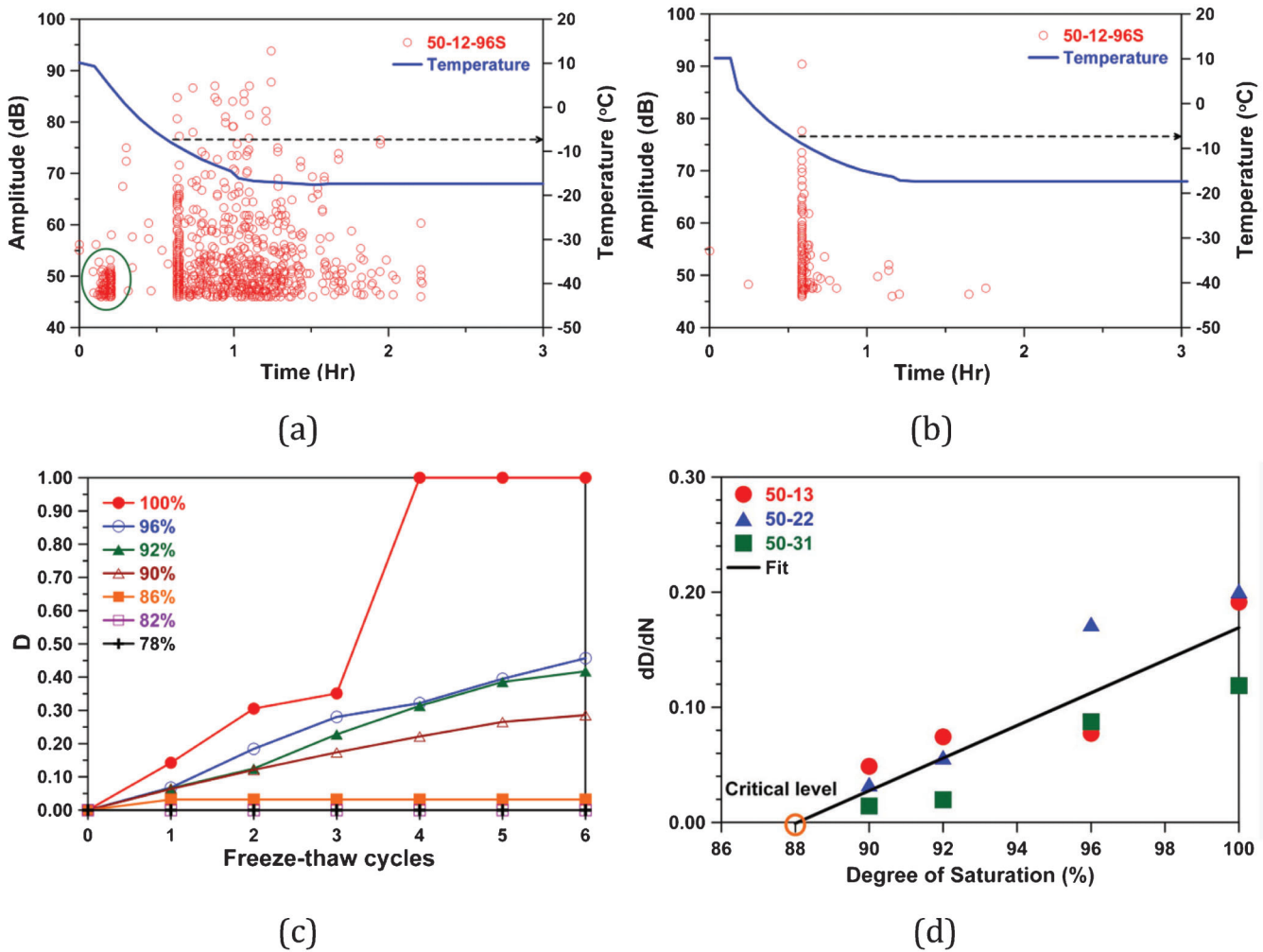
Figure 2.2 (a) Amplitude distribution for the first freeze-thaw cycle; (b) the amplitude distribution during the second freeze-thaw cycle; (c) decrease of the relative dynamic elastic modulus with freeze/thaw cycles of the specimen with 13% air content by volume of the paste; and (d) rate of decrease of relative dynamic elastic modulus with degree of saturation for different air content by volume of paste (*33*).

expansion coefficient mismatch between the paste and aggregate (*33*). During the second cooling and heating cycle, the damage attributed to thermal loading does not occur since the cracking due to COTE mismatch occurred on the first temperature cycle (*42*). Figure 2.2 (a) and (b) shows that the acoustic events begin to increase dramatically after the temperature drops below -8°C in both cycles. The damage at the point (below -8°C) is likely attributed to formation of ice and cracking inside the specimen due to pore confinement and dissolved ions in pore solution (*35,43*).

The relative dynamic elastic modulus is frequently used as an index to evaluate the extent of damage (*33*). The velocity of wave transmitting was used to determine the relative elastic modulus, (i.e., Et/E$_o$) and a damage parameter (D) using Equation 2.1.

$$D = 1 - \frac{E_t}{E_o} = 1 - \left(\frac{V_t}{V_o}\right)^2 \qquad (2.1)$$

where E_o and V_o are dynamic elastic modulus and average pulse velocity, respectively, before a freeze-thaw test; and E_t and V_t are the dynamic elastic modulus and average pulse velocity, respectively, after each freeze-thaw cycle. Figure 2.2 (c) illustrates the damage index with increasing cycles of freezing and thawing. The damage initiates during the first cycle when the degree of saturation is above 86~88%. The specimens with lower degree of saturation do not show damage while specimens with a higher degree of saturation show rapid deterioration. The saturated specimens (S = 100%) cannot sustain more than three cycles before complete failure occurs. Figure 2.2 (d) shows the rate of damage (dD) development per freeze/thaw cycle (dN) (as determined by the slope of Figure 2.2 (c)) for specimens with different degrees of saturation.

A critical degree of saturation occurs at approximately 86–88% for this mixture and appears to be independent of the air content. This means that regardless of the quantity and quality of the air, a specimen with a degree of saturation that is higher than the critical degree of saturation cannot even sustain a single freezing cycle without accumulating a significant amount of damage (*12,34,37*) as shown in Figure 2.2(d). The critical degree of saturation may however depend on the quality of air distribution and the volume of the air. The quality of the air system is related to the critical flow distance while the quantity of the air voids (volume of air) is related to the critical degree of saturation.

2.2 Effect of Air Entrainment on Water Absorption in Air Entrained Concrete

2.2.1 Materials, Mixture Proportioning, Sample Preparation, Sample Conditioning, and Testing Procedure

Mortars were prepared to assess how long it takes the concrete to become critically saturated when exposed to fluid. The mortars prepared herein were consistent with those described in section 2.1. Cylindrical specimens (25 mm height × 100 mm diameter) were used for the water absorption test. The cylindrical specimens were cut 24 h after casting from a larger cylindrical sample and sealed in two layers of plastic. The specimens were stored at 23 ± 1°C at 50 ± 1 (RH) after 28 days where they were kept for more than a year to equilibrate. A procedure similar to ASTM C1585-04 (*44*) was used to monitor fluid absorption. After conditioning, the outer circumference of the specimen was sealed with two layers of epoxy resin. After the epoxy hardened, the specimens were placed under water. Two small spacers were placed under the sample to provide a small gap between the bottom of the container and the lower surface of the sample. This allowed water absorption from both circular surfaces.

2.2.2 Results and Discussion

A water absorption test was performed where the amount of absorbed water (I) by mass was determined and normalized by the cross-sectional area exposed to water as outlined in ASTM C1585-11:

$$I = \frac{m_t}{a \cdot d} \qquad (2.2)$$

where m_t is the change in specimen mass at time t in grams; a is the area of the both sides exposed to water, in.mm^2; and d is the density of water in g/mm^3.

Figure 2.3 (a) illustrates the sorption results for the specimens with the low (13%) and high (31%) air contents. The specimens show a similar sorptivity (rate of water absorption or the slope of the curve) however, over time the specimens with higher volumes of air absorb more water. This occurs because the air voids provide space for water (*43*); however, the diffusion of air and the overpressure in the air bubbles slow the water absorption which corresponds to the long time to saturation (*18,45*). Figure 2.3 (b) shows data from Figure 2.3 (a); however, the vertical axis is plotted in terms of degree of saturation (S). The horizontal axis is shown as the square root of time while the upper horizontal axis corresponds to the actual time. The most striking feature of the graphs is the fact that at the same time the degree of saturation is substantially lower in the specimens with entrained air. At the end of the initial 6-h sorption period, samples with lower air content show higher degree of saturation. This suggests that for an equal time of exposure to water, the specimen with the higher air content has a lower degree of saturation. The secondary rate of increase in degree of saturation can be fitted with a linear function to estimate the amount of absorbed water over a long period of time. This implies that the non-air entrained concrete (red points in Figure 2.3 (b)) would be critically saturated after less than a week while the air entrained concrete would take 6 years to reach critical saturation under these conditions. This difference may
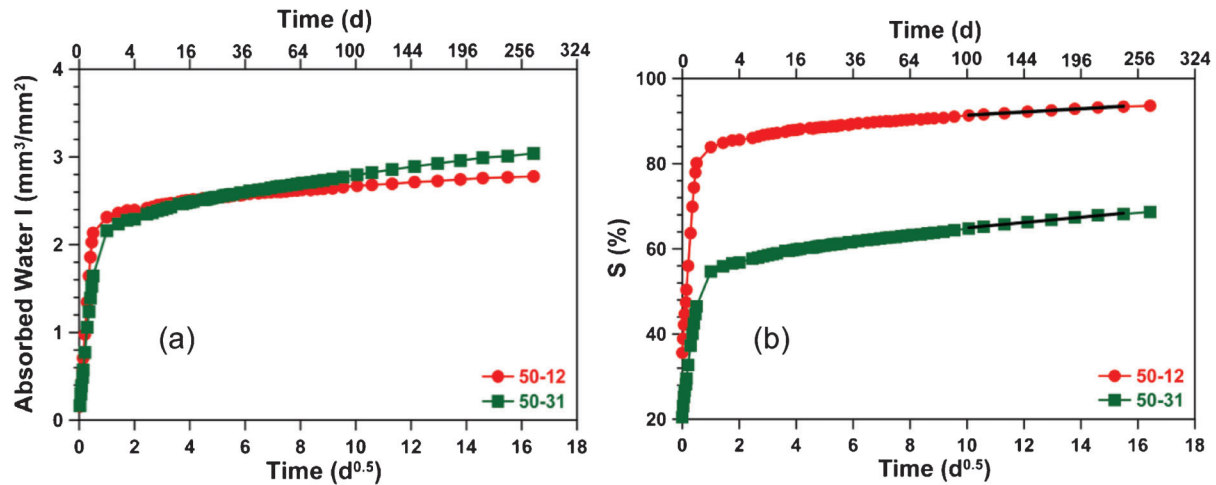
Figure 2.3 (a) Effect of air content by volume of paste and initial moisture on water absorbed for samples conditioned at 50% RH; (b) results of sorption test provided as increase in the degree of saturation for samples conditioned at 50% RH (*33*).

be attributed to the fact that entrained airs have larger pore size; thereby having a small capillary suction pressure. This may result in a longer time to fill larger pores by water.

2.3 Using Acoustic Emission and Heat Flow Techniques to Quantify Freeze and Thaw Damage in Mortars Containing Deicing Salt

Pure water freezes at $0°C$ when it is under one atmospheric pressure. As previously mentioned, however, the fluid inside pores of concrete is not pure water since it contains various alkali, chloride, and hydroxide ions. The presence of ions in pore solution causes that pore solution to freeze at a temperature lower than what is expected of pure water, i.e., $-8°C$ as observed by Li et al. (*12*). This decrease in the freezing point of pore solution in porous materials occurs due to surface interactions, confinement, and the presence of capillary pressures (*17,46*). When deicing salts are added to the surface of pavements and bridge decks, the concentration of ions in the pore solution is increased. In general, the use of more salt produces a higher concentration of ions in pores and leads to a greater depression of the freezing point.

In an aqueous NaCl solution, four phases exist including NaCl solution, ice, NaCl, and $NaCl \cdot 2H_2O$ (hydrohalite). When one phase changes to another phase, latent heat is either released or absorbed. Therefore, energy transfer can be used to indicate that a freezing or thawing event (i.e., a phase change) is taking place (*21,47*). The amount of latent heat and its corresponding freezing or thawing temperatures are specific material properties that can be used to differentiate different materials and different phases in a composite system.

A longitudinal guarded comparative heat flow technique (*48*) was used as a part of this study to quantify when phase changes occur in concrete (mortar) saturated by deicing salts. The acoustic emission was used to relate this phase change with damage. For more description see (*16*).

2.3.1 Materials, Mixture Proportioning, Sample Preparation and Conditioning

A single mortar mixture was used that was similar and was prepared in a similar fashion to that described in section 2.1 with a sand volume fraction of 55% and a water-to-cement ratio (*w/c*) of 0.42 by mass. After 28 d of curing, 25.4 mm × 25.4 mm × 50.8 mm (1 in. × 1 in. × 2 in.) samples were cut from cast bar. Samples were then placed in a vacuum oven at $65°C \pm 1°C$ and a pressure of 20 mm Hg $\pm$ 5 mm Hg for 7 d to empty the pore space. The samples were then placed in a desiccator and fully saturated (i.e., 100% degree of saturation) with a de-aerated NaCl solution by vacuum pump as described in section 2.1 of this chapter. Samples were wrapped with a thin plastic sheet to protect the samples against subsequent moisture exchange with their surrounding environment and the top and bottom cross section plastic covers were removed to ensure better connection with thermal pads during the freeze-thaw tests. In addition, a small circular hole was made in the side plastic of each sample to attach the AE sensor.

2.3.2 Testing Design and Procedure

Samples were saturated using NaCl solutions with concentrations of 0, 0.7, 3, 5, 6, 8, 10, 13, 15, 18, 23.3, and 26% NaCl by mass to investigate the effect of solution concentration on freeze-thaw damage. Dry control samples were also prepared for comparative testing. A longitudinal guarded comparative colorimeter (LGCC) was used according to ASTM E1225-09 (*48*) and ASTM D5470-12 (*49*) to produce heat flow. Heat flow was also monitored versus temperature change. A test sample was inserted between two 25.4 mm × 25.4 mm × 25.4 mm (1 in. × 1 in. × 1 in.)

meter bars (Pyroceram Code 9606) with known thermal properties Figure 2.4 (a).

A temperature gradient was established in the test sample by using a low temperature cold plate cooler as shown in Figure 2.4. Thermally conductive pads with a thickness of 3 mm were used at the Pyroceram/mortar sample and Pyroceram/cold plate interfaces. Seven thermocouples were positioned at different heights to measure corresponding temperatures and heat flow through the LGCC.

Before and after the freeze-thaw test, two coupled AE sensors were used to perform active AE measurement through the length of the sample. During the freeze-thaw test, one AE sensor was used to record a continuous passive AE measurement. Each mortar sample was run through one freeze-thaw cycle in order to determine freezing and thawing temperatures of solution. Temperature was controlled to vary from 24°C to -40°C. The initial temperature of the test was set to remain at 24°C for one hour to allow the sample to equilibrate. After the initial temperature became stable, the bottom surface was cooled by controlling the temperature of the cold plate. The cold plate was cooled at a rate of 2°C/h within 32 h. At -40°C, the temperature was kept constant for 4 h to allow the sample to again reach equilibrium. Then, the temperature was increased to 24°C at a rate of 4°C/h within 16 h.

2.3.3 Results and Discussion

The heat flow consumed or released by the mortar sample (i.e., heat flow inward or outward sample) can be estimated by Equation 2.3:

$$\Delta Q_{Sample} = (q_B - q_T).A \qquad (2.3)$$

where: ΔQ_{sample} is the heat flow (W) consumed/released by mortar sample, q_T is the heat flow per unit area (W/m^2) through top Pyroceram meter bar, q_B is the heat flow per unit area (W/m^2) through bottom Pyroceram meter bar, and A is the cross section area of the sample (m^2).

Figure 2.5 shows the temperatures of the sample and Pyroceram meter bars at seven different locations. Heat flows were also calculated and indicated in Figure 2.5 for one dry sample and for wet samples containing 0%, 5%, or 23.3% NaCl solution. Freezing and thawing peaks were observed corresponding to different phase changes (i.e., water, ice, and NaCl·2H$_2$O). In fact, these peaks are associated to the energy (i.e., latent heat) released/absorbed during freezing/thawing due to phase change. The freezing process can be considered as an exothermic behavior since the system releases heat to the surrounding environment. The thawing process can be considered as an endothermic behavior.

Water and salt solutions may freeze at a temperature below their freezing point. This phenomenon is known as super-cooling or under-cooling (50). NaCl-rich solution in the pores of the mortar sample could freeze at a lower temperature than expected from the NaCl solution phase diagram, but would be expected to thaw at the same liquidus temperature. Figure 2.6 shows the temperature of the phase change detected on thawing and good correlation is observed with the typical NaCl phase diagram. Indeed, under-cooling action was observed during the cooling process for mortar samples saturated with NaCl solutions. For samples containing solutions with a NaCl concentration of more than 13%, two freezing points were observed corresponding to the two exothermic events observed during cooling Figure 2.5 (d). The second freezing point for high concentrations could be attributed to formation of ice in the pore structure, while the origin of the first freezing point (unexpected freezing point) is unknown, as its temperature is above the NaCl solution liquidus line. For sample containing 18% salt solution, two thawing points were observed associated to liquidus and eutectic phase changes during heating process.

Figure 2.7 (a) shows the total cumulative acoustic energy recorded during one freeze-thaw cycle for samples saturated with different concentrations of NaCl solution. The damage index (D) for mortar samples is also shown in Figure 2.7 (b). It should be noted that the amount of damage varies with the concentration of NaCl solution. Two levels of high damage or AE activity (i.e., humps) can be seen. The damage that occurs at the lower concentrations of NaCl solution may be similar to what was observed during scaling tests, where more damage occurred due to a

(a)   (b)

Figure 2.4   Experimental setup: (a) mortar sample and Pyroceram specimens on the two stage cold plate; (b) entire experimental setup with insulation and AE sensor (*16*).
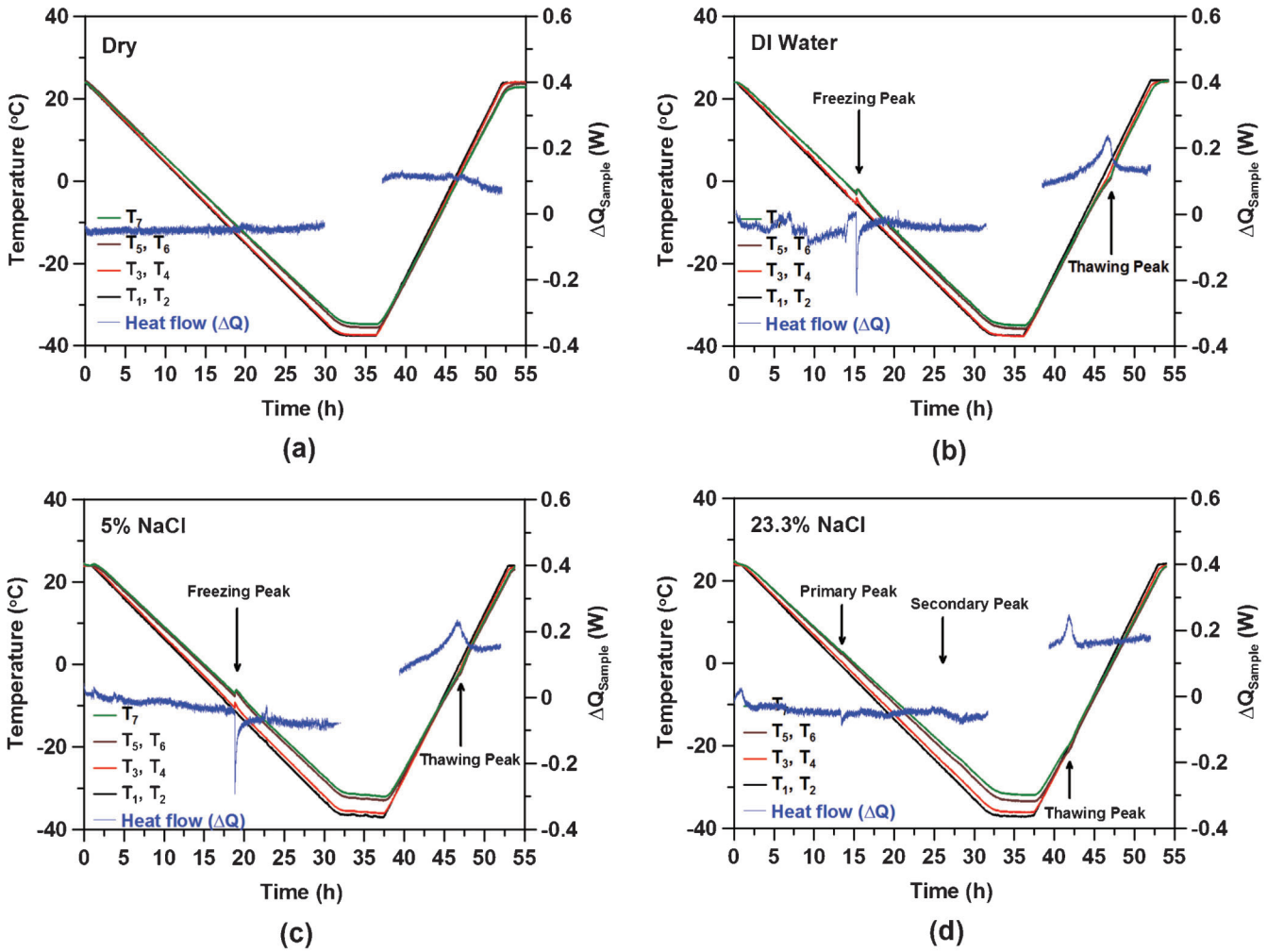
Figure 2.5 Temperatures of sample and Pyroceram meter bars at different locations together with corresponding consumed/released heat flow (ΔQ_{Sample}) versus time (*16*).
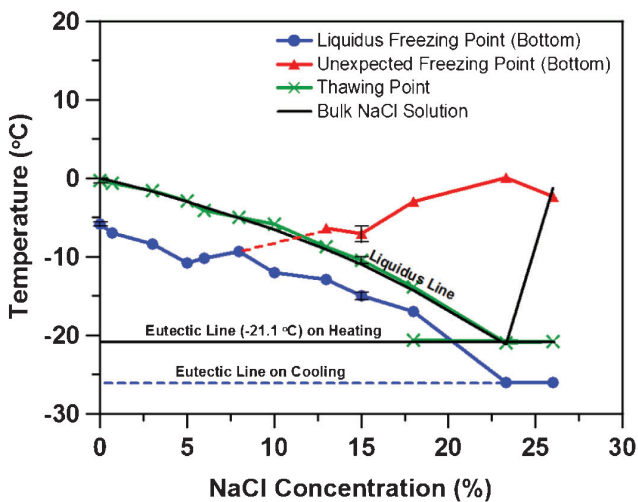
Figure 2.6 Freezing and thawing points of samples saturated with different NaCl solutions compared to the freezing points of bulk NaCl solution (*16*).

pessimism salt concentration between 3% and 5% NaCl (*51,52*). A greater damage also occurred with a higher NaCl concentration solution, which appears to be caused by the combination of different freezing mechanisms or formation of an alternative phase (*16*).

2.4 Summary

This chapter discussed the use of acoustic emission to monitor freeze-thaw damage using both passive and active AE. It was observed that freeze-thaw damage is related to critical degree of saturation (86–88% for these samples). For specimens having a degree of saturation greater than 86–88%, damage began to occur during the first freeze-thaw cycle. The critical degree of saturation appears to be independent of the air content; however, the volume of air and quality of the air void system likely has a strong relation to the time that it takes the concrete to reach the critical degree of saturation.

While water absorption using a procedure like ASTM C 1585-04 (*44*) may provide an index of water absorption, the differences between non-air entrained
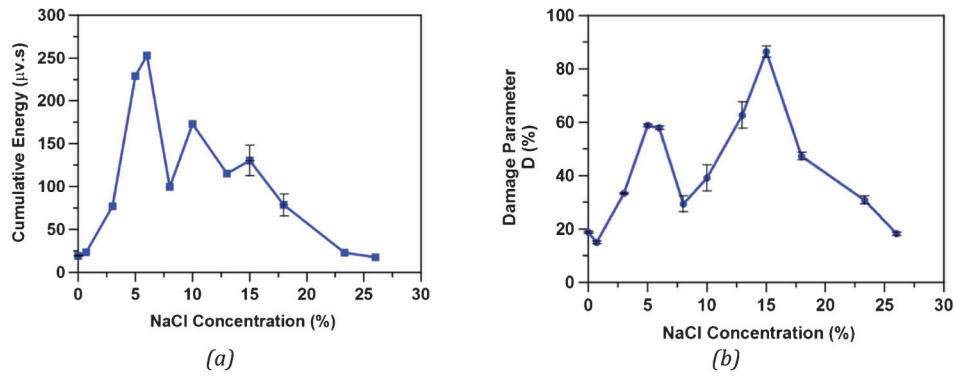
Figure 2.7   Total cumulative acoustic energy due to freeze/thaw damage (a) and decrease of the relative dynamic elastic modulus (damage parameter) due to freeze and thaw damage (b) for samples saturated with different NaCl solutions (*16*).

and air entrained systems were small when only mass gain was investigated. However, when examined in terms of the degree of saturation the plain and air entrained materials show a clear distinction. The non-air entrained system took less than a week to reach 88% saturation and the air entrained system is estimated to require approximately 6 years. A new procedure was used based on the longitudinal guarded comparative heat flow technique to detect phase changes so they can be correlated with acoustic emission events. Samples saturated with salt solution showed greater damage with respect to those saturated with pure water.

3. DEICING SALTS: PROPERTIES AND THEIR INFLUENCE ON DRYING AND WETTING

3.1 Introduction

Concrete pavements in the midwestern United States have shown premature deterioration at joints. While several causes have been suggested for the distress that develops at some joints, it is clear that the movement of moisture is an important aspect for several of these distress mechanisms including those associated with freeze-thaw and/or physical salt attack (*12,21*). As such, the wetting and drying of concrete may be of great importance in understanding joint durability. This chapter describes how deicing salt modifies transport due to changes in the activity of the solution, surface tension and viscosity as a function of concentration and temperature. The implications of the fluid properties on the drying behavior are discussed as they relate to the non-linear diffusion coefficient, which will be useful for modeling drying processes. The influence of deicing salts on wetting mechanisms is shown for sorptivity tests. A simple model is proposed to relate wetting process to fluid properties. Additionally, the change in the pore space available for gas transport is investigated by performing oxygen permeability and oxygen diffusivity tests in samples which were previously exposed to deicing salts.

3.2 Background

Moisture diffusion is known to be related to the moisture content and pore size distribution (*53,54*). In addition, internal moisture profiles influence the rate of hydration, electrical properties, fluid transport, and many aspects of durability. While there are numerous studies on transport, very few explicitly focus on experimentally determining the non-linear diffusion coefficient and few explicitly examine the influence of the pore fluid properties on the transport. This work examines how the pore solution composition is influenced by deicing salts and how this alters the pore fluid properties such as surface tension, viscosity and activity. This work will show how the composition of the pore fluid can influence the rate of fluid ingress into and egress from concrete.

In the concrete literature, the majority of the interest in deicing salts research is related to durability (*55*), on hysteresis during drying and wetting (*12,56*), on freeze-thaw and salt solutions damage (*16,57,58*) or crystallization pressure (*17*). Spragg et al. (*31*) examined changes in density, activity, surface tension and viscosity as a function of the concentration of salt solutions; however, a limited number of measurements have been reported in literature.

The influence of deicing salt on pore solution properties and transport processes has not been sufficiently studied. Some studies reported the reduction in sorptivity of aqueous solution in presence of deicing salts (*31,55,59,60*). Despite the large interest of the concrete community to the drying process (*53,61,62*), few studies can be found on the drying when salts are present in the pore fluid. Drying in presence of deicing salts has been studied for rocks (*63*) and to investigate salt weathering processes (*64*). Similarly, very few studies are available in literature that discuss gas transport in concrete previously exposed to deicing salts. Only one study was found where salt saturated concretes were used for transuranic waste repository (*65,66*). This project will provide some information that can be used to describe the influence of salt on drying from a more fundamental perspective.

3.3 Influence of Deicing Salts on Liquid Properties

Three common deicing salts were analyzed in this study at different concentrations: 0–23% for sodium

chloride (NaCl), 0–32% for calcium chloride (CaCl$_2$) and 0–30% for magnesium chloride (MgCl$_2$). Commercially available deicing salts were used in this study for all tests. It should be noted that the solutions were prepared using de-ionized water and were not done using typical pore solution. In a cement paste, therefore, there may be other ionic species that are not accounted for with this formulation.

Viscosity measurements for deicing salt solutions were performed using an Anton-Parr rheometer (model Physica MCR 301). In the rheometer, the solution was maintained at constant temperature; the viscosity can be found from the torque applied to the fluid that causes a shear.

The surface tension for the deicing salt solutions was measured using a Du Noüy Ring Tensiometer (*67*). The method is based on determining the force that is required to detach a wire ring from the surface of the solution. A series of three measurements were performed for each solution using the approach described by Pease et al. (*68*).

For systems containing deicing salt solution considered in this study, an equation proposed by Kaminsky (*69–71*) can be used to describe the variation of viscosity with concentration of the solute at atmospheric pressure. (Equation 3.1):

$$\eta = \eta_{\text{water}}\left(1 + C_1 \cdot V_{\text{salt}}^{1/2} + C_2 \cdot V_{\text{salt}} + C_3 \cdot V_{\text{salt}}^2\right) \quad (3.1)$$

where η is the viscosity at a certain temperature and pressure (Pa·s), η_{water} is the viscosity of pure water at the same temperature and pressure (Pa·s) and V_{salt} is the concentration of the aqueous solution (%). The empirical coefficients C_1, C_2 and C_3 (-) depends on both solute and solvent properties (*70,72,73*) and are provided in Table 3.1.

Experimentally obtained viscosity results for calcium chloride, magnesium chloride and sodium chloride solutions at 23° ± 0.02°C are presented in Figure 3.1 where viscosity of salt solutions is presented as a function of the concentration, by mass.

The change of viscosity with temperature can be described using an Arrhenius-type of law, introduced by Andrade (*74,75*) as described by Equation 3.2:

$$\eta = A \cdot \exp\left(\frac{E_a}{RT}\right) \quad (3.2)$$

where A is a constant that changes with concentration (Pa·s); E_a is the activation energy (J·mol^{-1}); R is the universal gas constant (8.314 N·m/K·mol); and T is the temperature (°K). The viscosity was experimentally obtained in the temperature range between 5°C and

TABLE 3.1
Fitting parameter from Equation 3.1 for salt solutions

	C_1 (-)	C_2 (-)	C_3 (-)
NaCl	0.1134	-0.0551	0.0027
CaCl$_2$	−0.1810	0.0285	0.0080
MgCl$_2$	−0.1202	0.0385	0.0081
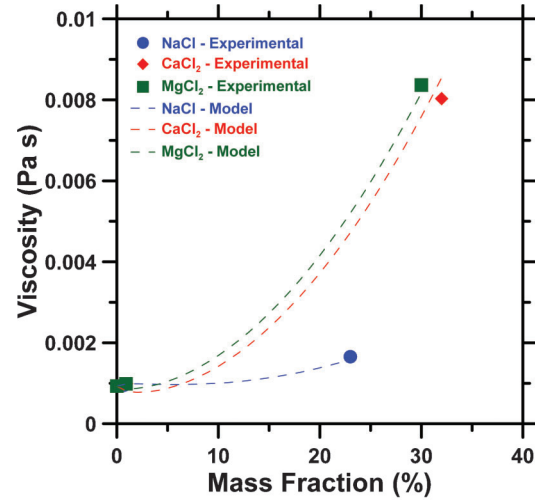
Figure 3.1 Viscosity as function of mass concentration for salt solutions at 23°C (*32*).

38°C. Experimental data was fitted to Equation 3.2 evaluating the constant A and the activation energy for each solution analyzed. The results are shown in Figure 3.2, where the model obtained with the calculated parameters is compared to experimental data.

To describe the change in surface tension, the semi-empirical formulation proposed by Szyszkowski (*76*) (Equation 3.3) was used:

$$\gamma = \gamma_{water} - RT\Gamma^{\infty} \ln\left(1 + \frac{C}{b}\right) \quad (3.3)$$

where the concentration is given as C at temperature T. γ_{water} represents the surface tension of water at the same temperature and of Langmuir adsorption coefficients Γ^{∞} (mol·m^{-2}) and b (mol·l^{-1}).

Surface tension measurements performed at 23 ± 1°C are shown in Figure 3.3. In Figure 3.3, the curves were obtained by fitting the Szyszowski equation to experimental values of surface tension. In Figure 3.4,
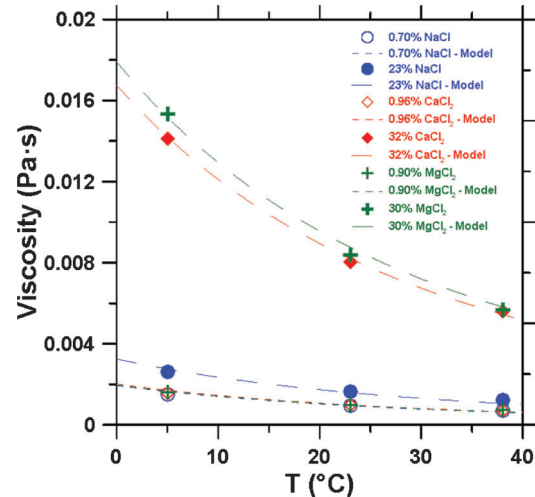
Figure 3.2 Effect of temperature on viscosities of salt solutions (*32*).
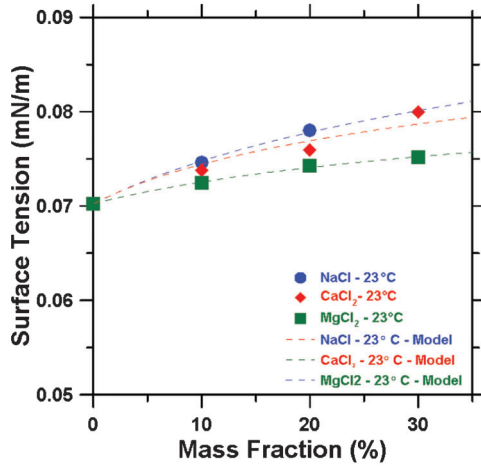
Figure 3.3 Surface tension measurements for different salt solutions at 23°C (*32*).

the influence of temperature is shown comparing experimental values (symbols) with curves from the Szyszowski's model (dotted lines) for calcium chloride solutions. A good correspondence between experimental values and model is shown.

3.4 Influence of Deicing Salts on Drying Mechanisms

Desorption tests and moisture diffusion tests were performed on mortar that had a w/c of 0.42 and 55% of fine aggregates by volume. More details on the materials used can be found in Chapter 2.

For the desorption test, mortar cylinders (34 mm of diameter and 50 mm of height) were cast and kept sealed for 28 days and then demolded. Thin slices were cut using a wet saw and then stored at 23°C $\pm$ 0.1°C and 50% $\pm$ 2% RH, in a CO_2 free chamber. Prior to testing, samples were saturated in limewater or salt solutions.

For the moisture diffusion test, cylindrical samples (diameter of 102 mm (4 in.) and length of 204 mm (8 in.)) were prepared. The samples were demolded at an
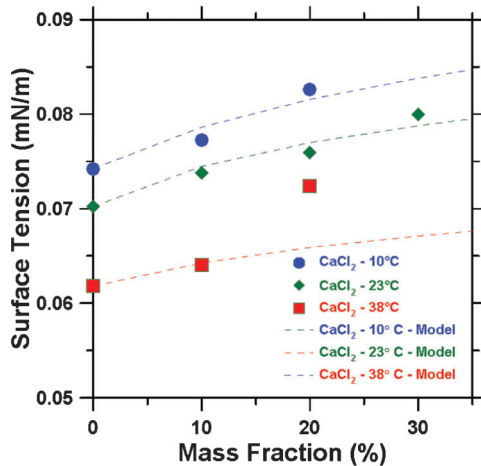
Figure 3.4 Influence of temperature on surface tension measurements for $CaCl_2$ solutions (*72*).

age of 24-hours and then sealed in double plastic bags for approximately 8 months. The samples were then cut using a wet saw to obtain 9 samples with a height of 50 $\pm$ 2 mm (2 in.) and diameter of 102 $\pm$ 2 mm (4 in.) and 9 samples 10 $\pm$ 2 mm (0.2 in.) thick and with diameter of 102 $\pm$ 2 mm (4 in.). The samples were prepared according to STADIUM Lab® procedure.

The non-linear moisture diffusion coefficient was calculated from a desorption isotherm measured using a dynamic vapor desorption analyzer (TGA Q5000). During the desorption test, the samples have subjected to a constant temperature while the relative humidity was varied using controlled steps and the mass recorded as a function of time (*32,77,78*).

For the moisture diffusion test, according to the procedure suggested in STADIUM Lab® procedure, the 18 samples were weighted and their dimensions were taken. The specimens were subsequently epoxy-coated on the side surfaces to ensure a one-dimensional moisture flow during drying. The samples were then submerged in each solution (lime water, 32% $CaCl_2$ and 30% $MgCl_2$) and kept submerged until their mass variation became lower than 0.5% with respect to the initial mass over a 7 days period. Samples were then exposed to drying, storing them in a temperature and humidity controlled chamber (at 23 $\pm$ 0.1°C and 50% $\pm$ 0.1% RH). Their mass was monitored at 1, 2, 3, 4, 5, 6, 7, 9, 11, 13, 15, 21, 28 days etc. until the percentage of mass variation was lower than 0.5% with respect to the initial mass of the sample.

The change of the drying mechanism in presence of deicing salts has been studied by analyzing two factors: the alteration of the equilibrium relative humidity of the solution and of the non-linear moisture diffusion coefficient (*79*).

The equilibrium relative humidity is the relative humidity that corresponds to the transition between condensation and evaporation. It is dependent on fluid properties and on the pore size, according to Equation 3.4 (*63,80*):

$$RH_{eq}(r) = a_w \cdot e^{-\frac{z\gamma M}{\rho_l RT\gamma}\cos\theta} \tag{3.4}$$

where a_w is the water activity of the solution (-), γ is the surface tension (N/m), M is the molar mass of the liquid (kg/mol), ρ_l is the density of the liquid (kg·m^{-3}), θ is the contact angle (deg), and r is the pore radius (m). The contact angle is assumed to be zero in this study (*81*). From Equation 3.4, it is apparent that the alteration in liquid due to the presence of deicing salts will affect the equilibrium relative humidity as well (*80*).

The equilibrium relative humidity (RH_{eq}) as a function of the pore radius is presented in Figure 3.5 (a) for the case of calcium chloride solutions. Specifically, the increase of surface tension and the decrease of water activity cause a decrease in the equilibrium relative humidity. The equilibrium relative humidity can be thought of as the boundary between evaporation ($RH < RH_{eq}$) and condensation ($RH > RH_{eq}$) (*63*). A decrease in RH_{eq} corresponds to a lower
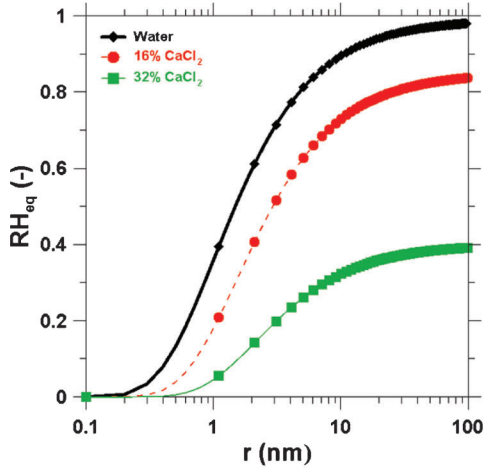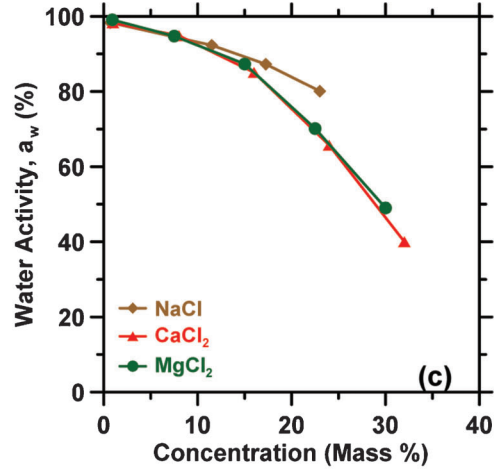
(a)   *(b)*

Figure 3.5 (a) Equilibrium relative humidity as function of pore radius for water and calcium chloride (CaCl$_2$) solutions (*80*); (b) water activity as function of the concentration of deicing salt solutions (*31*).

external humidity required to initiate the drying process for samples containing salts. This has practical implication in concrete as the sample containing deicing salt solutions will remain saturated longer than a sample containing water (*31,80*).

It is common to describe the drying processes of cementitious materials using Fick's second law (Equation 3.5), where the diffusion coefficient, D_S, is non-linear with respect to moisture content (relative humidity or degree of saturation, S is shown here) (*49,82,83*).

$$\frac{\partial S}{\partial t} = \frac{\partial}{\partial x}\left[D_s(S)\frac{\partial S}{\partial x}\right] \quad (3.5)$$

where S is the degree of saturation (-), x is position from the surface (m), and t is drying time (s).

It is common to refer to the diffusion coefficient, D_s, as the sum of two contributions that are considered to simultaneously participate (Equation 3.6): the advective liquid flow represented by a liquid diffusion coefficient D_{S_L} and the water vapor diffusion described by a vapor diffusion coefficient D_{S_V} (*78,84,85*).

$$D_S(S) = D_{S\_l}(S) + D_{S\_v}(S) \quad (3.6)$$

The formulations for D_{S_L} (Equation 3.7) and for D_{S_V} (Equation 3.8) come from the work of Mainguy (*86*) and Philip and de Vries (*87*). Both the liquid and the vapor contribution are written as a function of the degree of saturation S (ratio between the mass of the fluid and the mass of the fluid at saturation) (*84*). The liquid portion of the diffusion coefficient is defined as:

$$D_{S\_l}(S) = -\frac{dp_c(S)}{dS}\cdot\frac{K_l}{\phi\cdot\eta}\cdot k_{rl}(S) \quad (3.7)$$

where p_c is the capillary pressure, K_l is the intrinsic liquid permeability (m^2), Φ is the porosity (-), η is the viscosity of the liquid (Pa·s), and k_{rl} is the relative liquid

permeability (-). The vapor portion of the diffusion coefficient is considered as in Equation 3.8:

$$D_{S\_v}(S) = -\frac{dp_c(S)}{dS}\cdot\left(\frac{M}{\rho_l\cdot RT}\right)^2$$
$$\cdot D_{ve}(S)\cdot\frac{p_{vs}}{\phi}\exp\left(\frac{M}{\rho_l\cdot RT}\cdot p_c(S)\right) \quad (3.8)$$

where D_{ve} is the effective water vapor diffusion coefficient, and p_{vs} is the saturation water vapor pressure (2810.06 Pa at 23°C (*88*)). The liquid and vapor contribution of the diffusion coefficient for the mortar considered in this study are shown in Figure 3.6. The model presented in Figure 3.6 has been obtained by fitting Equation 3.7 and Equation 3.8 to
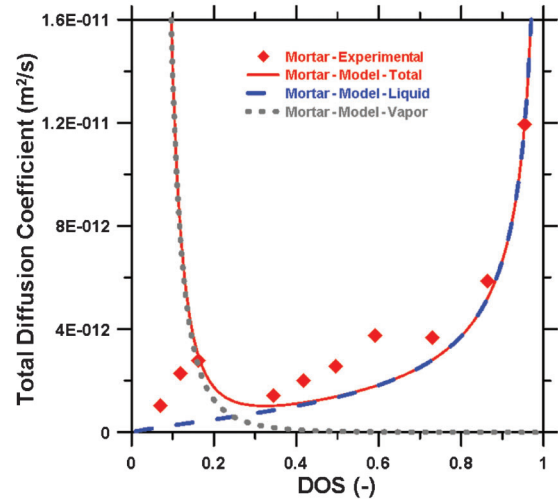
Figure 3.6 Vapor, liquid and total diffusion coefficient for mortar samples initially submerged in water.

the experimental diffusion coefficient evaluated as in (*77,84*).

From Equation 3.7 and Equation 3.8, it can be seen that both contributions are the function of the liquid properties; and specifically the vapor portion of the diffusion coefficient is dependent on the surface tension and density of the liquid, while the liquid portion of the diffusion coefficient results to be the function of the surface tension, density and viscosity of the fluid.

To investigate the effect of deicing salts on the diffusion coefficient, desorption tests were performed on mortar samples previously submerged in calcium chloride solutions. The results are presented in Figure 3.7. It should be noted that the "model curves" have been obtained accounting for the change in surface tension, density, and viscosity during drying, implementing Equation 3.1, 3.2 and 3.3 in Equation 3.7 and Equation 3.8. However, the possible reaction between salt and matrix was not accounted for in this model.

It can be seen from Figure 3.7 that the effect of deicing salts causes: (1) a shift of the curve towards lower relative humidity values due to change in the equilibrium relative humidity (Equation 3.4); (2) a change in the shape of the curve due to surface tension and viscosity changes. From the comparison between the model and the experimental diffusion coefficient, a reasonable correspondence is obtained in capturing the shift due to relative equilibrium changes. However, the shape of the curve predicted differs from those experimentally obtained. A higher effect of viscosity on the diffusion coefficient is predicted by the model that shows indeed a steeper decrease of the diffusion coefficient at high relative humidities when proceeding towards low relative humidity values (during drying). The differences observed between experimental data and the model may be related to the salt reaction, binding with the matrix, or salt crystallization process

Figure 3.7 Total diffusion coefficient of mortar samples submerged in water and calcium chloride solutions.

during drying which is not accounted for in the model used in this study.

The results shown in the previous paragraph have been confirmed by performing a moisture diffusion test on larger mortar samples that were previously submerged in salt solutions (Figure 3.8). It is evident that the amount of water lost from samples previously submerged in deicing salt solutions is considerably lower than the amount lost from those submerged in limewater. It should be noted that even though the initial salt solution concentration was 32% for calcium chloride and 30% for magnesium chloride, the actual concentration in the samples is thought to be lower to explain the drying at 65% RH. Additionally, it is expected that some micro-structural changes occurred during the sorption process due to the presence of deicing salts. This might have caused a partial pore blocking and a consequently lower initial degree of saturation in the samples containing salts compared to the samples submerged in pure water.

3.5 Influence of Deicing Salts on Wetting Mechanisms

Spragg et al. (*31*) have shown that the amount of fluid absorbed during sorptivity tests by samples which are equally conditioned reduces in presence of deicing salts. This effect was also shown to be the function of the solution concentration and of the type of salt. A portion of the results is summarized in Figure 3.9 (*31*) where the fluid absorbed (mass) by mortar samples conditioned at 50% RH is plotted as a function of time. The decrease absorbed fluid is evident already at low concentration. These tests were conducted using commercially available deicing salts.

A simple model that describes the wetting process for sorptivity test is represented by Kelham's equation (*89*). In this model, the penetration depth of the fluid is expressed as the function of the absorbent properties and of the absorbate properties (Equation 3.9).

$$\chi(t) = \sqrt{\frac{4K_i\gamma\cos(\theta)t}{\phi\eta r}} \qquad (3.9)$$

where χ is the penetration depth (m), K_l is the previously introduced intrinsic permeability (m^2), γ is the surface tension (N/m), θ is the contact angle (deg), Φ is the porosity (-), η is the viscosity, and r is the pore radius (m). Using the parameters previously determined for the mortar used in this study (K_l and Φ) and implementing Equation 3.1, 3.2 and 3.3 in Equation 3.9, a preliminary estimation on the penetration depth has been obtained for calcium chloride solutions. The results are presented in Figure 3.10 where the penetration depth is shown as a function of calcium chloride solution concentration at various absorbing time. The model shows the reduction in fluid absorption in presence of deicing salts as a function of salt solution concentration. Specifically, the change is proportional to the square root of the surface tension to viscosity ratio. It should be noted however that the model assumes that there are no changes in the microstructure
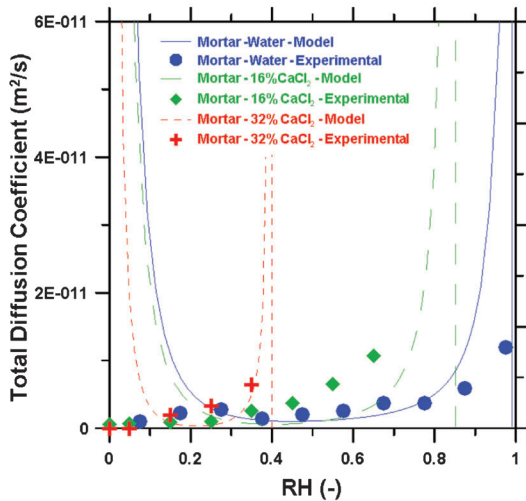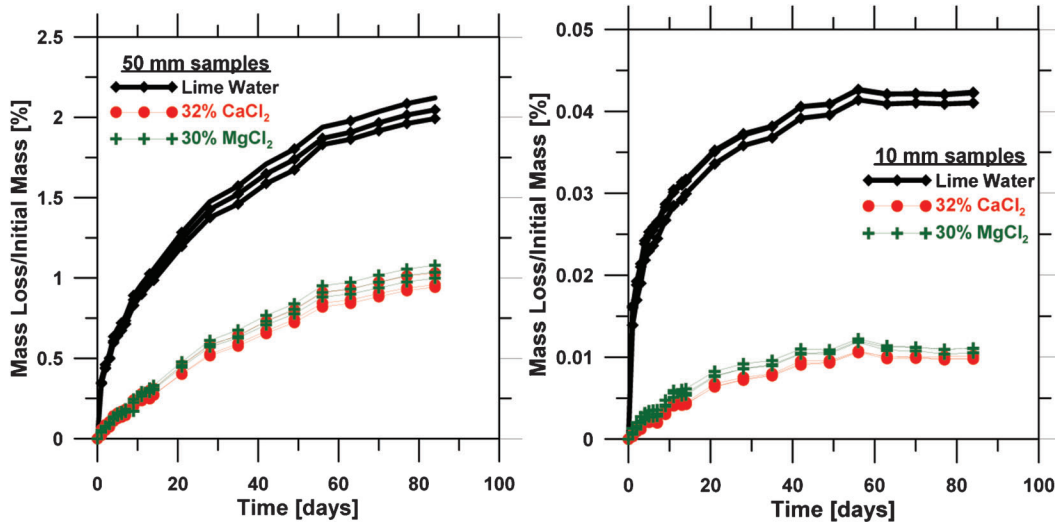
Figure 3.8 Mass loss from drying test for samples saturated with water, calcium chloride and magnesium chloride solutions.

during sorption. Recent works have shown that changes in the microstructure are likely to occur due to the presence of salts. Consequently, the penetration depths might be different in reality than the values shown in Figure 3.10 and likely a non-linear behavior with respect to concentration is expected.

3.6 Reduction of Gas Transport for Concrete Exposed to Deicing Salts

As shown in the previous paragraph (3.3 and 3.4), the presence of deicing salts alters the degree of saturation of concrete materials due to modification of fluid properties and of the non-linear diffusion coefficient. This also means that the pore space available for gas transport is reduced in presence of

deicing salts. The influence of deicing salts on gas permeability and diffusivity is presented.

Gas permeability, gas diffusivity and desorption tests were performed using the same type of mortar introduced in section 3.4.

Cylindrical samples (diameter of 102 mm (4 in.) and length of 204 mm (8 in.)) were prepared, demolded at an age of 24 hours and then sealed in double plastic bags for approximately 12 months. For oxygen permeability, the cylinders were cored using a 68 $\pm$ 2 mm diameter bit. The samples were then cut using a wet saw to obtain samples with a height of 25 $\pm$ 2 mm (1 in.) for oxygen permeability measurements. For oxygen diffusivity measurements larger cylinders were obtained (102 mm (4 in.) of diameter and 50 mm (2 in.) length). Specimens were initially oven dried at 50° $\pm$
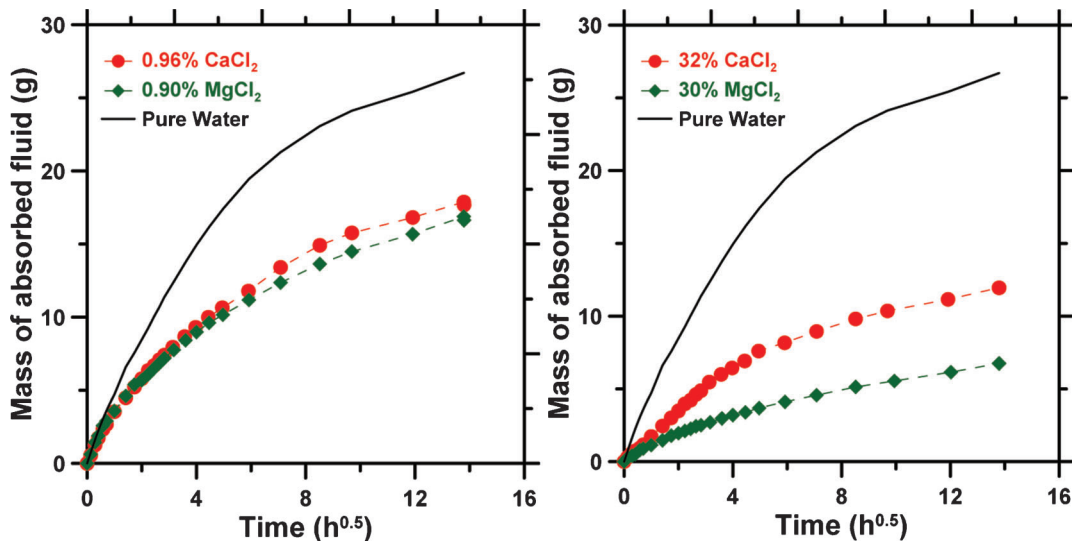
Figure 3.9 Sorptivity tests conducted on samples conditioned at 50% RH using different type of deicing salts (calcium chloride and magnesium chloride) in different concentration (*31*).
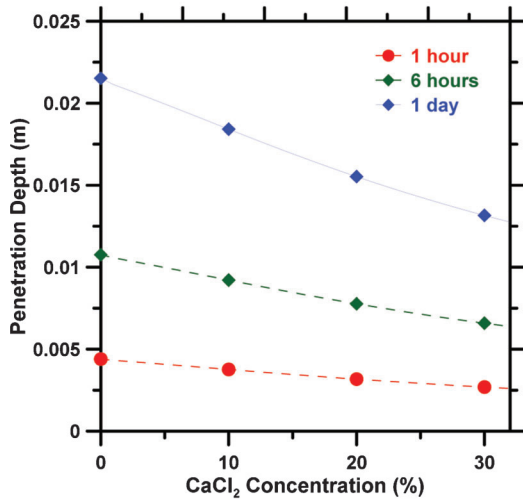
Figure 3.10 Penetration depth as function of calcium chloride solution concentration after 1 hour, 6 hours and 1 day of exposure to fluid absorption.

0.5° C and 30% $\pm$ 1% RH until constant mass and subsequently submerged in different aqueous solutions until constant mass: deionized water, 16% and 32% calcium chloride ($CaCl_2$), 15% and 30% magnesium chloride ($MgCl_2$) and 17.5% sodium chloride (NaCl). The specimens were then conditioned in a temperature and humidity controlled chamber at 65%° $\pm$ 1% RH and at 23°C $\pm$ 0.5°C until equilibrium ($\Delta m < 0.1\%$).

Oxygen permeability has been measured using a falling head permeameter (90,91). This test involves the measurement of a unidirectional flow of oxygen through the specimen generated by the pressure gradient between the upper and the lower side of the

sample. The testing procedure has been performed according to Alexander et al. (87). More details on the test method and on the calculation can be found in Villani et al. (75).

The oxygen diffusivity was measured using an instrument originally developed by Lawrence (92). The test is performed by exposing one surface of the disc to a stream of pure oxygen and the opposite face to a stream of pure nitrogen at the same pressure. The unidirectional flow of oxygen is measured by monitoring the difference in oxygen concentration between the beginning and the end of the test in the nitrogen cell. More details on the test procedure and on the calculation can be found in Villani et al. (79).

Oxygen permeability results are presented in Figure 3.11. The error bars indicate the variability (in terms of standard deviation) between four. The results of oxygen permeability and oxygen diffusivity are also shown in Figure 3.12 as function of the degree of saturation.

It is apparent from Figure 3.11 and Figure 3.12 that despite samples were all conditioned at the same relative humidity (65% RH), the samples that contained salt solutions showed a higher degree of saturation at equilibrium. When the degree of saturation increases a reduction is observed for both the oxygen permeability and diffusivity. A decrease in the case of oxygen diffusivity can be seen when the DOS is higher than 60% since the main vapor filled pores involved in gas transport are becoming filled with fluid and the vapor phase is becoming disconnected. This is in accordance to previous research results that related the degree of saturation with transport properties (93). The lower degree of saturation seen in the case of magnesium chloride might be related to the slightly lower
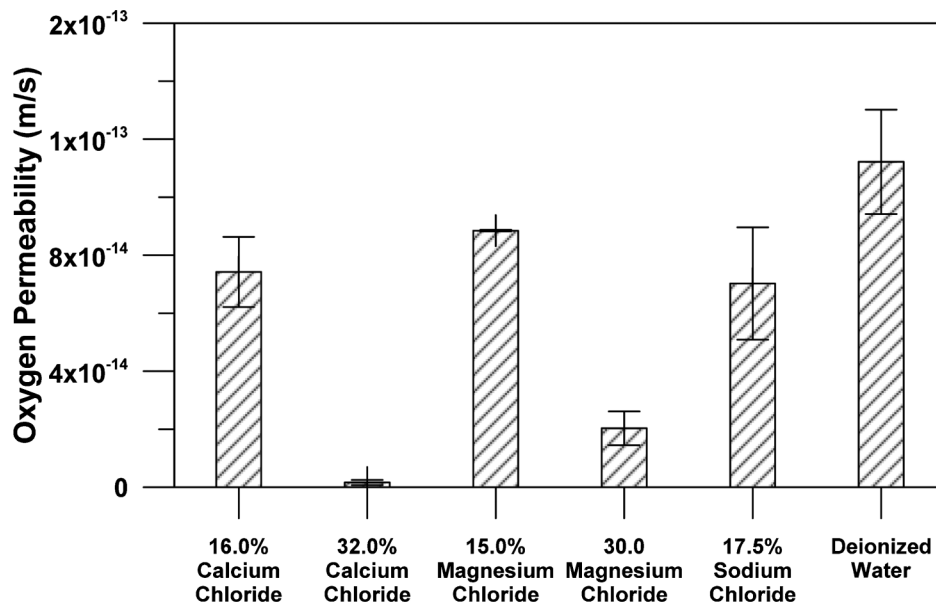
Figure 3.11 Oxygen permeability results for samples initially submerged in high and intermediate deicing salt solution concentration.
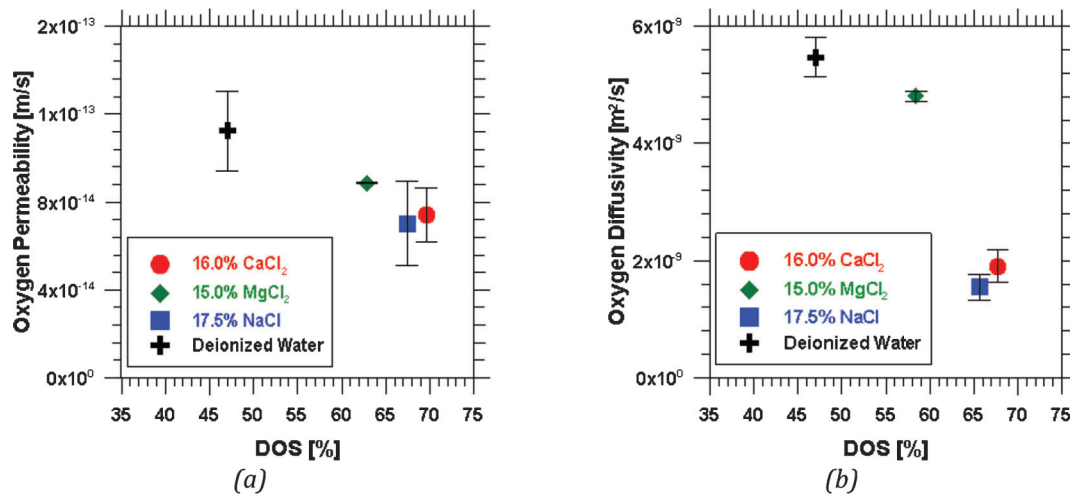
Figure 3.12 (a) Oxygen permeability results and (b) oxygen diffusivity results as function of the degree of saturation for samples initially submerged in intermediate concentration deicing salt solutions.

concentration also confirmed in the chloride profile (*79*) or due to microstructural change due to the reaction between magnesium chloride and paste (for example, magnesium (Mg^{2+}) and chloride (Cl^-) ions tend to deplete calcium hydroxide ($Ca(OH)_2$) forming magnesium hydroxide $Mg(OH)_2$ and calcium chloride or the magnesium may also substitute for the calcium in calcium silicate hydrate).

Additional causes such as further hydration, salt precipitation due to drying, or Friedel's salt formation ($3CaO \cdot Al_2O_3 \cdot CaCl_2 \cdot 10H_2O$) (*55*) might have altered the results of gas transport. The influence of hydration is considered to be negligible in this study since the samples are sufficiently aged; therefore, the possible reduction in porosity for further hydration is likely not substantial. The effect of salt deposition during drying has been investigated for lower salt concentration (*79*) and its effect seems to be relatively small, assuming that no precipitation occurred at pores. However, this may not be the case for high concentration.

3.7 Summary

Understanding premature deterioration at joint in concrete pavement can benefit substantially from understanding the role of deicing salts on the fluid properties and its transport properties. Specifically the fluid properties (activity, surface tension and viscosity) alter the drying and wetting behavior.

The changes that occur in solution properties in presence of deicing salts are discussed. Surface tension and viscosity were analyzed when changing concentration and temperature. The presence of deicing salts alters both viscosity and surface tension of the liquid. These effects were also shown to be a function of temperature. Models from literature were successfully fitted to describe the change in viscosity and surface tension when changing the concentration or temperature.

The presence of deicing salts changes the drying behavior. The non-linear diffusion coefficient and equilibrium relative humidity (the humidity that must be reached to initiate drying) are influenced by salt concentration. Samples containing deicing salts can be expected to have higher degree of saturation. This has practical implication in concrete as the sample containing deicing salt solutions will have a higher degree of saturation and will remain saturated for a longer time.

The wetting process was also briefly discussed considering sorptivity test (*31*) using deicing salt solutions. A simple model was also applied that predicts the penetration depth in time, based on known fluid properties (square root of the surface tension to viscosity ratio).

Oxygen permeability and diffusivity tests were conducted that have shown a considerable reduction of gas transport in the presence of deicing salts. This result is thought to be the effect of mainly three factors: 1) increased degree of saturation of the sample which has been proved to considerably affect gas transport; 2) salt deposition during drying which is believed to have had only a small influence on measurements performed; and 3) chemical compounds formation such as Friedel's salts. The last aspect was not analyzed in this specific study and further research is needed to better understand its possible influence.

4. LABORATORY EVALUATION OF THE FIELD CORES

4.1 Introduction

Some of the 10–20 years-old concrete pavements located in various parts of Indiana, which otherwise perform well, show signs of premature deterioration (in the form of excessive cracking, spalling, loss of material in the direct vicinity of the joint and development of "bulb-shaped" damage zones under the sealed parts of

the joints) primarily in areas near the longitudinal joints; in several cases, the transverse joints areas have been affected as well.

Some of the typical examples of the distress observed in these pavements are presented in Figure 4.1. More details can be found in the report by Arribas-Colón et al. (*11*).

This chapter of the report presents the results of laboratory work performed on concrete core samples collected from several locations around the state of Indiana. The samples were collected from both distressed and un-distressed concrete pavement joints as well (for comparative purposes) from the middle of the panels in an effort to determine the underlying causes of the observed joint distresses. The age of the pavement varied, as did the mixture compositions and severity of the environmental exposure.

The results presented in this chapter include examination of cores from the following locations:

(a)   The onramp from US 67 to east-bound I-465 located in the SW section of Indianapolis, IN;
(b)   W 86th Street (near Michigan Road) located in the north section of Indianapolis, IN;
(c)   SB I-65 (near MLK Street exit) in Indianapolis, IN
(d)   SR 933 near South Bend, IN (section between Darden Road and Willow Street)
(e)   A four-mile stretch of I-94 between the junctions with US 421 and US 20 (exits 34 and 40) near Michigan City, IN.

4.2 Collection of Cores

When selecting the coring, an attempt was made to obtain specimens for various cases presented in Figure 4.2 and listed below:

- A – damaged area of the transverse joint
- B – damaged area of the longitudinal joint near the junction of the longitudinal and transverse joints
- C – damaged area of the longitudinal joint away from the transverse joint
- D – mid-span of the slab, un-damaged section
- E – un-damaged transverse joint adjacent to the damaged transverse joint
- F – un-damaged area of the longitudinal joint away from the transverse joint

A number of specimens needed for various types of tests were prepared by dissecting each of the collected cores as shown in Figure 4.3. The specimens for air-void system analysis had planar dimensions of 4.3 × 4.3 in. and were generally collected from the top section of the core. In some cases, the damage to the cores during removing from the joints was so extensive that it was not possible to obtain the specimens directly from the top section of the core. As a result, these specimens were obtained from the lower portion of the core.

4.3 Testing

In an attempt to identify the underlying causes of deterioration, the cores were subjected to the following examinations:

- Analysis of air void system in hardened concrete (ASTM C457) (*94*)
- Optical microscopy analysis
- Evaluation of freeze-thaw resistance (modified ASTM C666) (*95*)
- Evaluation of resistance to chloride ions penetration by AASHTO T277 (*96*) chloride ion penetration (RCP) test

Figure 4.1   Examples of joint damage in the existing pavements.
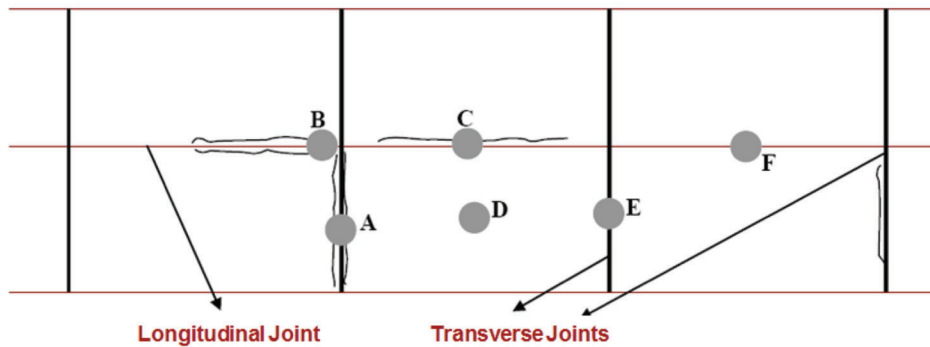
Figure 4.2 Location of cores within pavement structure.

- Scanning Electronic Microscopy (SEM) analysis of concrete microstructure and energy dispersive spectroscopy (EDS) analysis of secondary deposits in the air bubbles
- Evaluation of the rate of water absorption (sorptivity) as per ASTM C1585 (*44*)
- Determination of the depth of chloride ions penetration (concentration of chloride ions at various depths of the specimen).

4.3.1 Analysis of the Air Void System

The analysis of the air void system of specimens extracted from various cores was performed according to the ASTM C457 (*94*) Modified Point Count Method using one of the two procedures: (a) manual procedure and (b) image analysis procedure.

During the manual procedure the results were recorded separately for each line of traverse in order to determine the distribution of air voids with depth of the core (the results for every four lines were averaged to increase the accuracy). In addition, an attempt was made to distinguish between the entrained and entrapped voids. The selection of entrapped voids, although arbitrarily, was based on the size (larger than

about 1 mm), shape (irregular rather than round) and location (mostly adjacent to at least one particle of aggregate). Further, it should be pointed out that voids which were infilled with secondary products were not counted (regardless of whether they appeared to be entrapped or entrained) as such voids were difficult to distinguish and it was assumed that at this stage they do not contribute to the freeze-thaw resistance of concrete.

When using the image analysis procedure the polished surfaces of the cores were scanned and the resulting images were analyzed by a computer program that replicated the Modified Point Count Method of the ASTM C457 method (*8,94,97*). The image analysis method of air voids analysis was found to provide objective and repeatable results with good level of accuracy. However, this method does not distinguish between entrained and trapped air voids. On the other hand, this method identifies all infilled air voids as paste and thus yields the results similar to those obtained during the manual method.

The results of the air void system analysis are shown in Table 4.1. All air void system parameters given in this table (with the exception of I-94 cores with labels shown in *italic* which were collected by image analysis method) were determined using the manual method.
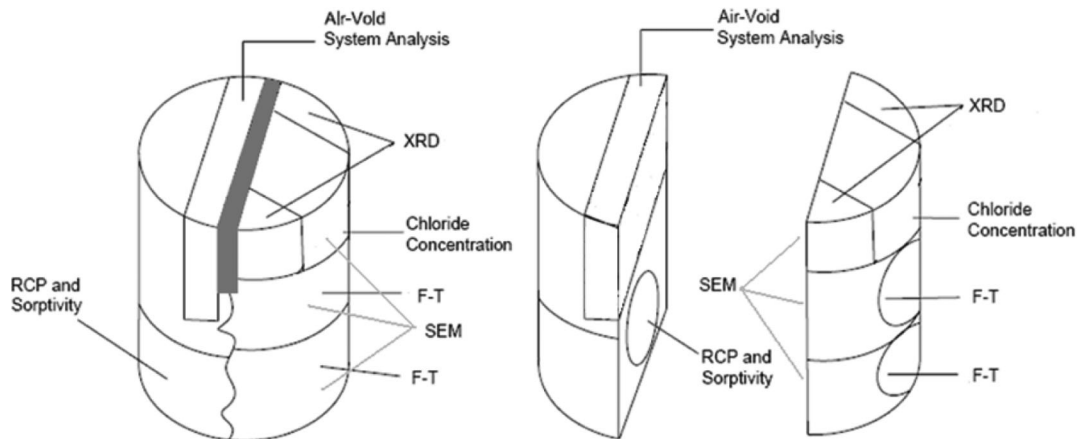
Figure 4.3 Schematic of test specimen locations within each core.

TABLE 4.1
Summary of test results from air-void system analysis

Location	Label	Total air content (%)	Entrained air content	Void frequency (voids/mm)	Specific surface (mm²/mm³) target (>25)	Spacing factor (mm) target (<0.200)	Descending trend in void frequency with depth	Filled air voids observed	Durability factor (%)	RCP
US 67	**US67 1A**	5.8	3.8	0.17	11.5	0.39	Yes	Yes	53.2	
	US67 2F	5.2	3.5	0.19	14.4	0.36	Yes	Yes		
	US67 3E	5.2	3.0	0.19	15.0	0.32	Yes	Yes		
	US67 4D	5.3	3.1	0.28	21.0	0.21		Yes	90.3	Low
	US67 5F	6.3	5.5	0.5	31.6	0.17	Yes	Yes	89.1	Mod
	US67 6D	4.0	2.1	0.11	10.7	0.52				
	US67 7F	5.5	4.2	0.32	23.3	0.20				
	US67 8A	4.3	2.4	0.09	8.8	0.62	Yes	Yes	5.5	
	US67 8E	n/a								
	US67 9D	6.4	6.2	0.49	31.0	0.13				
	US67 10D	3.8	3.5	0.54	56.5	0.10				
W. 86th St. BL (west of the lights at W. 86th and Payne Rd. intersection)	86BL 1D	3.4	3.1	0.43	50.8	0.11			76.6	Vlow
	86BL 2D	6.3	4.9	0.43	27.0	0.16				
	86BL 3D	4.2	4.1	0.43	40.2	0.13	Yes			
	86BL 4D	4.5	4.3	0.40	36.1	0.14				
	86BL 5D	4.9	4.5	0.34	27.9	0.16				
	86BL 6D	5.4	5.3	0.43	32.0	0.14				
W. 86th St. AL (east of the lights at W. 86th and Payne Rd. intersection)	86AL 1D	3.7	3.7	0.18	19.9	0.29			92.4	Low
	86AL 2D	4.1	2.5	0.10	9.9	0.55				
	86AL 3D	5.2	3.7	0.33	25.2	0.20	Yes			
	86AL 4D	4.3	2.5	0.17	16.2	0.33				
	86AL 5D	5.3	4.1	0.23	17.5	0.28				
	86AL 6D	5.2	4.4	0.23	17.7	0.27				
	86AL 7A	3.5	2.9	0.08	9.2	0.63	n/a	Yes	82.0	Mod
	86AL 8B	4.7	3.8	0.15	12.4	0.41	Yes	Yes	26.2	High
	86AL 9C	3.8	3.2	0.10	10.5	0.53	Yes	Yes	55.1	High
	86AL 10E	6.0	4.7	0.21	14.3	0.31	Yes		60.1	
	86AL 11C	4.1	4.1	0.14	14.0	0.39	Yes	Yes	70.1	High
SR 933	SR933 0D*	4.5	3.7	0.14	14.0	0.4	n/a	Yes	64.3	Low
	SR933 1D	4.6	4.4	0.28	23.9	0.22			99.9	Vlow
	SR933 2E	5.7	4.2	0.23	16.1	0.28	Yes	Yes	98.2	Low
I-65	**I65 2C**	5.9	5.3	0.11	7.7	0.42	n/a		55.2	Low
	I65 3B	4.9	3.9	0.08	6.8	0.67				
	I65 4C	4.0	2.7	0.11	10.9	0.41				
	I65 5C	5.1	3.7	0.13	10.0	0.44				
	I65 6F	7.9	6.1	0.17	8.8	0.41	n/a		45†	Low

19

TABLE 4.1
(Continued)

Location	Label	Total air content (%)	Entrained air content	Void frequency (voids/mm)	Specific surface (mm²/mm³) target (>25)	Spacing factor (mm) target (<0.200)	Descending trend in void frequency with depth	Filled air voids observed	Durability factor (%)	RCP
I-94	*1C1*	2.9			21.8	0.28		Yes	91.6	Test not performed due to equipment problems
	1D1	5.4	2.1		16.8	0.28		Yes	96.4	
	1D2	7.9			18.9	0.18			86.4	
	1F2	3.5			20.4	0.28		Yes	93.1	
	1J1	3.6			18.8	0.28		Yes	95.0	
	1S3	7.0			21.6	0.18		Rare	93.0	
	1W1	5.0			11.6	0.41		Rare	96.1	
	2D1	9.1			19.3	0.15		Yes	90.5	
	2F1	3.9			20.4	0.25		Yes	94.3	
	3D1	5.0			27.3	0.18		Rare	96.5	
	3F1	3.1			33.4	0.18		Yes	96.5	
	3J2	6.3			24.4	0.15			96.6	
	3S3	5.6			27.6	0.15			98.9	
	4D1									
	4F1	5.0	3.0		26.2	0.18			95.3	
	5D1	6.3	3.8		23.8	0.15		Yes	96.6	
	5F1	5.4	2.6		19.2	0.23		Yes	95.9	
	5W1								94.4	

NOTE: Only empty air voids were included in the count. **Boldface** indicates cores from damaged joints. n/a denotes the specimens which were not obtained from the very top part of the core. J–next to construction joint, undamaged (.1 in. from joint), W–wheel path (.2 ft from transverse joint), S–shoulder (.2 ft from joints). The labels shown in *italics* denote cores for which the air void system was evaluated using the image analysis method.

* Average of five specimens obtained from the same core.

† Sample taken from core showing unusual cracking damage.

4.3.2 Optical Microscopy Analysis

The optical microscopic analysis of the specimens was performed using the same pieces of polished flat specimens that were used for the air-voids analysis. The examination of the surfaces was conducted at the magnification of about 60X. A sulfate compounds staining technique was used on samples from 11 cores to identify potential deposits of these materials in the air voids concrete. The staining process involved immersing samples for 2 min in a solution of barium chloride and potassium permanganate. At the end of the immersion period the samples were carefully cleaned with deionized water (3 times) and left to dry for 24 hours after which the surfaces of the specimens were photographed in the optical microscope.

4.3.3 Freeze-Thaw Resistance

The resistance of concrete to cyclic freezing and thawing was evaluated using a modified "A" procedure of ASTM C666 method (95). The modifications adopted for the purpose of this research were primarily related to the use of nonstandard test specimens. Specifically, instead of using the standard prismatic specimens the non-standard concrete discs (about 0.9 in. thick and 4.0 in. in diameter) cut from individual cores 9as shown in Figure 4.3) were used. When conducting the test, a total of 12 disks (in four rows of three disks each) were placed vertically in the standard 3 in. × 4 in. × 16 in. freeze-thaw machine metal containers. Due to the above configuration and the cylindrical shape of the specimens, there were few places in each container where the specimens were surrounded by more than 3 mm of water (maximum allowed by ASTM C666 (95)). However, the effect of this modification is believed to be minor.

The relative dynamic modulus of elasticity was determined for each disk after every 36 freeze-thaw cycles. The impulse excitation method, completely described (for disk-shaped specimens) in the annex to ASTM E1876 (98) was used to monitor the change in resonant frequency. Even though the resonant frequency in both the first and the second natural modes was monitored, it was often not possible to obtain the second mode frequency after some degradation of specimens already occurred. Therefore, only the frequency obtained in the first natural mode was used for calculation of the relative dynamic modulus of elasticity. The values of relative dynamic modulus of elasticity at 300 cycles were used to calculate the values of durability factor (DF) following the procedure of ASTM C666 (95). These values are shown in Table 4.1

4.3.4 Resistance to Chloride Penetration (RCP)

The measurement of the resistance concrete to chloride ion penetration (RCP test) was performed according the AASHTO T277 (96) standard procedure using the 2-in. thick discs extracted from the bottom pat parts of the cores) see Figure 4.3.

4.3.5 Scanning Electron Microscopy (SEM) Examination

The concrete specimens used for SEM examination were extracted from different locations within the individual cores as shown schematically in Figure 4.4.

All SEM specimens were prepared using standard microscopy polishing techniques and the images were collected in the backscattered mode. In addition, several of the observed microstructural features (especially deposits present in the infilled voids) were further analyzed using the energy dispersive x-ray analysis (EDXA) in order to determine their chemical composition.

4.3.6 Sorptivity

The measurements of the rate of water absorption (or sorptivity) were performed according the ASTM C1585 (44) using the 2 in.-thick discs removed from the bottom part of the cores (see Figure 4.3). The physical setup used to conduct the test is shown in Figure 4.5.

4.3.7 Depth of Chloride Ions Penetration

The depth of penetration of the chloride ions was determined by grinding layers of concrete in ~2 mm increments and analyzing the amount of water soluble chlorides in the resulting powders using the ion chromatography technique. The parts of cores from the mid-span of the pavement were ground downwards starting from the surface. The parts of cores from the vicinity of the joints were ground in layers parallel to the surface of the joint (laterally and inward starting at the surface of the joint). The grinding directions are shown in Figure 4.6.

4.4 Test Results

4.4.1 Analysis of the Air-Void System

As seen in Table 4.1, the amount and the quality of the air void system varied, depending on the location

Figure 4.4 Location of the SEM specimens within the core.

Figure 4.5 Setup for the sorptivity testing.

In contrast, all cores obtained from W 86th Street AL location had relatively low entrained air content varying from 2.5% (cores 2D and 4D) to 4.7% (core 10E). The cores from this location also exhibited high scatter in the spacing factor, with values ranging from 0.20 mm (core 3D) to 0.63 mm (core 7A). It can also be noticed that for all damaged cores (7A, 8B, 9F and 11C) the measured spacing factor was 0.39 mm or higher. Core 9F appeared to be undamaged (no surface damage) but was deteriorated beneath the surface.

The entrained air content of all three cores obtained from SR 933 was about 4.0%. The spacing factor for the cores from mid-span of the slab was 0.41 mm (core 0D) and 0.23 mm (core 1D). The core obtained from the undamaged transverse joint (2E) had a value of spacing factor of 0.28.

The total air content of 7.9% (entrained air content of 6.1%) obtained for the only undamaged core from I-65 (6F) was the highest among all cores retrieved from that location (Table 4.1). The lowest total air content of 4.0% (2.7% of entrained air content) was found for core 4C. All cores had relatively high spacing factor of about 0.41 mm, including the undamaged core 6F. The only exception was core 3B, for which the spacing factor was a very high value of 0.67.

Analysis of the results for the cores extracted from the pavement on I-94 reveals that the existing air void system in the concrete placed in the panels near the deteriorated longitudinal joint (1C1, 1D1, 1J1, 1W1) did not have spacing values within the range recommended for freeze-thaw. Contrary to this, all cores extracted from the vicinity the un-damaged (and un-sealed) joints (3F1, 4F1 and 5F1) had an adequate air void system at the time of sampling.

In general, the average values of spacing factor in the undamaged cores were always lower than that in the damaged cores, indicating potential for better freeze-thaw resistance of the former. However, one should keep in mind that the distinction between the entrapped and entrained air while based on a predetermined criteria (shape and size of the void) was inherently arbitrary and that only the voids that appeared empty

and the condition of the core. As an example, for the group of cores collected from the ramp of the US 67 the air content (both total and entrained) was highest for cores 5F and 9D (5.5–6.0%). The air content in all other cores was about 4% or less, which is significantly lower than 6.5% typically specified for PCC pavements exposed to freezing and thawing (*99,100*). The lowest entrained air content was obtained for cores 6D and 8A (2.0–2.4%). Accordingly, these two cores exhibited the highest values of spacing factor (0.52 mm and 0.62 mm, respectively), which is considerably above 0.20 mm considered to be indicative of frost-resistant concrete (*99,100*). Both damaged cores (1A and 8A) had relatively high spacing factor (0.39 mm and 0.62 mm, respectively).

All cores from W 86th Street BL location had relatively uniform amount of entrained air (in the range of about 3.0–5.0%). However, the values of spacing factor for these specimens were found to be very low (0.11 mm to 0.16 mm), which is below recommended value of 0.20 mm. Thus, the good parameters of air-void system of cores collected from that location appear to explain the lack of observable damage at the joints.

Figure 4.6 Grading directions for (a) mid-span cores and (b) joint cores.

when examined under the optical microscope (at magnification of 60X) were counted in determining the air content. As a result, the data collected for the samples collected from the middle of the panels (cores D) are probably more accurate than those collected from the vicinity of the joints as the mid-panel locations have lesser amounts of the infield voids.

4.4.2 Optical Microscopy Analysis

The optical microscope examination of polished specimens from the cores (at 60x magnification) identified several cases of in-filling of the air voids with secondary mineral deposits. This infilling was especially evident in the case of smaller air bubbles) as shown in Figure 4.7 (b) (*101*) and was typically associated with concrete obtained from damaged joints although in some cases it was also evident in concrete from some mid-spans and some undamaged joints.

The analysis of micrographs shown in Figure 4.7 reveals that (at first glance somewhat surprisingly) the empty air voids are present in the upper portion of the pavement and the infilled voids are present about 1 inch below the surface. However, it should be pointed out that this particular core (#1A) has been obtained from the damaged transverse joint which (at this location) contained silicon sealing material which was adhering to the face of the joint and thus blocking direct access of the moisture and the salt brine to the interior of the concrete near the top part of the joint. The presence of the sealant appears to have been effectively preventing precipitation of secondary products and infilling of the air voids. On the other hand, the part of the joint directly below the sealer must have experience the condition of full saturation which resulted in progressive infilling of the voids. This observation implies that the "original" parameters of the air-void system could have been well within the expected limits, but become compromised over time, perhaps because trapping of the moisture under the seal, poor drainage, locking-up of joints, water ponding, etc.).

The hypothesis presented above was further confirmed by the existing relationship between the vertical (downward from the surface) distribution of voids frequency and the degree of voids infilling (see the last two columns of Table 4.1). Specifically, it has been observed that 9 out of 12 specimens for which the void

frequency decreases with depth also show substantial infilling of the air voids. The only exceptions are samples from cores 3D, 4D and 10E which have been extracted either from the middle of the panels (location D) or from the undamaged transverse joint (location E).

An example of the decrease in voids frequency with the distance (depth) from the surface exposed to the moisture is shown in Figure 4.8. It is clear that within about 1 inch (~25 mm) from the surface of the core the void frequency was two to three times higher than that observed in the lower section of the specimen.

The observed infilling the existing air voids system obtained through optical observations puts in question its adequacy to resist damage from future freezing and thawing cycles. This is because the infilling of the smaller entrained air voids will significantly increase the air void spacing factor while it will only slightly decrease the total entrained air void volume (*7*).

4.4.3 Freeze-Thaw Resistance

When analyzing the values of durability factor (DF) presented in Table 4.1 for specimens from mid-panel cores (location D in Figure 4.2) extracted from US67, W86th St., SR 933 and I-65 it can be seen that in all cases the DF was higher than 60%. Although there is no common industry standard with respect to the minimum value of the DF required for adequate freezing and thawing performance, a value of 60% is frequently adopted for that purpose. When using this value, there are several cores collected from the vicinity of the damaged joints (US 67 1A, US 67 8A, 86AL 8B, 86AL 9C) which have DF lower than 60%. For specimens extracted from the I-94 cores, all values of the DF were greater than 85%. However, even for this case the DFs of samples from cores taken at the joint (1F-5F) were lower than those for samples from cores from the corresponding samples from the mid-span (1D-5D) with the exception of joint core from section 3 (see Figure 4.9).

4.4.4 Resistance to Chloride Penetration (RCP)

As can be seen from Table 4.1, all specimens extracted from the mid-panel cores (location D in Figure 4.3) had either very low or low chloride ion
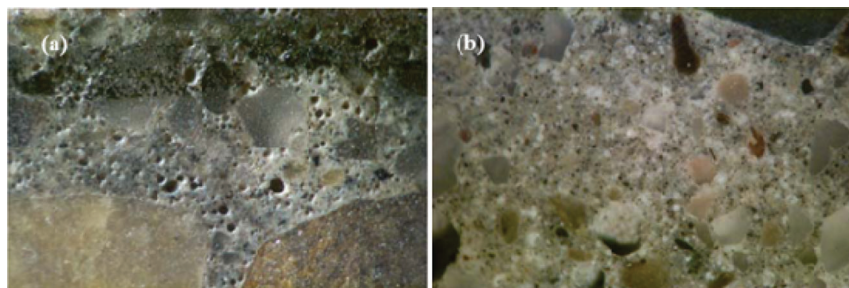
Figure 4.7 (a) Empty air voids in the top portion and (b) infilled air voids in the bottom (about 1 in. below the surface) portion of the specimen obtained from core #1A (ramp US-67) (*101*).
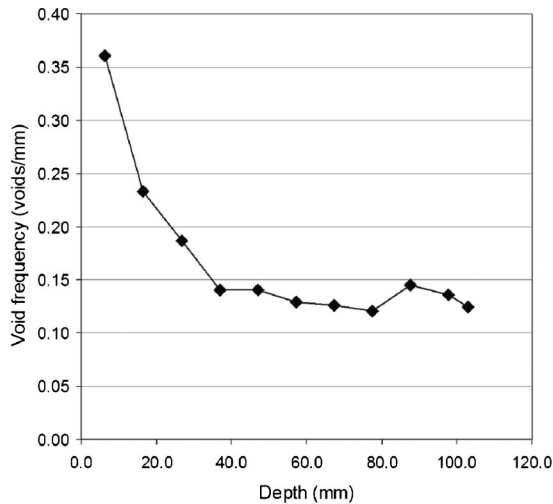
Figure 4.8 Void frequency vs. depth for US 67 core #1A (*101*).

penetrabilities (as per classification provided in the ASTM T 277 (*96*)). The penetrabilities of specimens from the un-damaged jonts(locations E and F in Figure 4.3) were classified as either low or moderate while the penetrabilities of specimens from damaged joints (locations A, B and C in Figure 4.3) were classified as moderate to high (the only exception being specimen I65 3B).

4.4.5 Scanning Electron Microscopy (SEM) Examination

The examination of the microstructure of specimens using the scanning electron microscope equipped with the energy dispersive X-ray detector (SEM-EDX) revealed significant differences in the appearance and composition of the matrix, as well as the degree of

infilling of the voids. These differences were found to depend on both, the location of the core itself (see Figure 4.2) and the location of the SEM specimen within the core (see Figure 4.4).

In general, microstructure of concrete obtained from the mid-section of the panel (locations D in Figure 4.2) consists of typical products of cement hydration (i.e., C-S-H gel, monosulfate (AFm phase), some ettringite (AFt phase) and occasional deposits of Friedel's (calcium aluminate chloride hydrate) and numerous empty or only partially infilled air voids. In contrast, the microstructure of concrete from the area of the damaged joints will often contain comparatively larger deposits of ettringite and Friedel's salt as well as numerous air voids completely or partially filled with either ettringite ($3CaO \cdot Al_2O_3 \cdot 3CaSO_4 \cdot 32H_2O$) or with Friedel's salt ($3CaO \cdot Al_2O_3 \cdot CaCl_2 \cdot 10H_2O$). In their paper on delayed ettringite formation (DEF) Stark and Bollmann (*102*) suggested a change in thermodynamic stability of monosulfate at low temperatures that leads to formation of ettringite (through partial decomposition of monosulfate). They also found that freeze-thaw cycling in 3% NaCl solution resulted in transformation of monosulfate to Friedel's salt and ettringite.

Interestingly, the microstructure of concrete retrieved from bottom parts of cores located at the damaged joints will often resemble the microstructure of concrete retrieved from the mid-span cores, indicating the critical role the water and moisture play in driving the observed changes.

To illustrate the above trends Figure 4.10 presents the micrograph of the microstructure of concrete from the top part (SEM location # 1 in Figure 4.4) of the core retrieved from the middle of the panel (location D in Figure 4.2). Figure 4.11 shows a higher magnification of the same microstructure indicating the presence of ettringite, monosulfate and either empty or partially infilled air voids.
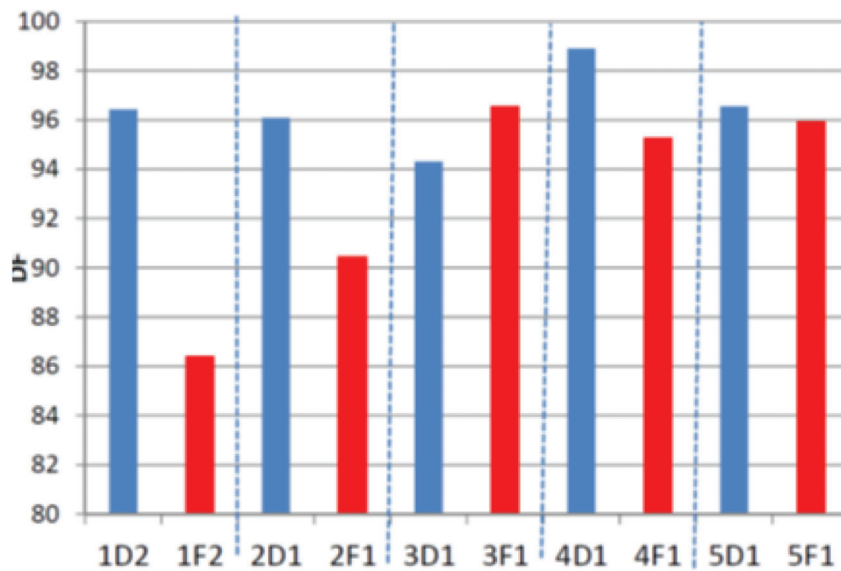
Figure 4.9 Average DF of F-T specimens taken at the sawn joint compared to corresponding mid-span of the same panel (*11*).
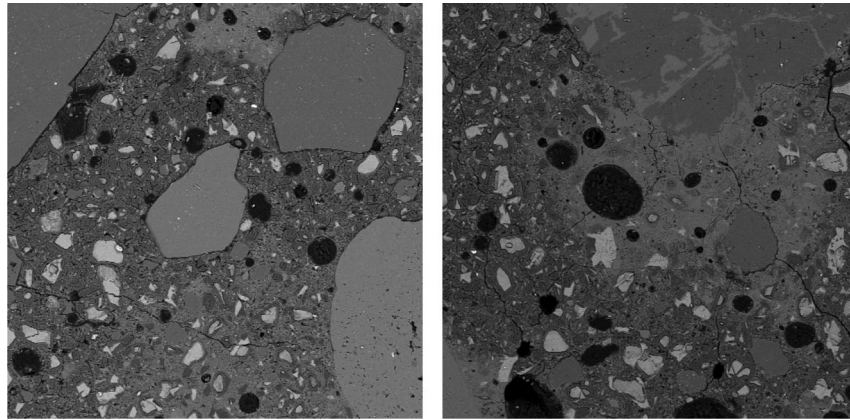
Figure 4.10 Microstructure of concrete near the top (SEM #1 in Figure 4.4) of the core mid-slab core (86AL 1D) with numerous empty air voids (*101*).

Finally, Figure 4.12 shows the microstructure of concrete from the bottom (SEM #3 in Figure 4.4) of the same core (86AL 1D) as shown in Figures 4.10 and 4.11. It can be seen that the microstructure shown in this figure is very similar to the microstructure shown in Figure 4.11 and consists of the C-S-H gel with some deposits of ettringite and Friedel's salt as well either partially filled or empty air voids.

In contrast, Figures 4.13 and 4.14 presents the micrograph of the microstructure of concrete from the core retrieved from the area of the damaged longitudinal joint (location C in Figure 4.2). Specifically, Figure 4.13 shows the microstructure of concrete from the top part (SEM location # 1 in Figure 4.4). The microstructure appears to contain sizeable deposits of ettringite as well as numerous air voids also completely infilled with ettringite. Figure 4.14 shows the microstructure of concrete from the area near the bottom of the longitudinal joint (SEM location # 2 in Figure 4.4). The microstructure contains numerous air voids completely infilled with secondary deposits of ettringite.

4.4.6 Sorptivity

Unfortunately, the results of the sorptivity testing were rather mixed. However, is can be stated that most of the cores retrieved from the joint areas showed higher water absorption rates than cores from the mid-span, with the highest rates observed in cores taken at damaged joints. One exception was the very high water absorption rates of the mid-span core that had slag coarse aggregate (SR933, #0D). Since many variables that were not the subject of this study can strongly influence the results of the sorptivity test, a more detailed analysis of these results is not warranted.

4.4.7 Depth of Chloride Ions Penetration

To determine the changes in the amount of chlorides present in the specimens as a function of the location of the concrete sampling layers within the individual cores, the process of collecting of powdered concrete samples from the mid-span cores started with the top-most layer (located at surface of the pavement) and continued
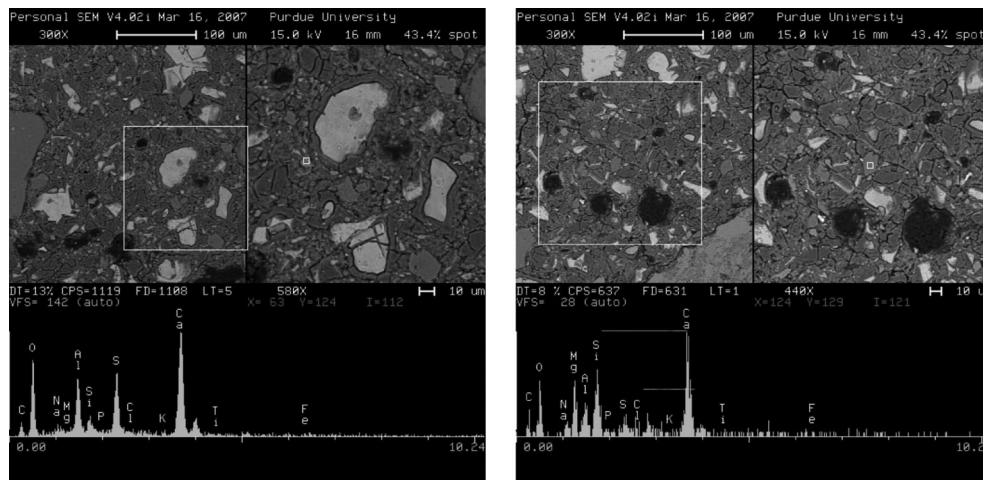
Figure 4.11 Higher magnification of the microstructure of concrete near the top (SEM #1 in Figure 4.4) of the core mid-slab core (86AL 1D) with local deposit of ettringite, monosulfate and either empty or partially filled air voids (*101*).
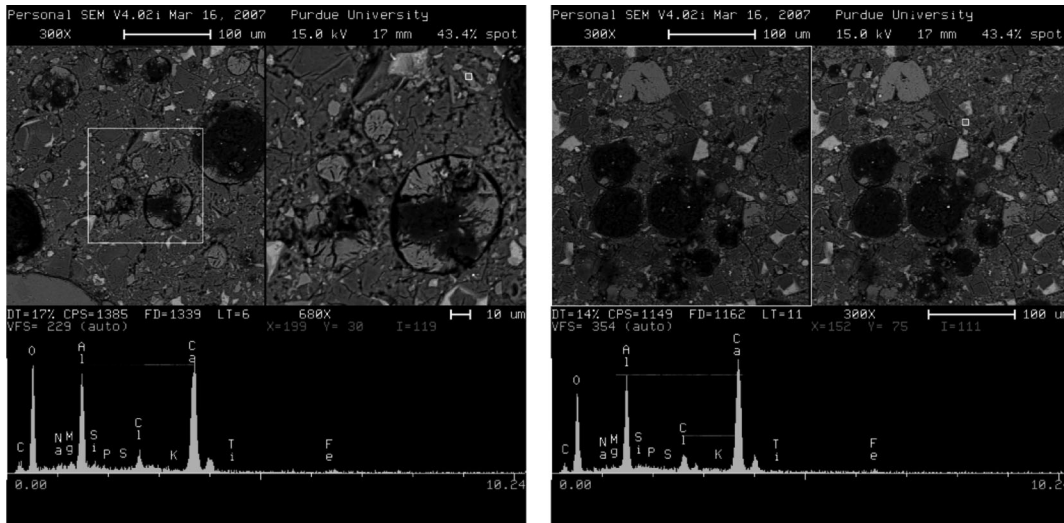
Figure 4.12 Microstructure of concrete near the bottom (SEM #3 in Figure 4.4) of the core mid-slab core (86AL 1D) with local deposit of ettringite, monosulfate, Friedel's salt and either empty or partially filled air voids (*101*).

downward toward the interior of the pavement. The process of collecting of powders from cores taken at joints started with the layer located on the vertical face of the joint and continued (in the horizontal direction) toward the interior of the core.

The results of the depth of chloride ions penetration are summarized in Figure 4.15 (for mid-span cores) and in Figure 4.16 (for cores from undamaged and damaged joints).

Although the chloride ion concentrations in mid-span cores were quite variable (ranging from 2–15 kg/m^3), they were highest in the top 10 mm of the pavement surface (see Figure 4.16) and then decreased significantly with depth, as expected. The chloride ion concentrations in cores from undamaged joints (left part of Figure 4.16) measured over the distance of

about 25 mm form the joint surface were fairly uniform and ranged from approximately 2–6 kg/m^3. In contrast, chloride ion profiles in cores from damaged joint varied significantly, with the lowest measurements near the joint surface (ranging from <0.5–6 kg/m^3), peak concentrations at depths of about 5–15 mm (ranging from approximately 6–11 kg/m^3) and relatively stable values of 4–6 kg/m^3 at distance of 22 mm or higher from the joint surface.

Analyzing the curves presented in Figure 4.15 it could be observed that the layer of concrete located between about 0.1 to 0.3 inches (~2.5 to 7.5 mm) below the surface of the mid-span cores (surface of the pavement) has the highest level of chlorides of any layers for each of the individual cores. It is probably reasonable to assume that this elevated level of
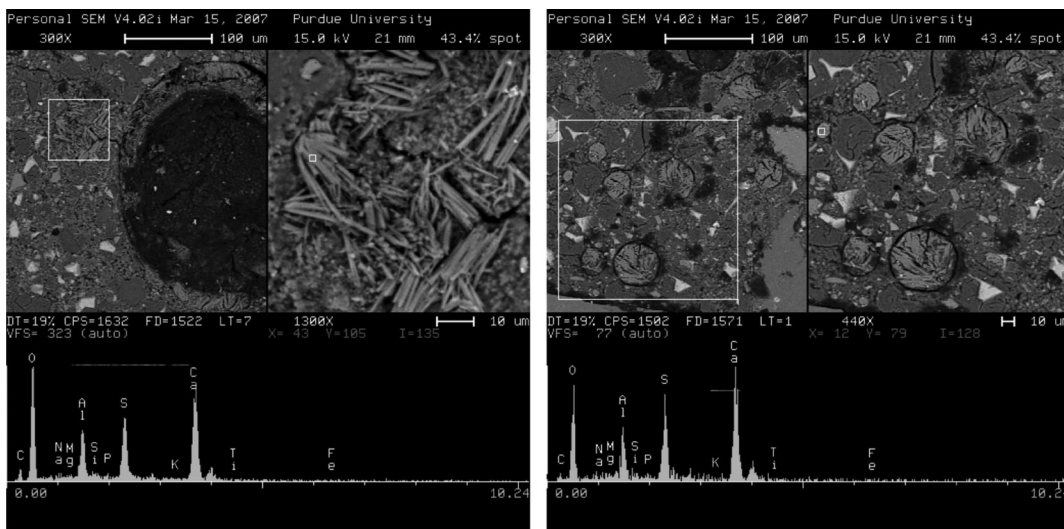
Figure 4.13 Microstructure of concrete near the top (SEM #1 in Figure 4.4) of the core located in the area of damaged longitudinal joint (core 86AL 11C) showing ettringite crystals infilling air void (left) and numerous pores in the matrix filled with ettringite (right) (*101*).
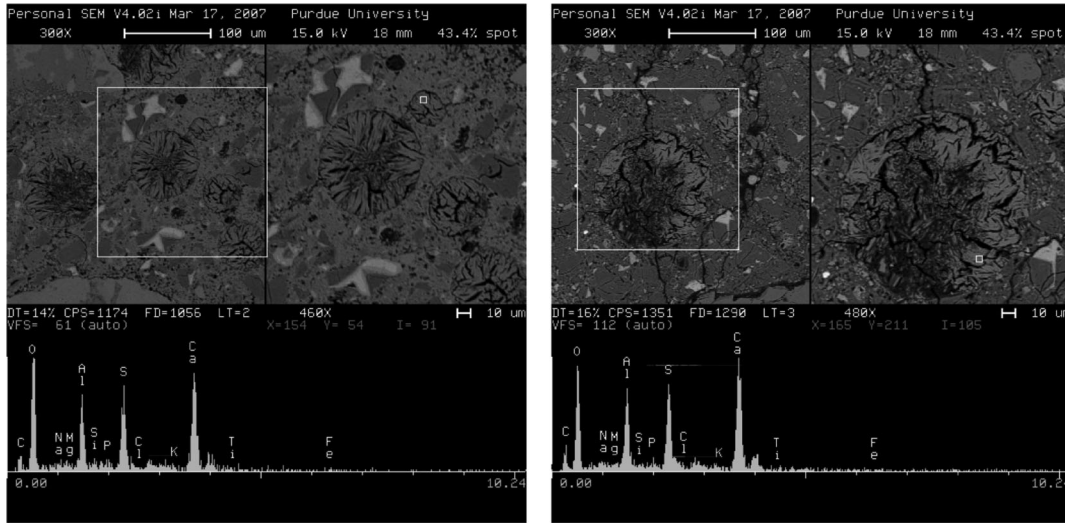
Figure 4.14 Microstructure of concrete near the bottom (SEM #2 in Figure 4.4) of the sealed and damaged longitudinal joint (core 86AL 11C) showing ettringite crystals infilling air numerous air voids (*101*).

chlorides is most likely the result of the accumulation of residue from the de-icing salts as these locations are not subjected to the direct wheel traffic. Similarly, relatively low (and uniform) levels of chlorides in the undamaged joints most (shown in the left part of Figure 4.16) seem to indicate low level of deicer penetration due to the presence of protective layer of the joint sealant. On the other hand, the elevated levels of chlorides observed behind the surfaces of the damaged joints are indicative of prolonged chloride exposure which is likely the result of water standing in the joints due to sealer failure and lack of effective drainage. That accumulation of water is particularly damaging during the winter months as the presence of deicing salts depresses the freezing point and increases the effective degree of saturation. The increased saturation will, in turn, lead to higher probability of freezing and thawing damage of concrete.

4.5 Summary and Conclusions

This chapter presents the results of the laboratory evaluation of concrete specimens obtained from field cores extracted from several Indiana pavements. The
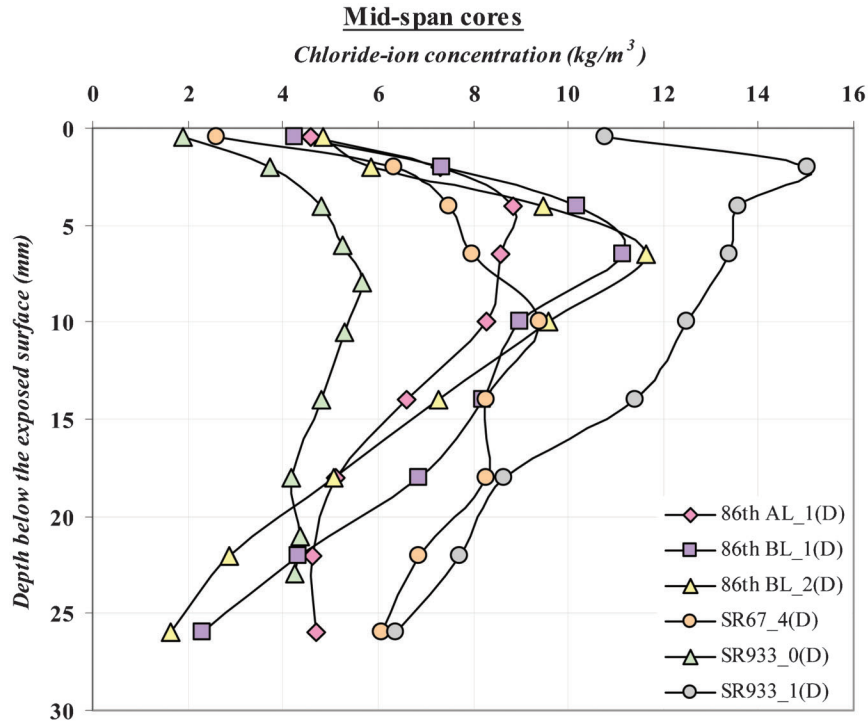
Figure 4.15 Chloride ion concentrations profile for mid-span cores (*11*).
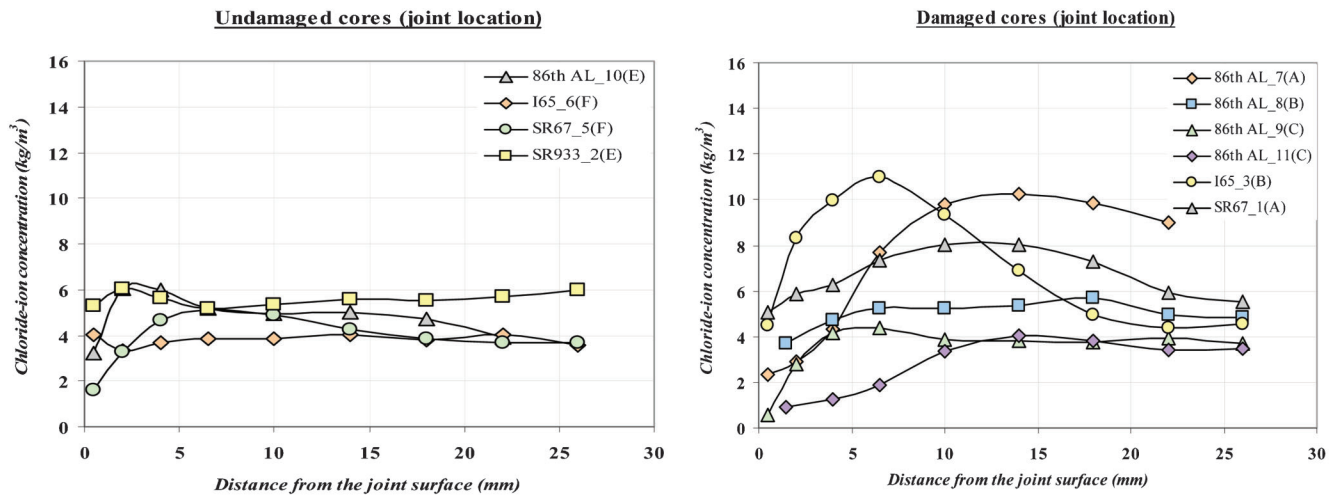
Figure 4.16 Chloride ion concentrations profiles (from joint faces inward) for undamaged joints (left) and damaged joints (right) (*11*).

areas of pavements selected for coring included both mid-panel and joint locations and incorporated both damaged and un-damaged joints. As already mentioned, the damage to concrete in the vicinity of the joints manifested itself by excessive cracking, spalling, loss of material in the direct vicinity of the joint and development of "bulb-shaped" damage zones under the sealed parts of the joints.

In general, the concrete from cores which came from the middle of the slabs (location D) had quite robust (in terms of characteristics associated with adequate freeze-thaw resistance) air void system. In addition, the concrete from mid-slab locations also showed good (as measured by the values of the durability factor) resistance to freezing and thawing cycles and its chloride ions penetrability was classified as either "very low" or "low". Although the air voids system parameters of concrete specimens obtained from cores which came from the undamaged joints (locations E and F) were, in general, less robust than the air voids system parameters of concrete from the mid-slab locations, they were still reasonably adequate. Most of these specimens had a durability factor above 60% and their chloride penetrability values could be classified as "low" to "moderate". In addition, although many of the specimens contained a considerable quantity of small (~10 μm) air voids filled with either ettringite, Friedel's salt or a combination of both, they also contained numerous empty or partially empty air voids.

The characteristics of the air voids system in samples from concrete which came from the cores extracted in the vicinity of the damaged joints (locations A, B and C) were the least robust when compared with characteristics of the air voids systems from the other two locations. These concretes displayed "moderate" to "high" chloride ion penetrability and achieved relatively low values of the F-T durability factors. Additionally, it was noted that these cores contained numerous

microcracks and infilled air voids (both small and large). The secondary (infilling) deposits contained ettringite, Friedel's salt or a combination of both.

It is generally accepted that secondary deposits filling the air voids are commonly seen in damaged concrete. It is therefore reasonable to assume that the ettringite and Friedel's salt deposits found in many air voids of the field concrete examined as a part of this research were most likely the result of the repetitive saturation of air voids with mineral-laden water that left precipitates behind in the air voids.

Without knowing the original air void system of the concrete, it is difficult to determine the exact cause of the observed damage. On one hand, it can be assumed that the air-void system in the original concrete was not adequate and thus resulted in F-T damage and microcracks. The presence of microcracks would increase the degree concrete saturation and facilitate the movement of moisture through the microstructure, thus leading to secondary mineral deposits in the air voids. These deposits would, in turn, lead to further reduction of the effectiveness of the air voids system. On the other hand, one can assume that some other mechanisms (or processes) first caused the infilling of the air void system. That infilling of the voids would subsequently result in an increased vulnerability to the freezing and thawing damage and formation of the microcracks which will lead to an increased absorption of water and salt brines. The increased rates of absorption (and thus reduced ability to resist deicer penetration), combined with higher degree of saturation the concrete will experience in the presence of the deicers all point toward the higher risk of freeze-thaw damage, especially if the water and salt brines are trapped below the layer of the sealant.

The results obtained from evaluation field specimens lead to the following conclusions:

1. Cores extracted from the damaged joint locations (type A, B and C) mostly exhibited poor (in-situ) air void system

characteristic, numerous micro-cracking, infilling of the air voids, higher rates of absorption, high values of RCP and low values of F-T durability factors.

2. The residual freeze-thaw (FT) resistance of concrete with infilled air voids (mostly from the vicinity of the damaged joints) was lower than that of concrete with lesser degree of voids infilling (mid-span locations).

3. The observed microstructural and chemical changes were consistent with the appearance of the microstructure of concrete undergoing prolonged saturation (through-solution mechanism for creating deposits in the air voids).

5. USE OF SOY METHYL ESTER POLYSTYRENE (SME-PS) AS A CONCRETE SEALANT

5.1 Background on SME

The previous sections of this report have shown that the ingress of water and salt can contribute to the deterioration of the joints in concrete pavements. It was discussed that there is potential to use a concrete 'sealer' to block the pores and to reduce water and salt ingress. One such 'concrete sealer' the Purdue research team has been investigating is soy methyl ester polystyrene (SME-PS).

Plant oils such as soybean oil are made up of long-chain fatty acids containing 14 to 20 carbon atoms. The oil can be converted into a methyl group through transesterification. The transesterification process converts methanol and the plant oil (triacylglycerides) into methyl esters. Methyl esters are biodegradable and nontoxic. In addition the SME is a good solvent for synthetic polymers such as polystyrene (PS) and polyvinyl chloride (PVC) (27).

The following section provides a review of results from tests where SME-PS was applied to concrete and the influence of the SME-PS was assessed. Golias compared SME-PS with two silane sealants—a solvent-based alkyalkoxysilane sealer (SBS) and a water-based alkyalkoxysilane penetrating sealer (WBS). The SBS was a solution of silane dissolved in isopropanol that had greater than 50% active ingredients. The WBS was an emulsion of silane in water that contained 40% silane (28). This comparison was made since these are sealants that are frequently used.

5.2 SME-PS as a Concrete Sealant

5.2.1 Fresh Properties

SME-PS was topically applied and admixed with fresh concrete to test its ability to retard the evaporation of water. SME-PS was topically applied to fresh concrete with 0.018 g/cm^2 (5% polystyrene) and samples were maintained at $23 \pm 1°C$, $50 \pm 4\%$ RH and their masses were continuously monitored. As shown in Figure 5.1, the samples topically treated with SME-PS had a reduction in mass loss by roughly one-third at about 20 hours.
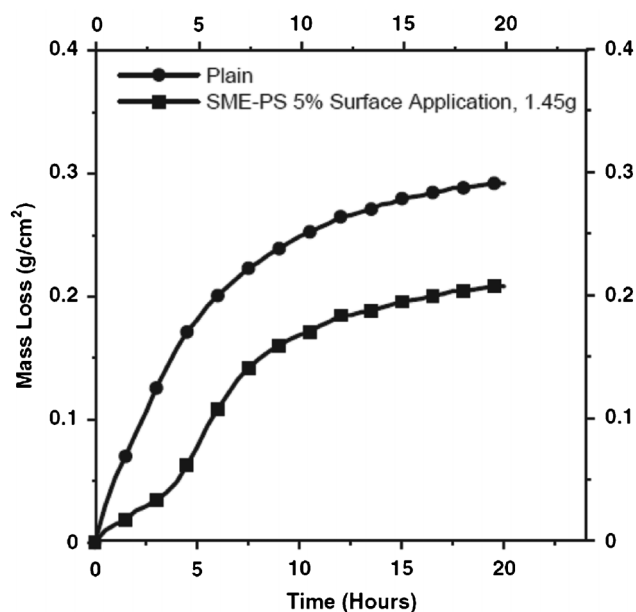
Figure 5.1 Evaporation of water over time in plain sample and sample topically treated with SME-PS.

5.2.2 Hardened Properties

The compressive strength was determined for plain samples as well as for samples admixed with a dosage of 1.25% SME-PS and different polystyrene contents. Figure 5.2 shows the compressive strength versus polystyrene content at each of the 3 ages tested.

The largest reduction in compressive strength was 18% for the SME-PS with 5% polystyrene at 28 days.
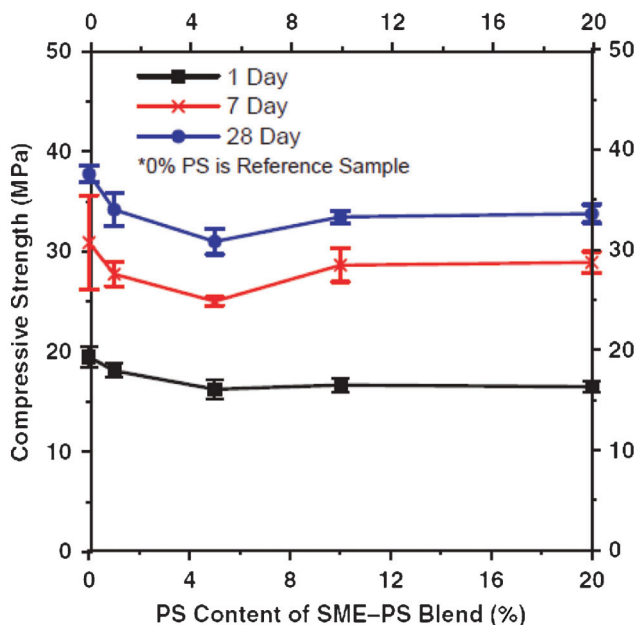
Figure 5.2 Compressive strength versus polystyrene content.

29

The reductions in compressive strength are noticeable however this can frequently be overcome in the mixture design.

Drying shrinkage tests were also performed on plain samples as well as samples with SME-PS with 1% and 20% polystyrene. It was observed that upon drying, the treated samples had less mass loss. The sample with 1% PS had a mass loss roughly 10% less than the plain sample. It was also observed that there was no substantial effect (either positive or negative) on shrinkage (27).

For fluid transport, samples admixed with SME-PS showed significant improvements with regards to absorption and ion diffusion. Both the SME and the polystyrene fill the pores and thus reduce water absorption. The treated samples dosed with 1.25% SME-PS had a 91% reduction in absorption after 8 days while the treated samples dosed with 2.5% SME-PS showed a reduction by 94% over the same time period. With regards to chloride ion diffusion, the depth of the treated samples dosed with 2.5% SME-PS was, on average, reduced by 68%. Thus, the use of SME-PS as an admixture can slow chloride ingress (27).

With regards to the topical application of SME-PS, it was observed that the SME-PS was able to penetrate the samples fairly quickly. Over a 5 hour period, the SME-PS with 5% PS was able to penetrate roughly 4 mm. For SME-PS application rates between 0.02 g/cm^2 and 0.036 g/cm^2, the SME-PS was able to reduce water absorption by 85% to 93% after 12 days (28).

The ability of SME-PS to penetrate concrete depends on a few different factors. One such factor is the moisture content of the concrete. Samples were conditioned at 23 ± 1°C at different relative humidities for 18 months. Roughly 20 g of SME-PS were then ponded on the samples for 48 hours. Figure 5.3 shows the water and SME-PS absorption after conditioning at different relative humidities. It clearly shows that the SME-PS is highly dependent on the moisture content (28) however it is worth noting that a greater penetration depth is observed in a dry concrete. This implies that when the SME-PS is being investigated for use as a sealer it is better to dry the surface pores.

Another such factor that affects the penetration of SME-PS is the length of the polystyrene chain. In this experiment, 5 g of SME-PS was ponded for 48 hours. One sample had pure SME while other samples had 5% polystyrene, each with different molecular weights (or chain lengths). As shown by the images in Figure 5.4 below, the penetration depth of the SME-PS decreases as the chain length of the polystyrene increases. Waste polystyrene is preferred due to its availability, its ability to maintain the SME at the surface however the chain is not so long that it greatly reduces absorption.

Time is the final factor that affects the SME-PS penetrability. Samples were submerged in SME-PS. At different time intervals, the samples were removed from the SME-PS and cut open to determine the penetration depth. Figure 5.5 shows the plot of the penetration depth over time (28). Again, the main factor is that the
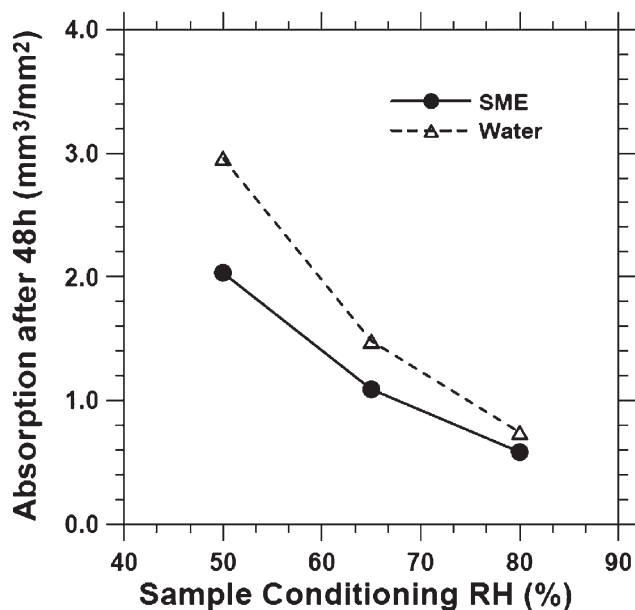
Figure 5.3 SME-PS and water absorption after 48 hours versus conditioning.

longer the SME-PS is allowed to absorb the more SME is absorbed and the deeper it can penetrate.

For water absorption, two doses of SME-PS were used. For Dose 1, samples were submerged in SME-PS for 6 hours while for Dose 2, samples were submerged in SME-PS for 24 hours. SBS and WBS were also tested. As is evident by Figure 5.6, the sealants significantly reduced the amount of absorbed water.

The SME-PS was able to reduce the water absorbed by 88% at 7 days while the silane sealants saw a 95% reduction in absorption. Over time, the effectiveness of the sealants decreases. The SME-PS saw a 77% reduction after 28 days while the silane saw a 90% reduction during the same time period (28).

In cold weather, SME-PS does not behave the same way as water, which is considered to be a single-phase liquid. SME-PS is made up of different fatty acid methyl esters (FAME), each of which has a different temperature at which phase changes occur. The first critical temperature is the cloud point whereby FAMEs start to lose solubility and form conglomerations of waxy crystals, which will form from the solution. For pure SME, the cloud point is typically 0°C while for SME-PS with 5 and 10 percent PS, the cloud point was 5°C. The pour point is the next critical temperature, which is at a lower temperature than the cloud point. At the pour point, the SME-PS turns into a gel-like substance, which typically occurs at -4°C. This is advantageous for concrete because it will clog the pores and help reduce fluid ingress (28). This has two implications as it relates to the use of the SME-PS as a sealer. First, the SME-PS is best applied in warmer weather and should not be applied when the temperature is approaching the cloud point. Second, the SME-PS is not expected to solidify and

a) SME Only   b) M_W 2,400   c) M_W 44,000   d) M_W 382,100
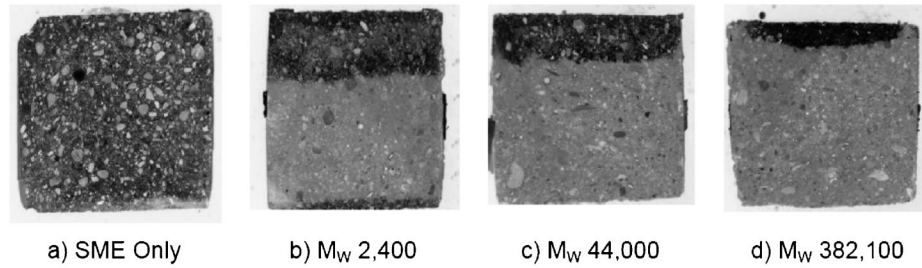
Figure 5.4 Penetration depth of SME-PS in black with varying PS chain lengths.

crack when it would freeze in practice. Rather the SME-PS would gel, then re-liquefy as the temperature heated allowing some redistribution and healing of the sealer.

A series of samples with different sealers was tested during freezing and thawing using ASTM C666 (*95*). After 75 cycles of freezing and thawing, both untreated concrete and concrete treated with SBS began to spall. After 100 cycles, both samples had the same amount of damage. It was observed that samples treated with a small dose of SME-PS did not show damage as shown by Figure 5.7 and Figure 5.8. Even when the SME-PS treated samples were damaged, the damage was still considerably less than the damage observed in the untreated samples (*28*).

When applied to concrete, silanes form a protective membrane. During freezing, silane sealants are vulnerable to thermal contraction, which can cause the sealant to crack. On the other hand, SME-PS absorbs into the pores and remains flexible after freezing.

While all the sealers were effective at reducing water absorption at 23°C, the same behavior was not observed at cooler temperatures. After 7 freeze-thaw cycles, SBS was the most susceptible to freeze-thaw. During freezing, SBS absorbed 85% of the volume of water that the untreated concrete had absorbed. SME-PS, on the other hand, was the least susceptible to changes caused by freezing—only losing roughly 20% of its effectiveness (*28*). As a result of this observation it appears that a testing procedure is needed to evaluate how the sealer performs when they are both exposed to water and undergoing thermal cycling. This however may be related to the surface coating properties.

The ability of SME-PS and the silanes to reduce the penetration of different chlorides was also examined. The solutions used were 32% calcium chloride ($CaCl_2$), 23% sodium chloride (NaCl), and 30% magnesium chloride ($MgCl_2$). After 21 and 42 days of ponding, samples were cut open and sprayed with 0.1M silver nitrate ($AgNO_3$). Photographs were taken of the samples and imported to determine the penetration depths. Figure 5.9 below shows the penetration depths for the different salt solutions where (a) is sodium chloride, (b) is magnesium chloride, and (c) is calcium chloride.

The SBS was the most effective in limiting salt ingress—it was able to eliminate the chlorides for $MgCl_2$ and $CaCl_2$ and was able to reduce the depth by 80% at 42 days for NaCl. The effectiveness of the SME-PS was related to its dosage rate. The reduction in depth for the larger dosage of SME-PS was roughly 10% greater than the reduction from the smaller dosage rate (*28*).

With regards to Alkali-Silica Reaction (ASR), Golias observed that the sealants were able to postpone the expansion. For dosages of 5 minutes, 2 hours, and 24 hours, the SME-PS was able to postpone the expansion by 1 day, 1 week, and 3 weeks respectively. The SBS sealant was able to postpone the expansion by roughly 6 weeks. It was further observed that despite the fact that doses 1 and 2 of SME-PS were able to delay the expansion, at later ages, those 2 samples actually had more expansion than the plain sample. This is probably due to the conditioning method prescribed in ASTM C1260 (*103*). After the 24 hours of saturation in water, the plain samples absorbed 5 times more water than the treated samples. Thus, the plain samples, during testing, absorbed less of the highly alkaline sodium hydroxide. The sealed samples, on the
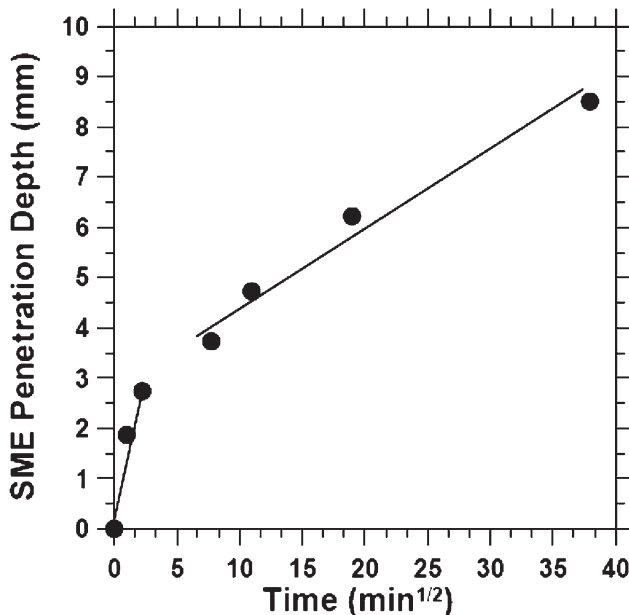
Figure 5.5 SME-PS penetration over time.
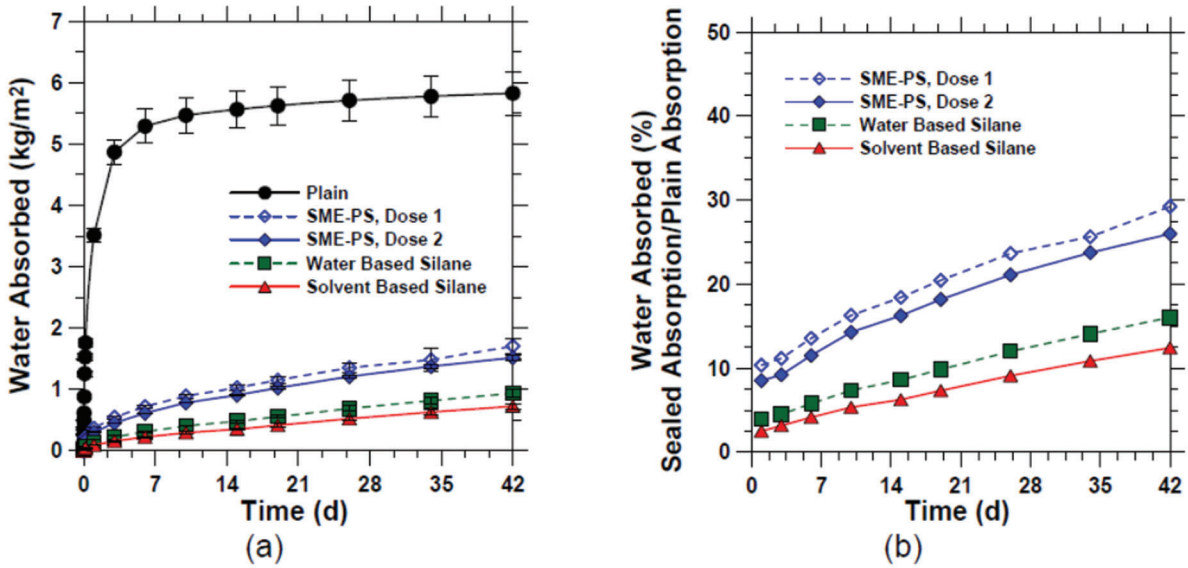
Figure 5.6 Water absorption where (a) is the amount absorbed and (b) is the percent reduction in absorption.

other hand, absorbed more fluid during the test, resulting in an exaggerated expansion (*28*).

5.3 SME-PS Application Instructions and Concerns

5.3.1 Introduction

A significant interest has been shown by various groups in using SME-PS as a treatment for concrete pavement joints. The goal of this treatment is to reduce premature pavement joint deterioration by minimizing the ingress of fluids such as water or the aqueous salt solutions that result from roadway deicing salt solution. In order to accomplish this goal SME-PS must be absorbed into the pores around the pavement joint, where it will remain, to minimize the fluid from within the joint from entering the surrounding concrete. Some care must be taken in the application and preparation

process in order to ensure that the sealant can be absorbed into the desired areas. The application process is quite simple, but each step of the process is necessary in order to ensure the availability of pores in the locations that require sealing.

5.2.2 Precautions

SME-PS is a solvent, which brings a few concerns with its use in the construction industry. This property can cause issues when SME-PS is being used in an area near asphalt or, less so, near paints. When exposed directly to asphalt and given a period of time the SME-PS will soften the asphalt, potentially up to a point where it can be removed with mechanical abrasion. This property has created both negative and positive situations. Although it can cause unwanted damage to asphalt that lies in areas near concrete pavements that
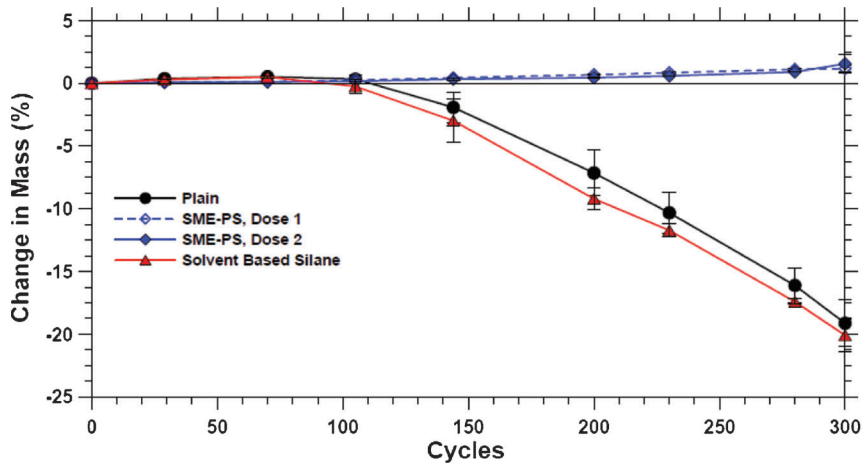
Figure 5.7 Mass change due to freezing and thawing.

Plain   SME-PS   SME-PS   SBS
             Dose 1   Dose 2
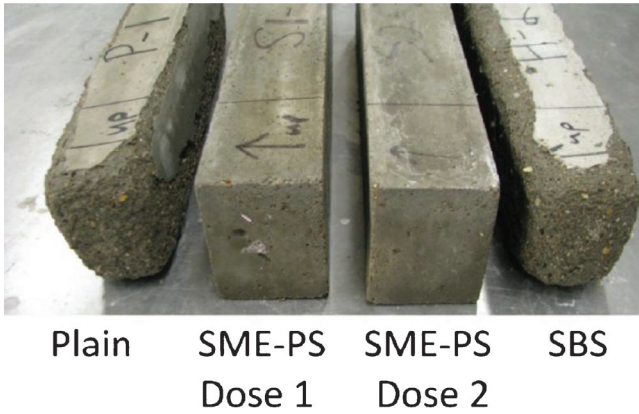
Figure 5.8   Samples after 280 cycles of freeze-thaw.

are being treated, it can be beneficial when removing ineffective areas of asphalt overlay that had been used in an attempt to seal the joints or cracks.

In locations where the removal of asphalt is desired, a three-stage process could be quite effective and require minimal labor. A first, light coating can be used to soften the asphalt seal. After a short period of time (less than one hour) some form of mechanical abrasion can be used to remove a portion of the seal and fully expose the joint. Once the joint is exposed, a second coat of SME-PS (applied as directed in the following sections) can be used to fully seal the joint. The only sided effect of this process (as opposed to traditional treatment of an already open joint) is that residual, softened asphalt can cause a slight discoloration in the SME-PS treated areas.

Up to this point the solvent properties have been of a lesser concern when used near a painted section. Although SME-PS has the potential to dissolve some paints, it has not been an issue in any field trials thus far. Laboratory investigation has shown that roadway

paints can be removed with SME-PS but require an extended exposure to the sealant (see Figure 5.10).

In one trial, paint stripes where exposed to significant amounts of SME-PS mopped onto the surface, as well as a significant amount of mechanical abrasion that was used to remove asphalt, yet the paint stripes remained unaffected by the process. Results of an asphalt removal project are shown in Figure 5.11. Asphalt had been mistakenly spilled onto a section of Kalberer Road on the north side of West Lafayette, IN. SME and absorptive pads were used to clean up the main portion of the spill. It is evident that this process had very little impact on the road paint.

The solvent properties of SME-PS can also cause issues with storage and equipment if not handled appropriately. This issue is easily mitigated by the selection of appropriate plastics for storage and application equipment. Polycarbonate (PC), polystyrene (PS), and acrylonitrile butadiene styrene (ABS) plastics should be avoided. This includes storage containers, sprayers, hoses, gaskets, and nozzles that will, at any point throughout the application process, come into contact with SME-PS.

5.2.3 Preparation

There are two main concerns that should be addressed in preparation for SME-PS application in pavement joints. The pores around the joint must be empty and they must be accessible. Ensuring accessibility is simple; remove any materials that may have entered the joint, wash away any slurry that may remain in the joint from saw-cutting, making sure that the inside faces of the joint are clean and exposed. It is recommended that an air compressor be used to blow air through the joint before application. The intent of this air current is to minimize the degree of saturation in the pores near the surface of the joint.
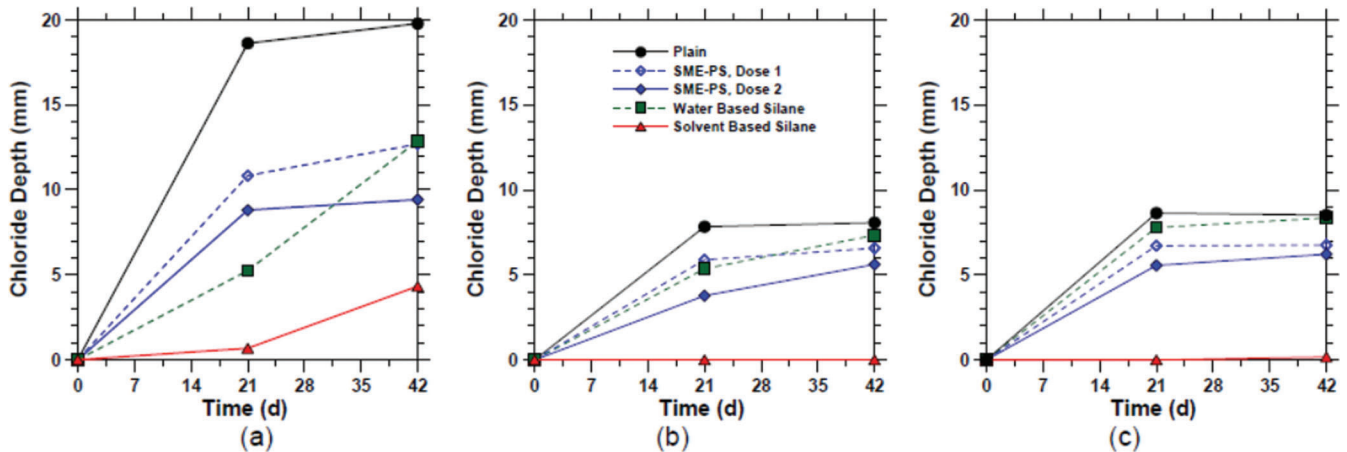
Figure 5.9   Chloride penetration depth for (a) sodium chloride, (b) magnesium chloride, and (c) calcium chloride.

Figure 5.10 Tests of compatibility of SME-PS with INDOT road paint under normal exposure (left) and extreme exposure (right).

In order to make sure that the pores of the concrete are open and available to absorb the applied SME-PS, weather before application should be monitored. It is highly recommended that application not occur within 24 hours of the most recent rainfall. Similarly it is advised that application not occur when the temperature is below the dew point, as this will allow water to condense within the pores after they have been assumed to be dry. If the temperature falls below the dew point on the day of application it is recommended that the area is retreated with compressed air, in order to accelerate vaporization of any water that may have condensed, prior to beginning application. There should

Figure 5.11 Asphalt spill on Kalberer Road before and after removal using SME-PS.

Figure 5.12 RL pro backpack sprayer used in field application of SME-PS.

be a 24-hour rain free period following application. The consequences of a shortened rain free period after application will be discussed in the following section.

5.2.4 Application

The application of SME-PS is a simple process. The field applications that will be discussed in the following section (section 5.4) have been performed with the use of a 4 gallon, RL Pro Flo-Master backpack sprayer with a fanning spray tip (shown in Figure 5.12). The objective of the application is to coat the inside faces of the joint and 2 in. (50.8 mm) inches at the surface on either side of the joint opening. For the best results, enough sealant should be applied so as to create a small reservoir at the base of the joint that can be absorbed into that critical area over the following hours. This process translates to an application rate of 160 ft^2 (14.9 m^2) per gallon of sealant. For a typical joint, assuming a 4 in. (101.6 mm) depth, this is also 160 linear feet (48.8 m) of joint per gallon.

The excess sealant will settle in the lowest locations. These locations will see a longer exposure time to SME-PS, and consequently a deeper penetration of the sealant. This is beneficial to the joint network because these locations are those that will also see similar settlement and the highest exposure to the deleterious fluids that lead to deterioration. If rain occurs within 24 hours after application much of this reservoir may be cleaned out of the joints before it has time to be absorbed into the concrete. This will leave these areas more vulnerable to fluid ingress. If rain occurs within the first three hours after application retreatment is recommended. In this case, much of the sealant on the joint faces and at the surface may be washed away before being fully absorbed into the surface.

5.3.5 Traffic Considerations

The application of SME-PS could create a slick surface until it can be absorbed into the surface. For

Figure 5.13 Demonstration of field application of SME-PS, on US-231 in Lafayette, IN.

new construction projects, there is minimal concern for traffic as the sealant can be applied and absorbed well before the project is open to traffic. Experience in field trials thus far has shown this to be of minimal concern. However, in order to avoid liability issues it is recommended that traffic be diverted from the joint for three hours following the application and that field personnel examine when they feel comfortable opening the pavement to the travelling public.

5.3.6 Potential Inclusion of Scent and Application Indicators

It has been discussed that many DOTs desire the inclusion of an indicator in order for inspectors to verify where sealant has been applied. The solvent properties SME-PS provide a simple solution for indicating sealed locations. Pigments can be dissolved into the sealant to show where the material has been applied. The color can be controlled by the particle size of the chosen pigment. If the particle size is slightly bigger than the size of the surface pores of the concrete, than the pigment will be screened at the surface and will be washed off with subsequent rainfalls. If the particle size is slightly smaller it will remain in the sealant and provide a long term discoloration. Scents have also been added to the SME-PS.

5.4 SME-PS Field Applications in Central Indiana

Several field trials of SME-PS have been initiated throughout central Indiana. These trials have been documented by recording videos of all treated joints for later reference so that any areas of damage can be monitored over time. Conditions on the day of application were also recorded including minimum, maximum, and mean temperatures, dew point, and wind speeds. As was mentioned in the previous section,

the application was conducted with the use of an RL-Pro Flowmaster backpack sprayer. In each case application was conducted with four walking passes along the joints, two in each direction, holding the nozzle of the sprayer about an inch (25 mm) above the joint opening as demonstrated in Figure 5.13. All sealant used in field trials contained 2% PS by mass.

5.4.1 US-231 in Lafayette, IN

The first field trial of SME-PS is a small section of southbound US-231. This section of highway was 12 years old at the time of application and was originally placed in the summer of 1999. The test section lies between the intersections with W 400 S and W 500 S and consists of twelve slabs with the previously installed backer rod and silicon sealant removed. These slabs were divided into two sections of six slabs with one slab in between them with the backer rod and sealant intact. The northern six slabs were treated with SME-PS following the procedures recommended in section 5.3. The southern six slabs were left untreated as a control section. The test area is shown on the map in Figure 5.14.

The application of SME-PS in the joints on US-231 was conducted on the morning of August 6, 2011 by INDOT maintenance personnel under the supervision of INDOT officials and researchers along with Purdue researchers. On the day of application the minimum temperature was 71.6°F (22.0°C), the maximum 89.1°F (31.7°C), and the mean 80.2°F (26.7°C). The mean dew point was 72°F (22.2°C), at the beginning of application the temperature was above this point. Wind speed was also recorded, as it can influence the moisture condition of the concrete. The mean wind speed was 4.0 mph (1.79 m/s), with a maximum sustained speed of 11.1 mph (4.96 m/s) and a maximum gust of 20.7 mph (9.25 m/s) (*104*).

For this application only the longitudinal joint between the two lanes of traffic was treated. During application the two lanes of traffic were reduced to a single lane and moved to the shoulder. The traffic pattern for application was established at 9:00am and returned to regular two-lane traffic flow at 1:00pm, approximately three hours after the application was complete.

During application it was noticed that the median barrier through this section of highway sits in a low spot, with the pavement on either side draining towards the barrier. This is likely to cause a high exposure to deicing salts during the winter months. The base of this barrier was treated with SME-PS as shown in Figure 5.15. The intent of this treatment was to provide an approximation of the exposure seen by vertical surfaces near salt water, such as bridge piers or abutments.

In January of 2013 the section was revisited and each area was documented with pictures and videos of the treated areas. These were compared to those taken on the day of application in order to determine if any new damage has become visible in either the joint or the
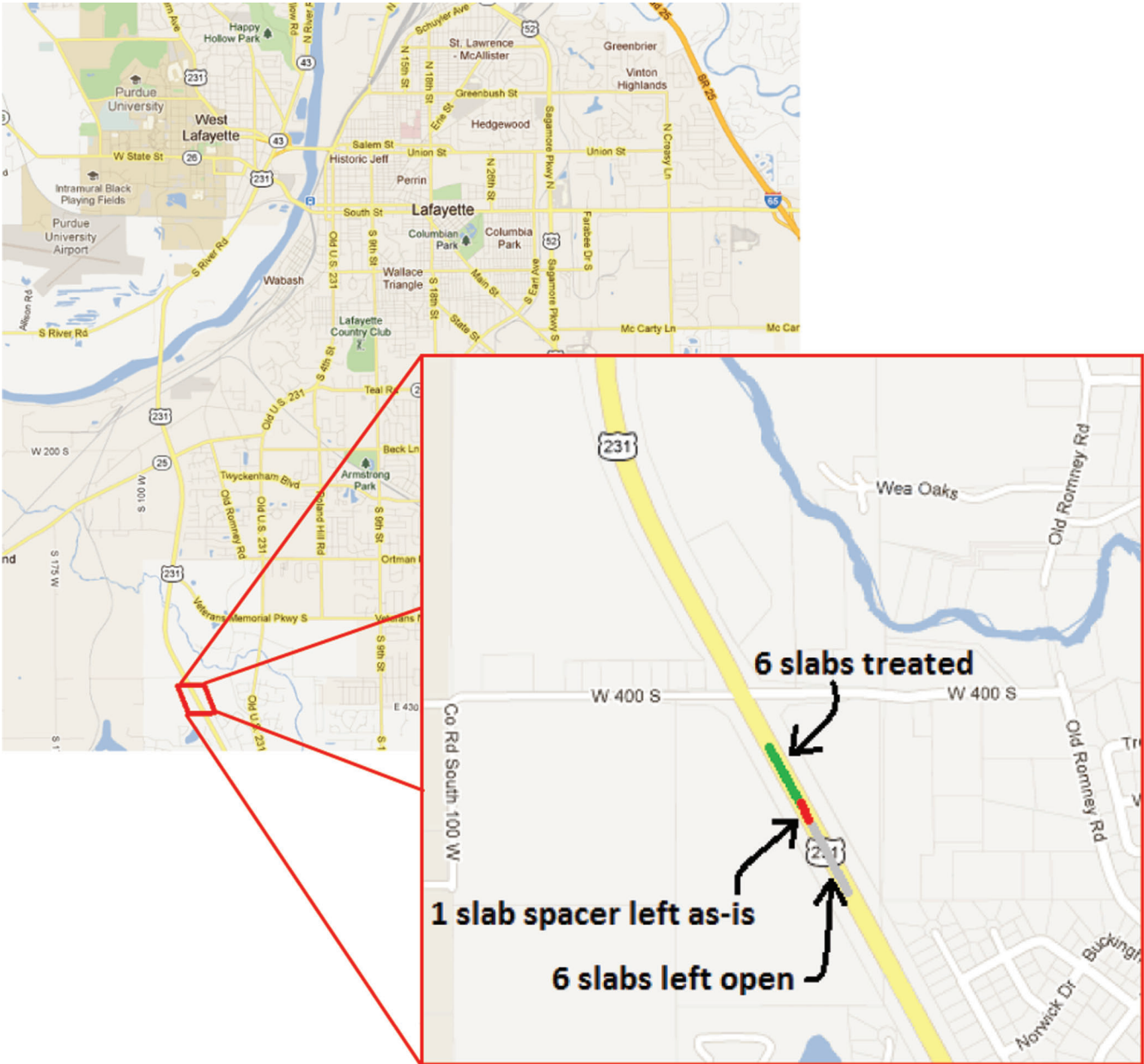
**Figure 5.14**   The location of the US-231 field trial section.
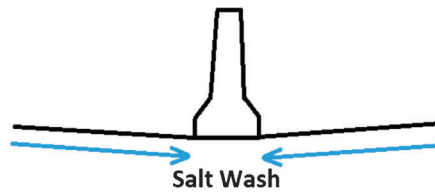
Figure 5.15   Treatment of the median barrier at the SME-PS test section on US-231.

36
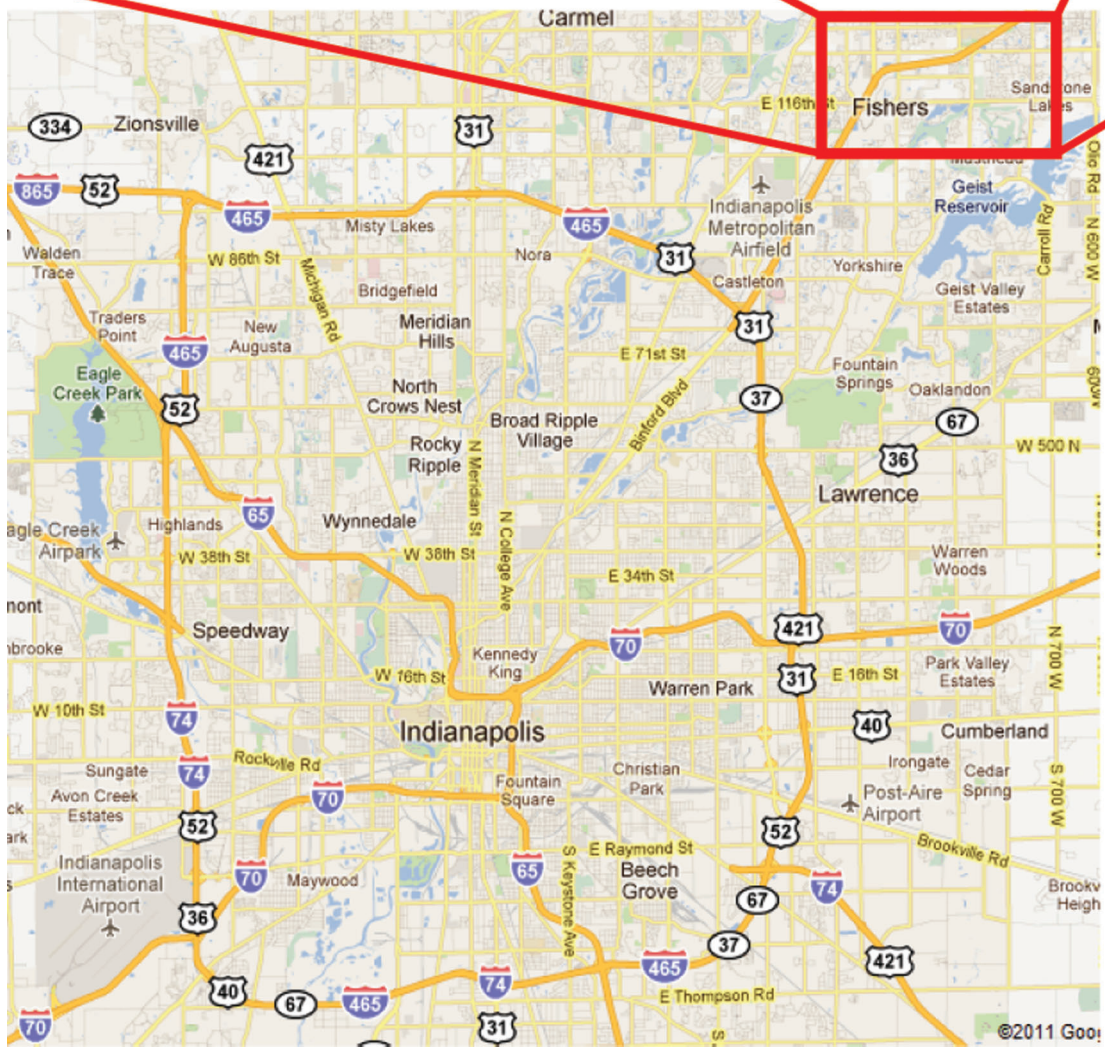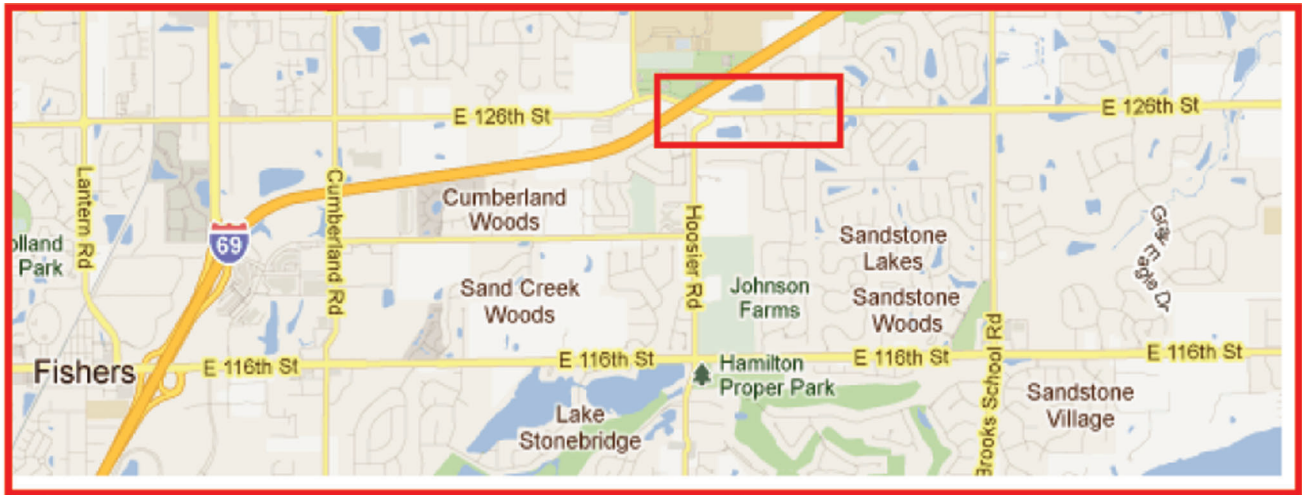
Figure 5.16 Location of the second SME-PS trial location, 126th Street, Fisher, IN, east of I-69.

barrier. In a side-by-side comparison, no new damage was found to have occurred in the 18 months between the time of application and the reevaluation. While data collected to this point has been rather qualitative, quantitative data will be taken for an analysis of long-term performance. Samples of the area will be taken either by coring and then subsequently grinding the cores into powdered samples of each millimeter throughout the depth of the core. These powders will be titrated in order to determine a profile of chloride content throughout the depth of the sample. Alternatively, a dry drill may be used to collect powdered samples in increments from the joint and similarly titrated to obtain a chloride content profile.

5.4.2 126th Street Fishers, IN—East of I-69

The second test section, and first where SME-PS has been applied to a newly constructed pavement, was on 126th street in Fishers, IN beginning to the east of the overpass at I-69. This section of roadway consists of two lanes in each direction, with turn lanes and uncurbed median in several locations throughout the test area. All of the longitudinal joints, over 3000 linear feet, in this section of pavement were treated, with the exception of the first 200 feet of joint east of the overpass bridge which was left untreated as a control section. At the request of INDOT/FHWA the transverse joints were sealed with traditional methods of backer rod and silicon sealant after the application of SME-PS was completed in the longitudinal joints. Treatment was performed by Berns Construction and began immediately east of the control section and continued to Raiders Blvd. A map of the location can be seen in Figure 5.16.

Sealing of this section occurred on October 25, 2011 with the coordination of BFS Engineering and Berns Construction who were managing the construction project. Application was conducted by members of the Berns construction team and can be seen in Figure 5.17. Feedback from these contractors after application was purely positive, saying that it was much simpler and faster than current sealing practices.

All of the application procedures and recommendations from Section 5.3 were maintained throughout this project.

Since this application occurred later in the construction season, temperature and dew point were monitored closely through the morning of application. The minimum temperature was 43.0°F (6.1°C), the maximum 73.0°F (22.8°C), and the mean 55.6°F (13.1°C). The mean dew point was 38.9°F (3.8°C). The mean wind speed for the day was 7.1 mph (3.17 m/s), with maximum sustained wind of 15.0 mph (6.70 m/s), and a maximum gust of 25.3 mph (11.31 m/s). All treated joints were videotaped for later reference in order to document damage from sawing so that it can be differentiated from any other damage that may occur.

5.4.3 126th Street Fishers, IN—West of I-69

The construction of 126th Street continued the following summer with the replacement of the portion west of the overpass at I-69. This test area begins at the intersection of Reynolds Drive and ends at the intersection with Cumberland Road. In this section all longitudinal and transverse joints were treated with SME-PS. The only exception being all of the joints in the last two slabs at the east end of this test section, commencing at the intersection with Cumberland Road. This test section is shown on the map in Figure 5.18. All treated joints were documented with videos for future reference.

Berns Construction performed application throughout this test section in coordination with BFS Engineering, similarly to the section East of I-69. Application occurred on September 25, 2012 and the section was opened to traffic one month after the joints were treated. On the day of application the minimum temperature was 39.0°F (3.9°C), the maximum 66.9°F (19.4°C), and the mean 57.7°F (14.3°C). The mean dew point was 49.1°F (9.5°C); application began slightly later in the day than other trials to ensure that the temperature was above the dew point. The mean wind speed for the day was 7.8 mph (3.5 m/s) with sustained winds of 11.0 mph (4.9 m/s).


**Figure 5.17** Application of SME-PS to 126th street in Fishers, IN, being performed by members of Berns Construction.

Figure 5.18 Location of 126th street field trial west of I-69 in Fishers, IN.

6. EVALUATION OF PENETRATING SEALANTS USING SORPTION TEST WITH THERMAL CYCLING

6.1 Introduction and Objectives

While many have looked at the ingress of chlorides due to its potential to cause corrosion to the embedded reinforcement steel (*105*), this work examines the penetration of chlorides due to the potential interaction with chemical species in the concrete with respect to the potential for deterioration. One method that has been found effective in reducing the amount of chloride ingress into the concrete matrix is the use of sealers, pore blocker, and water repelling materials. The use of these materials may be able to improve the service life of concrete pavements.

Concrete sealants can be used on freshly placed concrete or on concrete already in service. One question that arises however is how to test the performance of these sealants. There are current practices to determine the sealants effectiveness in reducing water ingress or chloride ingress at room temperature. However, it is not clear what happens when the sealant is exposed to freezing and thawing.

The objective of this study is to develop and evaluate a testing methodology to assess the impact of sealers, pore blockers, and water repelling materials for the ingress of fluids containing deicing salts. A proposed testing protocol is presented, which evaluates the sorption as the temperature is varied. This project examines various topical, penetrating, concrete sealants in order to investigate depth of penetration of the sealant into the concrete matrix and how this relates to the sealants ability to reduce chloride ingress through temperature cycling.

Research will compare different sealants to determine the depth of penetration into the concrete surface and to investigate if this is directly related to the sealants ability to reduce chlorides during freezing and thawing exposure. The further the sealant penetrates into the concrete, the more effective the sealant should be at reducing chloride ingress.

6.2 Experimental Approach

An experimental method to evaluate the effectiveness of sealants, pore blockers, and water repellants during thermal cycling is the focus of this study. A test was developed to closely replicate absorption in concrete that is exposed to fluids containing salts, such as deicing solutions. For this study it is of interest to look at concrete exposure to salt solutions in a freezing and thawing environment.

Figure 6.1 shows the experimental setup. This is very similar to ASTM C1585 (*44*); however, unlike the current standard where absorption is performed on a sample in room temperature water, this test exposes the sample to chlorides and freeze-thaw conditions. The test uses a cold-plate device to induce cooling from the bottom face of the concrete specimen. Note that the

cooling will take place in a one dimensional *heat flow*, or "bottom-up" fluid flow through the concrete. This would be a similar situation to concrete pavement, which has a single face exposed to deicing salts, although gravity would be acting in the normal downwards direction. It has been shown gravitational effects on fluid transport in the capillary pores, provided large cracks are not present, can be neglected when compared to the suction effects of the pore structure (*106*).

Samples are placed in a chloride solution, similar to the water used in absorption testing. Concrete specimens are placed in a container that is thermally conductive and resistant to corrosion. For this experiment, a galvanized steel, open-faced, box was used to contain the solution and sample. The box was covered with a plastic wrapping to minimize evaporation. A thermal pad (*Thermacool TC3000*) was placed in-between the cold plate surface and the container to effectively transfer heat from the cold plate to the container. A further discussion of thermal transfer for this setup can be found in Section 6.4.1. The samples should be placed such that they are not in direct contact with the container. This is to allow for absorption of the chloride solution throughout the exposed face of the concrete specimen. The system should be insulated such that temperature loss is a minimum. The container is to then be filled with the desired solution reaching no more than 0.15in [3mm] above the sample face. The deicing solution will not freeze during the testing and will serve as a thermal conductor from the container to the sample.

6.3 Materials and Specimen Geometry

6.3.1 Mixture Design

All samples used in this study were of the same mixture. The samples were a part of a large-scale cast using a commercial concrete mixture from a ready-mix
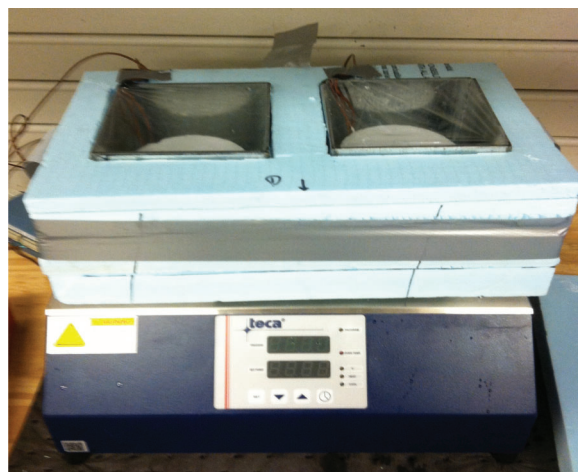
Figure 6.1 Schematic of experimental setup for freeze-thaw absorption with chloride solution.

concrete truck. The concrete was prepared with a w/c = 0.42. The fresh properties were tested in accordance with ASTM C172 (*107*), ASTM C143 (*108*), and ASTM C231 (*109*). The slump was 4 in. and the air content 6.2%. The coarse aggregate has an absorption of 0.58%, specific gravity at SSD of 2.77, and is AP#8 aggregate from U.S. Aggregates in Delphi, IN. The fine aggregate has an absorption of 1.33%, specific gravity at SSD of 2.65, and is #23 Swisher Road from Vulcan Aggregates in West Lafayette, IN. The mixture proportions are shown in Table 6.1. The batching ticket can be found in the appendix of this report.

6.3.2 Specimen Geometry and Preparation

Approximately 30, 4 in. × 8 in. concrete cylinders were cast in accordance with ASTM C192 (*41*) to be used as test specimens for this study. At 24 hours the specimens were removed from their molds and placed in plastic bags, to create a sealed condition. When the appropriate time for the specimens to be tested came, the cylinders were cut into 3-inch tall samples. The top and bottom inch of the cylinder were removed. For initial evaluation of chloride penetration, the samples have a height of approximately 3 inches. This is for preliminary experiments, but will be reduced to 2-inch samples for the final testing protocol to be consistent with ASTM C1585 (*44*) sample geometry. A height of 3 inches was chosen for preliminary testing to allow for potentially high absorption in the sample.

The circumference and one end of the samples were coated with a two-part epoxy (a similar cohesive moisture barrier would also be acceptable), leaving one face uncoated. This is to only allow fluid penetration through the desired face of the specimen. A plastic covering should be used at the top surface in future testing to eliminate potential pressure buildup at the epoxied face of the sample. However, for the purposes of this testing that was not done in order to reduce the possibility for the chloride solution collection and movement at the top surface. Application of the cohesive moisture should be according the manufacturers specifications, or enough to prevent any moisture from entering/ exiting the sample.

After the application of epoxy, the samples were placed in a 23 ± 1°C, 50 ± 1% RH environment until the sealant was applied, as applicable. Sample conditioning will be further discussed in Section 6.5.1. The sealants will then be applied to the un-epoxied face of the half-cylinders at the manufactures recommended rate of application. The samples should be left to dry after the application of sealant until there is no longer visible moisture from the sealant on the surface of the sample. Sealant application will be further discussed in Section 6.5.2.

6.4 Preliminary Testing Results

In order to develop a testing protocol for evaluating sealants, pore blockers, and water repellents, a series of

TABLE 6.1
Design quantities of materials used in concrete test specimens

Material	Design Quantity	Units
#8 Coarse agg., SSD	1800	lb/yd^3
#23 Fine agg., SSD	1240	lb/yd^3
Cement	658	lb/yd^3
Water	270	lb/yd^3
Water reducer	2.0	oz/100 lb cement
Air entrainer	1.2	oz/100 lb cement
Retarder	2.0	oz/100 lb cement

preliminary experiments must be conducted to determine appropriate parameters for testing. Variables such as temperature, number of cycles, concentration of solution, and rate of heating/cooling have been evaluated. It is desired to find a simple, practical, and effective way to test sealants. To do this, each test is evaluated on the basis of chloride concentration and depth of penetration of the chlorides. Each previously mentioned parameter is determined for the standard protocol based on the worst condition experienced by the concrete sample, i.e., the higher concentration/ further penetration into the concrete.

After each round of testing the samples were split in half, where one half of the split samples was sprayed with silver nitrate (AgNO$_3$) for visual evidence and the other half was titrated to give chloride concentration throughout the depth of the sample. Titration was completed according to ASTM C1556 (*110*) using surface grinding at depths of every 2 mm, as seen in Figure 6.2.

Comparative samples, i.e., sealed vs. unsealed, were used in some of the preliminary testing. All sealed samples for preliminary testing used Soy Methyl-Ester blended with 2% Polystyrene by mass (SME-PS), as was discussed in Chapter 5.

Figure 6.2 Surface grinding used obtain powder for titration. Samples were ground at depths of 2mm.

It should be noted that various conditioning times were used for the sets of samples in preliminary testing. With that being said, the results of samples in each preliminary test should only be compared to results of samples made from the same material and tested under a given set of conditions, as results from one test will not correlate with that of another.

6.4.1 Temperature Testing/ Cycle Length Determination

As in any freezing test, it is necessary to monitor the temperature throughout the test specimen. In order to represent pavements that are exposed to high concentrations of salt solution in a freezing and thawing environment, a condition must be replicated in which the capillary pore water freezes, but the chloride solution does not freeze. It has been shown that capillary water freezes around -3°C (*111*); however it was -8°C for the materials used here (*12*) potentially due to the composition of the material or due to under-cooling.

In order to monitor internal temperature throughout the sample, guarded thermocouple wiring was cast at known depths inside a sample. The sample was then cut and a temperature profile was developed for the sample. Temperature was also monitored throughout material where losses would occur. Figure 6.3 shows a schematic for the section view of the test setup, as well as locations of each thermocouple wire.

Figure 6.4 (a) shows the input program used to control the cold plate, while Figure 6.4 (b) shows the real-time temperature change throughout the sample (as noted above). It is desired to have the center of the sample reach *at least* -3°C (-8°C was selected in this case since the freezing temperature of capillary water varies and Li et al. (*12*) measured damage at -8°C) before commencing the thawing phase. From this data it can be concluded that in order to properly freeze the capillary water, while maintaining a liquid solution, the sample should be in a frozen state for at least 4 hours. In order to properly thaw the sample, a temperature of 10°C should be maintained for approximately 30 minutes.

6.4.2 Rate of Temperature Change

The next parameter of interest, after determining the duration of the freeze and thaw period, is the rate at which the temperature change during the cycle should occur. To investigate this parameter, two tests were run, in which the only variable was the rate of freezing. Figure 6.5 shows the two different freezing rates at which the samples were tested. Figure 6.5 (a) shows the test in which the freezing rate was "immediate", or quickly loaded. Figure 6.5 (b) shows the test in which the temperature drop took place gradually over the duration of the 4 hours, or slowly loaded.

For the rate of loading test, it was necessary to compare both sealed and unsealed samples at each of the loading rates. Alongside this test, specimens (both sealed and unsealed) we placed in a container with room temperature chloride solution and set aside until the completion of the cycling tests. This was used to look at the effects of altering solution properties.

Results. A plot of the chloride concentration vs. depth for the loading rate test can be seen in Figure 6.6 (a) and further analyzed in Figure 6.6 (b) and (c). It can be seen in both the sealed and unsealed samples, Figure 6.6 (c), that the chloride concentration is higher when the samples loaded at a slower rate. It is also interesting to note that the samples that were cyclically loaded had further chloride penetration than those that were absorbing solution at a constant temperature.

It can be seen in Figure 6.6 (b) that the samples in a room temperature environment do not contain as many chlorides as the cycled samples. This seems counter-intuitive since as discussed in Chapter 2 as the temperature decreases the viscosity (resistance to flow) of the solution increases and the diffusion coefficient would be decreased. What is aiding in the absorption of chlorides during the freezing and thawing cycles?

The internal temperature of the sample drops to a point in which freezing of capillary water occurs. At this temperature the chloride solution has not frozen and an osmotic pressure draws the chloride solution (still
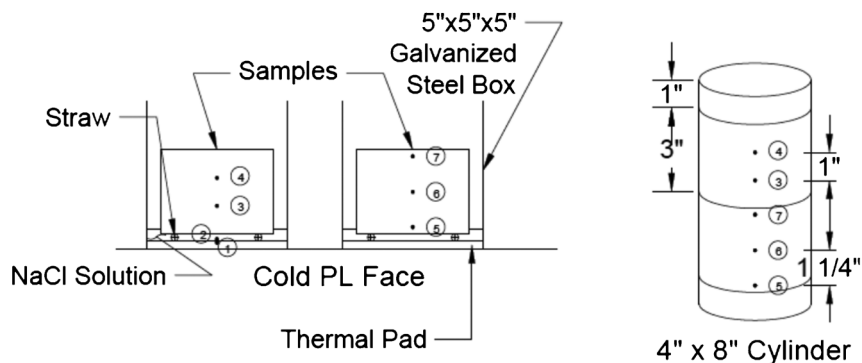
Figure 6.3 Section view of the test setup (left) and the locations of the thermocouple wiring in the cylinder (right).
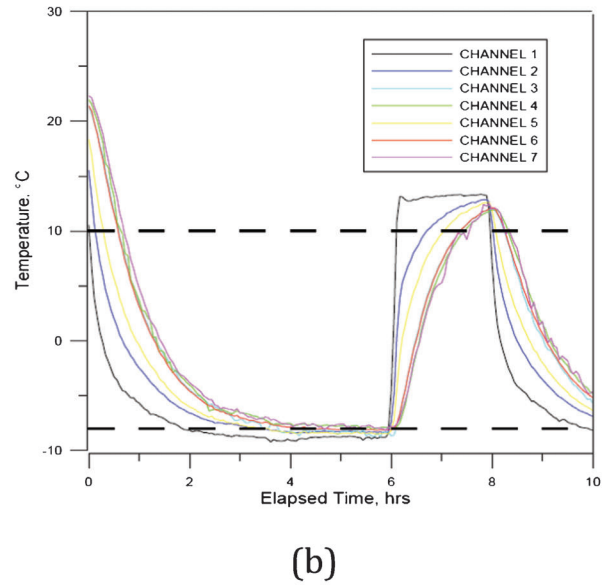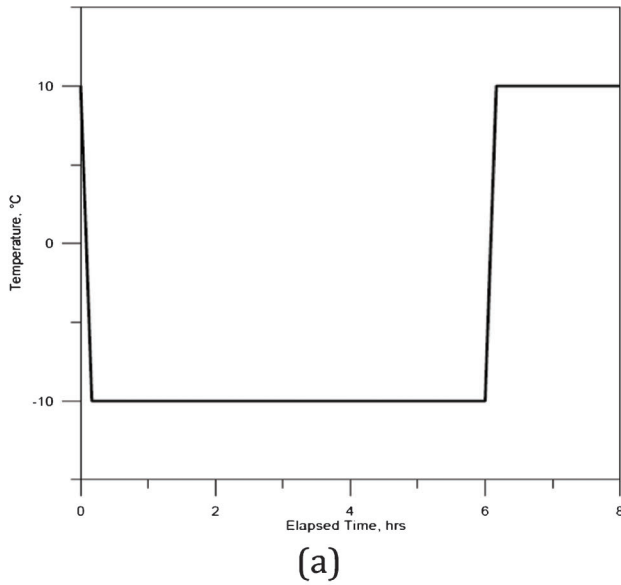
Figure 6.4 (a) Cycling of cold plate for temperature testing and (b) temperature output used to determine cycle lengths.

liquidous) further into the sample. This is part of an ongoing study being conducted at Purdue University.

6.4.3 Cycle Testing

Now that the cycles' length, minimum and maximum temperature of the cycles, and rate at which the temperatures are changing, have been determined, it is desired to know how many cycles the samples should run through. In order to do so, sealed samples with a high degree of saturation were tested at 10, 20, 30, 40,

50, 60 and 90 cycles. Only sealed samples were chosen because it was desired to know if any breakdown of the "barrier" provided by the sealant would occur. A high degree of saturation was used to see if there was a drastic change in chloride concentration as the number of cycles increased.

Through visual evidence it was noticed that no breakdown of the sealant occurred. This is concluded since maximum chloride penetration in each sample, regardless the number of cycles was approximately the same depth. It is also interesting to note than no scaling
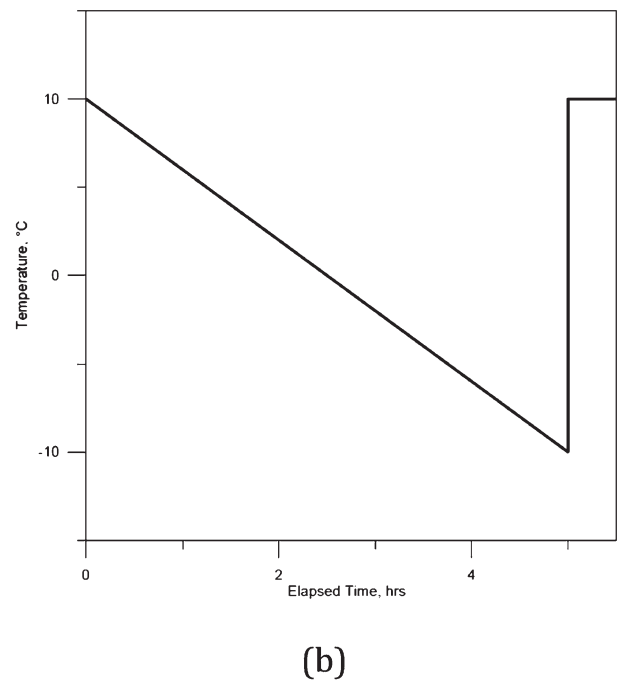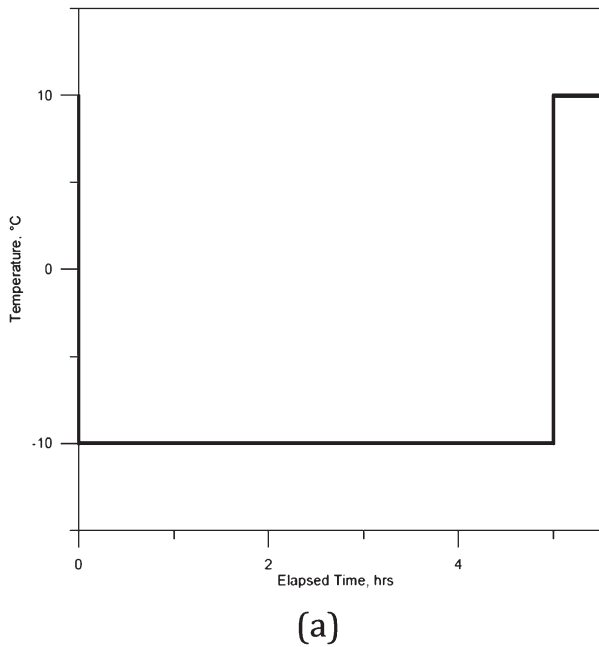
Figure 6.5 Cycling for determination of the freezing rate: (a) shows "quick" loading and (b) shows "slow" loading.

43
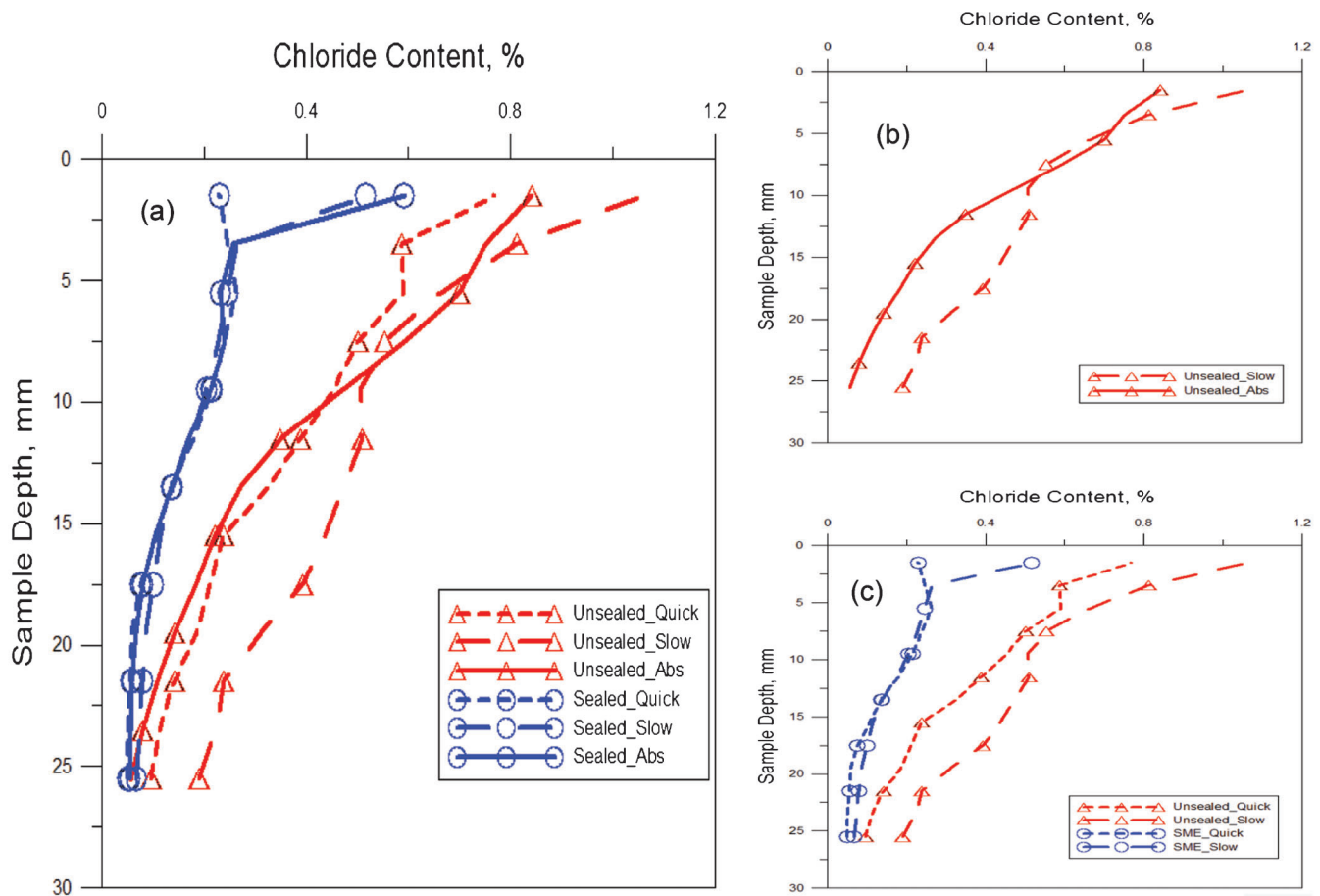
Figure 6.6 (a) Compares chloride concentration for sealed and unsealed samples at different loading rates; (b) demonstrates chloride pumping; and (c) is evidence that "slow" loading causes a higher concentration of chlorides further into the sample than quick loading.

of the sample face was visually noticed, even at 90 cycles (i.e., no flaking of concrete was found in the bottom of the pans, as would happen in an ASTM C666 (*95*)—Freeze and Thaw test). For practicality purposes, 35 cycles per test was chosen. Running 35 cycles at 5 hours a cycle will allow a single week of testing.

6.4.4 Solution Testing

This round of testing was used to determine the concentration of sodium chloride to be used in the standard testing procedure. The plot seen in Figure 6.7 shows that as the concentration of the solution increases, the chloride content throughout the sample increases. Although a lower concentration could theoretically penetrate further into the sample due to slightly lower viscosity, this was not seen here. For the purposes of our testing, a nearly saturated sodium chloride solution was used. This is not to say that other chloride solutions and concentrations couldn't be considered, however further studies may need to be done on keeping the desired concentration throughout the test, i.e., how often to flush the system. It should

also be noted that a concentration that allows the chloride solution to freeze should not be permitted.

6.5 Protocol for Sealant Testing

6.5.1 Sample Conditioning

Sample conditioning plays a major role in the absorption and rate of absorption in unsaturated hydraulic cement concretes (*112*). Absorption in concrete is generally described as the ability to take in water by means of capillary suction. A large fraction of concrete in service is only partly saturated and the initial ingress of water and dissolved salts is influenced, at least in part, by capillary absorption (*113*). Absorption has been used as an important factor for quantifying the durability of cementitious systems (*15,113–116*). Therefore, conditioning must be given proper focus in this study.

6.5.2 Uniform Application/Application Rate of Sealant

Obtaining a uniformly consistent application of sealers, pore blockers, and water repellants is a
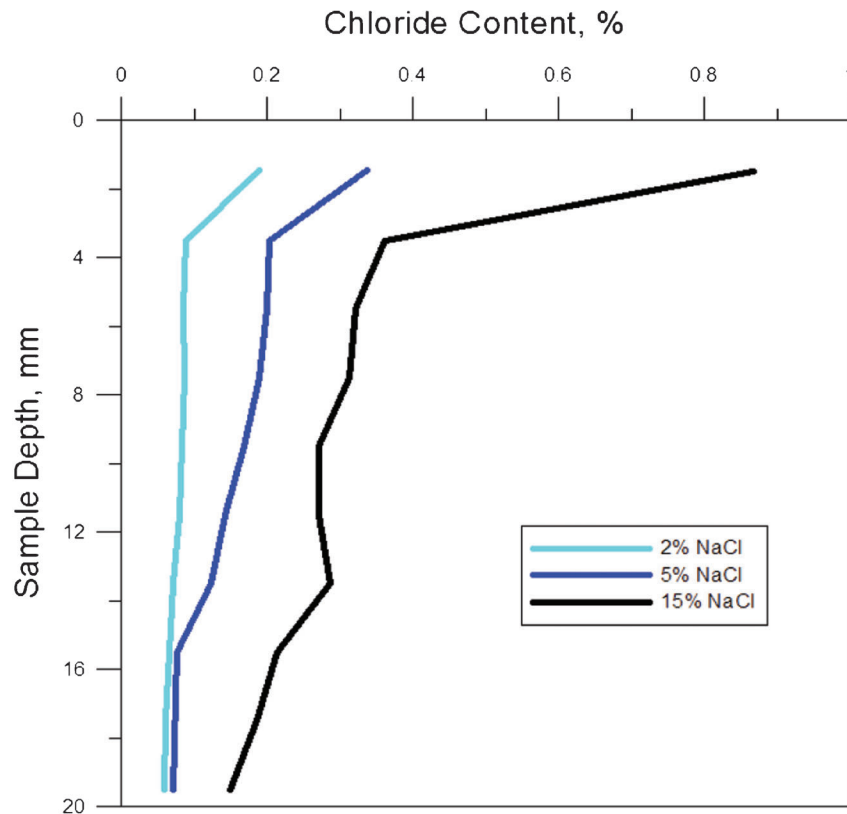
Figure 6.7 Chloride profile for solutions containing 2, 5, and 15% NaCl by mass.

necessity when trying to compare one manufacturer's product to another. In order accomplish uniform consistency a "flat-board" device in which the concrete samples could sit flush was created. This can be seen in Figure 6.8 (polystyrene is shown here; however, since some of the sealants are solvents, a non-degradable base is a better choice).

Application rate plays a role in the effectiveness of the sealant. Aside from the use of the flat-board, a light sprayer was used to apply each of the sealants. Each sealer was applied using an application rate of

Figure 6.8 Uniform application of sealants to cylindrical concrete samples.

125 ft²/gal, which fell within each manufacturer's recommendation for concrete applications.

6.5.3 Setup/ Cycling

Conditioning for this portion of the sealant testing was conducted by obtaining mass equilibrium in an over-dry condition. Samples were placed in a *Shel Lab* vacuum oven at 685 mm Hg at 50 $\pm$ 1°C to minimize damaging the microstructure. Sealant application in such a = dry state is not recommended for future testing as it creates an unrealistic concrete surface for which the sealant is applied.

After gathering data from the preliminary testing a protocol for testing various sealants has been developed. When the samples have been conditioned and sealed (this will vary based on what is being examined) the testing procedure will use cycling similar to that shown in Figure 6.5 (a), with 4¼ hours freezing at -10 $\pm$ 2°C, and ¾ hours thawing at +10 $\pm$ 2°C. The solution used for sealant testing will be a 23% NaCl (sodium chloride) by mass. Specimen dimensions are 2 in. in height by 4 in. in diameter. The samples will go through 35 cycles, which will take approximately 1 week per test. Quantitative measurements consist of massing the samples at cycles 1, 2, 5, and every 5 cycles until the conclusion of testing. Also, layered grinding and chloride titration will be completed to create a chloride profile.

6.6 Sealant Testing Results

6.6.1 Sealants Used

The use of silane, siloxane, and silicon sealants are common in today's construction industry (*117*). It has been shown that silicones are not an effective sealant in reducing both chloride and water absorption (*118,119*) and the only approved siloxane sealant on the Indiana Department of Transportations (INDOT) approved sealant list is no longer in production due to high volatile organic compound (VOC) content.

The sealants chosen for testing in this part of the study were two silane-based sealants, with differing percentages of alkylalkoxysilane (20% and 100%), along with Soy Methyl Ester (SME) containing 5% Polystyrene. The product data sheets for the silane sealants can be found in the appendix.

6.6.2 Penetration Depth

It was desired to test the penetration depth of each sealant. To do this, the effectiveness of the sealant will be investigated at depths of 0, 1, 2, and 5 millimeters below the surface to which the sealant was applied. The surfaces were removed to the desired depth after the application of the sealant and before testing. It is important that the sample top is flush when the sealant is applied and when the top surface is being removed.

6.6.3 Evaluation of Sealants

Figure 6.9 shows four plots, (a), (b), and (c) represent the chloride content of each of the tested sealants in the setup described in Section 6.5.3. Figure 6.9 (d) is a chloride profile summary showing all three sealants without any top surface removed. Top surfaces were removed at 1 mm, 2 mm, and 5 mm before testing, as seen in the three figures. The plots labeled '0mm' are samples in which no surface was removed. The plots labeled 'ABS' are samples in which no surface was removed and were placed in a room temperature chloride solution for the duration of the cycles. The chloride profile for each sample starts at the surface exposed to chloride, not at the original surface that was removed.

6.6.4 Discussion of Results

The "tails" seen at the top of the chloride profile plots represent sealant present in the powder for titration at that depth. The reason many chlorides are not present at the surfaces is that much of the pore volume is filled by the sealant and not chloride solution. The reason for the plot lines not reaching 0% chlorides can be attributed to background chlorides that are present is the sample before testing. Plot lines that do not approach zero are due to samples that have absorbed chlorides through the entire depth.

Also, it should be noted that the previously mentioned phenomenon of chloride pumping is not noticed in these samples (see unsealed absorption vs cycled plots) because capillary water is not present in these samples. It may seem apparent that chloride pumping is happening in the sealed samples, but this is simply due to the effect of freezing and thawing on the sample.

From the plots in Figure 6.9 (a), it can be concluded that the 100% silane sealant performs the best of the three sealants tested. Since the red line indicating 5 mm from the face of the sealants application has prevented fewer chlorides than the unsealed sample, the 100% silane sealant is effective at preventing chlorides at a depth of 5mm. The plot showing the 20% silane sealant, Figure 6.9 (b), indicates that the sealant is more or less ineffective at a depth of 2 mm and beyond, although there is a "tail" present on the 2 mm sample (meaning there is still a sealant present at this depth).

It can be seen that both the 20% and 100% silane sealants perform better than SME-PS, Figure 6.9 (c). Since these samples are oven dry, it has been noticed that at the low dosage rate the SME-PS was too easily absorbed. The SME-PS appears to require a higher dosage rate or some amount of capillary water to keep the sealant near the top surface of the sample. Since oven-dry conditions were used, SME-PS was absorbed into the sample instead of blocking the pores at the surface. Traces of SME-PS were found in the sample, through titration as notice in the "tail" of the chloride profile, at depths of up to 11mm. This indicates that the sealant was not held at the surface.

Figure 6.9 (d) shows a plot of all three sealants with the originally sealed surface. It can easily be determined which sealants performed best for this particular test. All three sealants prevented chlorides from being absorbed into the sample.

6.7 Summary and Conclusions

Premature deterioration of concrete pavement joints is a an issue of concern. One method that has been found effective in reducing the amount of chloride ingress into the concrete matrix is the use of sealers, pore blocker, and water repelling materials. The objective of this study was to develop a testing procedure to assess the impact of sealers, pore blockers, and water repelling materials to delay or prevent chloride solution ingress. Preliminary testing has been performed to develop a methodology, which closely replicates concretes field exposure to fluids containing salts. Chloride pumping has been found to expedite the absorption of chlorides in concrete that are exposed to freezing conditions. Uniform application is important when comparing various sealants. Sample conditioning cannot only have a large effect on the absorption/ absorption rate of concrete, but also on the application of the sealant. More testing should be done to apply this approach to samples that are conditioned to more closely represent the moisture conditions from the field.
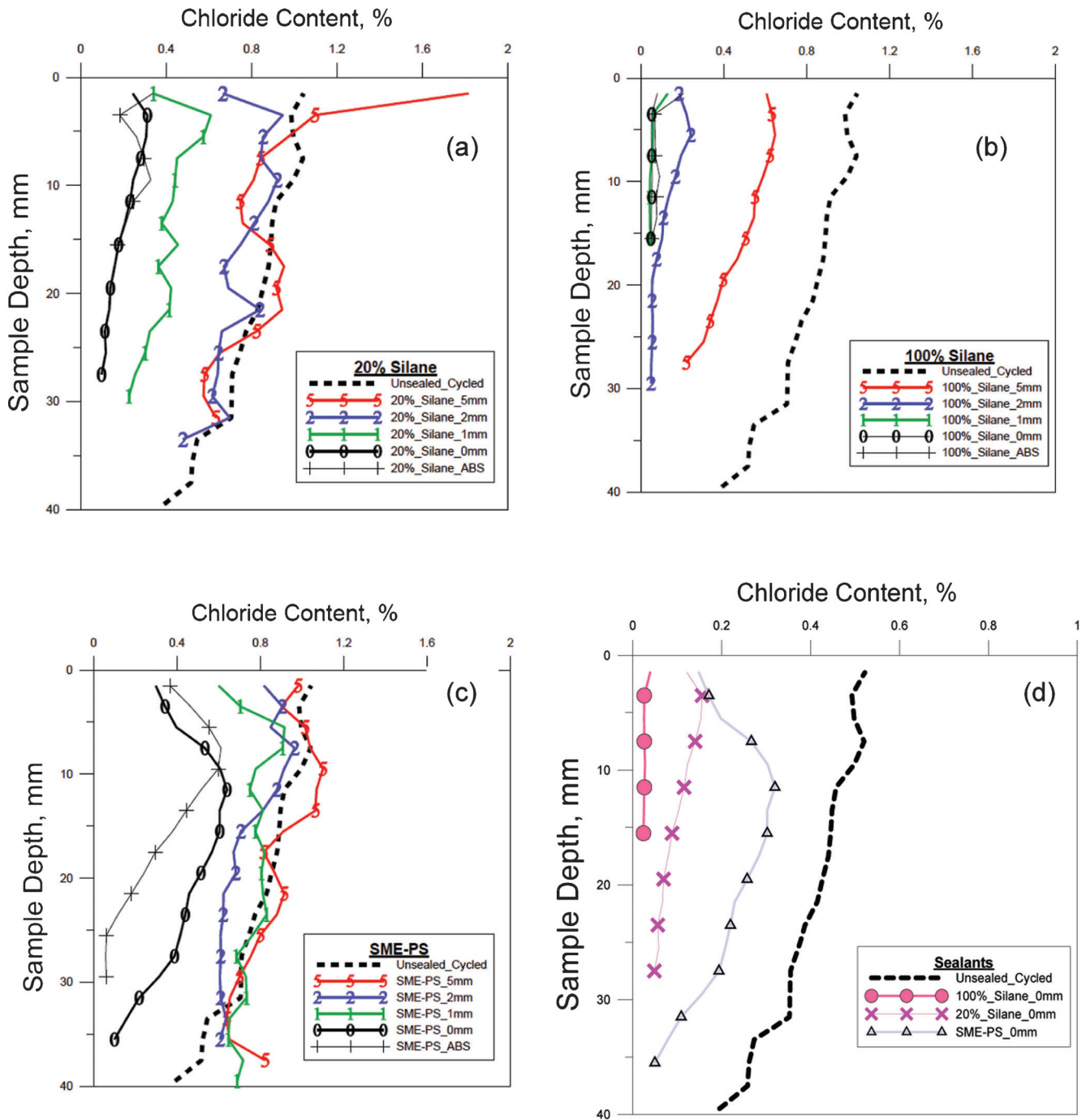
Figure 6.9 (a) Chloride profile for the 20% silane sealant used in this study; (b) chloride profile for the 100% silane sealant used in this study; (c) chloride profile for SME-PS (5% by mass) sealant used in this study; and (d) summary showing all three sealants without removal of the top surface.

7. SUMMARY

Concrete pavements represent a large portion of the transportation infrastructure. While the vast majority of concrete pavements provide excellent long-term performance, a portion of these pavements have recently shown premature joint deterioration. Substantial interest has developed in understanding why premature joint deterioration is being observed in jointed portland cement concrete pavements (PCCP). While some have attributed this damage to insufficient air void systems, poor mixture design, or chemical reaction between the salt and the paste, it is the hypothesis of this work that a component of this damage can be attributed to fluid absorption at the joints.

This report begins by discussing the importance of the level of concrete saturation on freeze-thaw damage. It was determined that damage can occur in samples

having a degree of saturation higher than some critical value (approximately 86%) after even one freezing cycle. When deicing salts are used, the freezing temperature is depressed; however, additional damage is observed as compared to just water. Additional damage appears to occur on thawing for systems with higher salt concentrations, presumably due to the phase change in the hydrohalite.

Second, this report describes the influence of deicing salt solutions on drying and wetting of concrete. The presence of deicing salts alters the viscosity, surface tension, and activity of the liquid. Models were presented for the solution properties as a function of temperature, as well as for sorption and drying. Samples containing deicing salts can be expected to have higher degree of saturation. This has practical implication in concrete, as the sample containing deicing salt solutions will have a higher degree of saturation and will remain saturated for a longer time.

Third, the report presents the results of laboratory work performed on concrete core samples collected from several locations around the state of Indiana. The samples were collected from both distressed and un-distressed concrete pavement joints as well as from the middle of the panels (for comparative purposes) in an effort to determine the underlying causes of the observed joint distresses.

Fourth, the report discusses soy methyl esters polystyrene blends (SME-PS) as a potential method to seal the concrete surface and to extend the service life of concrete pavements by limiting the ingress of salt solutions. SME-PS has been found to reduce salt ingress and freeze thaw damage. The report also discusses field application of the SME-PS blends for field investigation.

Finally, the report discusses the development of a test to assess chloride solution ingress during temperature cycling. The aim of this work is to provide background on some aspects that can lead to joint deterioration and to provide the pavement community alternatives on how sealers and deicers may be able to be used more efficiently to reduce joint damage. While still preliminary, this approach has the ability to shed light on how these sealers may influence the performance at joints, especially when the temperature is cycled.

REFERENCES

1. Weiss, J., and T. Nantung. Internal Proposal for the Joint Transportation Research Program of the Indiana Department of Transportation, Purdue University, West Lafayette, Indiana, 2007.
2. Castro, J., W. Li, M. Pour-Ghaz, M. Golias, B. Tao, H. Sun, and W. J. Weiss. *Durability of Saw-Cut Joints in Plain Cement Concrete Pavements.* Publication FHWA/IN/JTRP-2011/22. Joint Transportation Research Program, Indiana Department of Transportation and Purdue University, West Lafayette, Indiana, 2011. doi: 10.5703/1288284314649
3. Sutter, L., T. Van Dam, K. R. Peterson, and D. P. Johnston. Long-Term Effects of Magnesium Chloride and other Concentrated Salt Solutions on Pavement and Structural Portland Cement Concrete Phase I Results. In *Transportation Research Record: Journal of the Transportation Research Board*, No. 1979, Transportation Research Board of the National Academies, Washington, D.C., 2006, pp. 60–68.
4. Leech, C., D. Lockington, R. D. Hooton, G. Galloway, G. Cowin, and P. Dux. Validation of Mualem's Conductivity Model and Prediction of Saturated Permeability from Sorptivity. *ACI Materials Journal*, Vol. 105, No. 1, 2008, pp. 44–51.
5. Olek, J., M. Radlinski, and M. del Mar Arribas. Premature Deterioration of Joints in Selected Indiana Portland Cement Concrete Pavements. *Proceedings of the XXIII Conference "Awarie Budowlane,"* M. Kaszynska, ed. Wydawnictwo Uczelniane Politechniki Szczecinskiej, 2007, pp. 859–868.
6. Rangaraju, P. R., K. R. Sompura, and J. Olek. Investigation into Potential of Alkali-Acetate-Based Deicers to Cause Alkali-Silica Reaction in Concrete. In *Transportation Research Record: Journal of the Transportation Research Board*, No. 1979, Transportation Research Board of the National Academies, Washington, D.C., 2006, pp. 69–78.
7. Radlinski, M., J. Olek, M. del Mar Arribas, A. Rudy, T. Nantung, and M. Byers. Influence of Air-Void System Parameters on Freeze-Thaw Resistance of Pavement Concrete—Lessons Learned from Field and Laboratory Observation. *Proceedings of the 9th International Conference on Concrete Pavements*, San Francisco, August 17–21, 2008, pp. 824–835.
8. Radlinski, M., J. Olek, Q. Zhang, and K. Peterson. Evaluation of the Critical Air-Void System Parameters for Freeze-Thaw Resistant Ternary Concrete Using the Manual Point-Count and the Flatbed Scanner Methods. *Journal of ASTM International*, Vol. 7, No. 4, 2010, 14 pp.
9. Jain, J., A. Janusz, J. Olek, and D. Jozwiak-Niedzwiedzka. Physico-Chemical Changes in Plain and Fly Ash Modified Concretes Exposed to Different Deicing Chemicals. *Proceedings of the XIII International Congress on the Chemistry of Cement*, Madrid, Spain, 2011.
10. Jitendra, J., J. Olek, A. Janusz, and D. Jozwiak-Niedzwiedzka. Effects of Deicing Chemicals on Physical Properties of Pavements Concretes. In *Transportation Research Record: Journal of the Transportation Research Board*, No. 2290, Transportation Research Board of the National Academies, Washington, D.C., 2012, pp. 69–75.
11. Arribas-Colón, M., M. Radliński, J. Olek, and N. Whiting. *Investigation of Premature Distress Around Joints in PCC Pavements: Parts I & II.* Publication FHWA/IN/JTRP-2012/25 & FHWA/IN/JTRP-2012/26. Joint Transportation Research Program, Indiana Department of Transportation and Purdue University, West Lafayette, Indiana, 2012. doi 10.5703/1288284315019.
12. Li, W., M. Pour-Ghaz, J. Castro Sepúlveda, and W. J. Weiss. Water Absorption and Critical Degree of Saturation Relating to Freeze-Thaw Damage in Concrete Pavement Joints. *Journal of Materials in Civil Engineering*, Vol. 24, 2012, pp. 299–307.
13. Golias, M., J. Castro, A. Peled, T. Nantung, B. Tao, and J. Weiss. Can Soy Methyl Esters Improve Concrete Pavement Joint Durability? In *Transportation Research Record: Journal of the Transportation Research Board*,

No. 2290, Transportation Research Board of the National Academies, Washington, D.C., 2012, pp. 60–68.

14. Raoufi, K., J. Weiss, and T. Nantung. Numerical Assessment of Saw-Cutting: The Influence on Stress Development and Cracking. Presented at 6th RILEM International Conference on Cracking in Concrete Pavements, Chicago, Illinois, 2008.

15. Hooton, R. D, T. Mesisc, and D. L. Beal. Sorptivity Testing of Concrete as an Indicator of Concrete Durability and Curing Efficiency. *Proceedings of the 3rd Canadian Symposium on Cement and Concrete*, Ottawa, Ontario, 1993, pp. 264–275.

16. Farnam, Y., D. Bentz, A. Sakulich, D. Flynn, and J. Weiss. Measuring Freeze and Thaw Damage in Mortars Containing Deicing Salt Using a Low-Temperature Longitudinal Guarded Comparative Calorimeter and Acoustic Emission, *Advances in Civil Engineering Materials (ASTM)*, Vol. 3, No. 1, 2014, pp. 1–22, doi: 10.1520/ACEM20130095.

17. Scherer, G. W. Crystallization in Pores. *Cement and Concrete Research*, Vol. 29, 1999, pp. 1347–1358.

18. Yang, Z. F., W. J. Weiss, and J. Olek. Water Transport in Concrete Damaged by Tensile Loading and Freeze-Thaw Cycling. *Journal of Materials in Civil Engineering*, Vol. 18, No. 3, 2006, pp. 424–434.

19. Beaudoin, J., and C. MacInnis. The Mechanism of Frost Damage in Hardened Cement Paste. *Cement and Concrete Research*, Vol. 4, 1974, pp. 139–147.

20. Kaufmann, J. Experimental Identification of Damage Mechanisms in Cementitious Porous Materials on Phase Transition of Pore Solution under Deicing Salt Attack. *Bericht - Eidgenossische Materialprufungs- und Forschungsanstalt*, Vol. 2, No. 248. 2000.

21. Litvan, G. Frost Action in Cement in the Presence of Deicers. *Cement and Concrete Research*, Vol. 6, 1976, pp. 351–356.

22. Mehta, P. K., and P. J. Monteiro. *Concrete: Microstructure, Properties, and Materials*. McGraw-Hill, New York, 2005.

23. Powers, T. C. The Air Requirement of Frost-Resistant Concrete. *Proceedings of the Twenty-Ninth Annual Meeting of the Highway Research Board*, Vol. 29, 1949, pp. 184–211.

24. Powers, T. A Working Hypothesis for Further Studies of Frost Resistance of Concrete. *Journal of the American Concrete Institute*, Vol. 41, 1945, pp. 245–272.

25. Powers, T. C. *The Physical Structure and Engineering Properties of Concrete*. Bulletin 90, Research Department, Portland Cement Association, Washington, D.C., 1958.

27. Coates, K., S. Mohtar. B. Tao, J. Weiss. Can Soy Methyl Esters Reduce Fluid Transport and Improve Durability of Concrete? In *Transportation Research Record: Journal of the Transportation Research Board*, No. 2113, Transportation Research Board of the National Academies, Washington, D.C., 2009, pp. 22–30.

28. Golias, M. The Use of Soy Methyl Ester-Polystyrene Sealants and Internal Curing to Enhance Concrete Durability. Master's thesis, Purdue University, West Lafayette, Indiana, 2010.

29. Whiting, D. Penetrating Sealers for Conerete: Survey of Highway Agencies. In *Transportation Research Record: Journal of the Transportation Research Board*, No. 1284, Transportation Research Board of the National Academies, Washington, D.C., 1990, pp. 79–84.

30. Qian, Y., Y. Farnam, and J. Weiss. Using Acoustic Emission to Quantify Freeze-Thaw Damage of Mortar Saturated with NaCl Solutions. In *4th International Conference on the Durability of Concrete Structures*, West Lafayette, Indiana, 2014, pp. 1–7.

31. Spragg, R., J. Castro, W. Li, M. Pour-Ghaz, P.-T. Huang, and W. J. Weiss. Wetting and Drying of Concrete Using Aqueous Solutions Containing Deicing Salts. *Cement and Concrete Composites*, Vol. 33, 2011, pp. 535–542.

32. Villani, C., T. Nantung, and W. J. Weiss. The Influence of Deicing Salt Exposure on the Gas Transport in Cementitious Materials. *Proceedings of the Third International Conference on Sustainable Construction Materials and Technologies*, Kyoto, Japan, August 18–21, 2013.

33. Li, W., W. Sun, and J. Jiang. Damage of Concrete Experiencing Flexural Fatigue Load and Closed Freeze/Thaw Cycles Simultaneously. *Construction and Building Materials*, Vol. 25, No. 5, 2011, pp. 2604–2610.

34. Fagerlund, G. *Critical Degrees of Saturation at Freezing of Porous and Brittle Materials*. Report 34, Division of Building Technology, Lund Institute of Technology, Lund, Sweden, 1972.

35. Fagerlund, G. The Critical Degree of Saturation Method of Assessing the Freeze/Thaw Resistance of Concrete and the International Cooperative Test of the Critical Degree of Saturation Method of Assessing the Freeze/thaw Resistance of Concrete. *Journal of Materials and Structures*, Vol. 10, 1977, pp. 217–229 and 231–253.

36. Bentz, D. P., M. A. Ehlen, C. F. Ferraris., and E. J. Garboczi. Sorptivity-Based Service Life Predictions for Concrete Pavements. *7th International Conference on Concrete Pavements,* NIST, Orlando, Florida, 2011, pp. 181–193.

37. Litvan, G. G. The Mechanism of Frost Action in Concrete-Theory and Practical Implications. *Proceedings of Workshop on Low Temperature Effects on Concrete*, September 5–9, Sapporo, Hakkaido, Japan, 1988, pp. 115–134.

38. Litvan, G. G., and P. J. Sereda. Freeze-Thaw Durability of Porous Building Materials. ASTM STP 691. In *Durability of Building Materials and Components*, ASTM International, 1980, pp. 455–463.

39. Shimada, H., K. Sakai, and G. G. Litvan. Acoustic Emissions of Mortar Subjected to Freezing and Thawing. *ACI Materials Journal*, Vol. 126, 1991, pp. 263–278.

40. Beaudoin, J. J., and M. Cameron. Dimentional Changes of Hydrated Portland Cement Paste During Slow Cooling and Warming. *Cement and Concrete Research*, Vol. 2, No. 2, 1972, pp. 225–240.

41. ASTM C192-12. *A Standard Practice for Making and Curing Concrete Test Specimens in the Laboratory*. ASTM International, West Conshohocken, Pennsylvania, 2012.

42. Kaiser, H. Bewehren von stahlbeton mit kohlenstoffserverstarkten epoxiharzen. Ph.D. Thesis, Diss ETH Nr. 8918, EMPA, Zurich, Switzerland, 1989.

43. Helmuth, R. A. Capillary Size Restrictions on Ice Formation in Hardened Portland Cement Pastes. *Proceedings of the 4th International Symposium on Chemistry of Cement*, Paper VI-S2, 1960, pp. 855–869.

44. ASTM C1585-04. *Standard Test Method for Measurement of Rate of Absorption of Water by Hydraulic-Cement Concretes*. ASTM International, West Conshohocken, Pennsylvania, 2004.

45. Fagerlund, G. *The Long-Time Water Absorption in the Air-Pore Structure of Concrete*. Rep. TVBM-3051, Division of Building Technology, Lund Institute of Technology, Lund, Sweden, 1993.

46. Beddoe, R., and M. Setzer. A Low-Temperature DSC Investigation of Hardened Cement Paste Subjected to Chloride Action. *Cement and Concrete Research*, Vol. 18, No. 2, 1988, pp. 249–256.

47. Han, B., J. H. Choi, J. Dantzig, and J. C. Bischof. A Quantitative Analysis on Latent Heat of an Aqueous Binary Mixture. *Cryobiology*, Vol. 52, No. 1, 2006, pp. 146–151.

48. ASTM E1225-09. *Standard Test Method for Thermal Conductivity of Solids Using the Guarded-Comparative-Longitudinal Heat Flow Technique*. ASTM International, West Conshohocken, Pennsylvania, 2009.

49. ASTM D5470-12. *Standard Test Method for Thermal Transmission Properties of Thermally Conductive Electrical Insulation Materials*. ASTM International, West Conshohocken, Pennsylvania, 2012.

50. Debenedetti, P. G., and H. E. Stanley. Supercooled and Glassy Water. *Physics Today*, Vol. 56, No. 6, 2003, pp. 40–46.

51. Valenza, J. Mechanism for Salt Scaling. PhD thesis, Princeton University, Princeton, New Jersey, 2005.

52. Verbeck, G., and P. Klieger. Studies of Salt Scaling of Concrete. In *Highway Research Board Bulletin No. 150*, Portland Cement Association, Washington, D.C., 1957.

53. Bazant, Z. P., and L. J. Najjar. Drying of Concrete as a Nonlinear Diffusion Problem. *Cement and Concrete Research*, Vol. 1, 1971, pp. 461–473.

54. Pour-Ghaz, M., J. Castro, E. J. Kladivko, and W. J. Weiss. Characterizing Lightweight Aggregate Desorption at High Relative Humidities using a Pressure Plate Apparatus. *Journal of Materials in Civil Engineering*, 2012.

55. Sutter, L. *The Deleterious Chemical Effects of Concentrated Deicing Solutions on Portland Cement Concrete*. South Dakota Department of Transportation, Pierre, South Dakota, 2008.

56. Hong, K., and R. D. Hooton. Effects of Cyclic Chloride Exposure on Penetration of Concrete Cover. *Cement and Concrete Research*, Vol. 29, 1999, pp. 1379–1386.

57. Wang, K., D. E. Nelsen, and W. A. Nixon. Damaging Effects of Deicing Chemicals on Concrete Materials. *Cement and Concrete Composites*, Vol. 28, 2006, pp. 173–188.

58. Samson, E., and J. Marchand. Modeling the Effect of Temperature on Ionic Transport in Cementitious Materials. *Cement and Concrete Research*, Vol. 37, 2007, pp. 455–468.

59. McCarter, W. J. Assessing the Protective Qualities of Treated and Untreated Concrete Surfaces Under Cyclic Wetting and Drying. *Building and Environment*, Vol. 31, 1996, pp. 551–556.

60. MacInnis, C., and Y. R. Nathawad. The Effects of a Deicing Agent on the Absorption and Permeability of Various Concretes. In *Durability of Building Materials and Components, ASTM STP* 691, P. J. Sereda and G. G. Levitan (Eds.), American Society for Testing and Materials, 1980, pp. 485–496.

61. Scherer, G. W. Theory of Drying. *Journal of the American Ceramic Society*, Vol. 73, 1990, pp. 3–14.

62. Scherer, G. W. Stress from Crystallization of Salt. *Cement and Concrete Research*, Vol. 34, 2003, pp. 1613–1624.

63. Benavente, D., M. A. Garcia del Cura, and S. Ordonez. Salt Influence on Evaporation from Porous Building Rocks. *Construction and Building Materials*, Vol. 17, 2003, pp. 113–122.

64. Rodriguez-Navarro, C., and E. Doehne. Salt Weathering: Influence of Evaporation Rate, Supersaturation and Crystallization Pattern. *Earth Surface Processes and Landforms*, Vol. 24, 1999, pp. 191–209.

65. Pfeifle, T. W., and F. D. Hansen. Salt-Saturated Concrete Strength and Permeability. Proceedings of 4th Materials Engineering Conference, Washington, D.C., 1995.

66. Davies, P. B. *Evaluation of the Role of Threshold Pressure in Controlling Flow of Waste-Generated Gas into Bedded Salt at the Waste Isolation Pilot Plant*. Sandia National Laboratories, 1992.

67. Adamson, A. W. *Physical Chemistry of Surfaces*. John Wiley & Sons, Inc., New York, 1990.

68. Pease, B., H. Shah, and J. Weiss. Shrinkage Behavior and Residual Stress Development in Mortar Containing Shrinkage Reducing Admixtures. *ACI—Special Publication on Concrete Admixtures*, 2005, pp. 285–302.

69. Jones, G., and M. Dole. 1929. The Viscosity of Aqueous Solutions of Strong Electrolytes with Special Reference to Barium Chloride. *Journal of the American Chemical Society*, Vol. 51, 1929, pp. 2950–2964.

70. Wang, P., A. Anderko, and R. D. Young. Modeling Viscosity of Concentrated and Mixed-Solvent Electrolyte Systems. *Fluid Phase Equilibria*, Vol. 226, 2004, pp. 71–82.

71. Kaminsky, M. Experimental Investigation on Viscosity of Dilute Aqueous Strong Electrolyte Solutions at Different Temperatures. *Physical Chemistry*, Vol. 12, 1957, pp. 206–231.

72. Jones, G., and S. T. Talley. The Viscosity of Aqueous Solutions as a Function of the Concentration. *Journal of the American Chemical Society*, Vol. 55, 1933, pp. 624–642.

73. Out, D., and J. Los. Viscosity of Aqueous Solutions of Univalent Electrolytes from 5 to 95°C. *Journal of Solution Chemistry*, Vol. 9, 1980, pp. 19–35.

74. Andrade, E. N. The Viscosity of Liquids. *Nature*, Vol. 125, 1930, pp. 309–310.

75. Abdulagatov, I. M., A. B. Zeinalova, and N. D. Azizov. Viscosity of Aqueous Electrolyte Solutions at High Temperatures and High Pressures. Viscosity *B*-coefficient. Sodium Iodide. *Journal of Chemical and Engineering Data*, Vol. 51, 2006, pp. 1645–1659.

76. Szyszkowski, B. V. Experimentelle studien über kapillare eigenschaften der wässerigen lösungen von fettsauren. Z. *The Journal of Physical Chemistry*, 64, 1908, pp. 385–414.

77. Anderberg, A., and L. Wadso. Method for Simultaneous Determination of Sorption Isotherm and Diffusivity of Cement-Based Materials. *Cement and Concrete Research*, Vol. 38, 2008, pp. 89–94.

78. Pour-Ghaz, M., R. Spragg, and J. Weiss. Moisture Profiles and Diffusion Coefficients in Mortars Containing Shrinkage Reducing Admixtures. *Proceedings of the International RILEM Conference on the Use of Superabsorbent Polymers and Other New Additives in Concrete Technical*, 2010, pp. 197–206.

79. Villani, C., R. Spragg, M. Pour-Ghaz, and W. J. Weiss. The Influence of Pore Solutions Properties on Drying in Cementitious Materials. *Journal of the American Ceramic Society*, Vol. 97, No. 2, 2014, pp. 386–393. doi: 10.1111/jace.12604.

80. Villani, C., R. Spragg, M. Pour-Ghaz, and W. J. Weiss. The Role of Deicing Salts on the Non-Linear Moisture Diffusion Coefficient of Cementitious Materials During Drying. *Proceedings of the 10th International Symposium on Brittle Matrix Composites*, Warsaw, Institute of Fundamental Technological Research PAS, 2012, pp. 101–114.

81. Selander, A. *Hydrophobic Impregnation of Concrete Structures—Effects on Concrete Properties*. Royal Institute of Technology, Stockholm, Sweden, 2010.

82. Samson, E., J. Marchand, K. A. Snyder, and J. J. Beaudoin. Modeling Ion and Fluid Transport in Unsaturated Cement Systems in Isothermal Conditions. *Cement and Concrete Research*, Vol. 35, 2005, pp. 141–153.

83. Nilsson, L.-O. Long-Term Moisture Transport in High Performance Concrete. *Materials and Structures*, Vol. 35, 2002, pp. 641–649.

84. Baroghel-Bouny, V. Water Vapour Sorption Experiments on Hardened Cementitious Materials: Part I: Essential Tool for Analysis of Hygral Behaviour and its Relation to Pore Structure. *Cement and Concrete Research*, Vol. 37, 2007, pp. 414–437.

85. Nilsson, L.-O. *Hygroscopic Moisture in Concrete: Drying*, Measurements & Related Material Properties. Division of Building Materials, Lund Institute of Technology, Lund, Sweden, 1980.

86. Mainguy, M. Non-Linear Diffusion Models in Porous Media—Application to Leaching and to Drying of Cementitious Materials (in French). PhD. dissertation, ENPC, Paris, France 1999.

87. Philip, J. R., and D. A. de Vries. Moisture Movement in Porous Materials under Temperature Gradients. *American Geophysical Union*, Vol. 38, 1957, pp. 222–232.

88. Wexler, A., and L. Greenspan. Vapor Pressure Equation for Water in the Range 0 to $100°C$. *Journal of Research of the National Bureau of Standards*, Vol. 75, 1971, pp. 213–230.

89. Kelham, S. A Water Absorption Test for Concrete. *Magazine of Concrete Research*, Vol. 40, 1988, pp. 106–110.

90. Ballim, Y. 1991b. A Low Cost, Falling Head Permeameter for Measuring Concrete Gas Permeability. *Concrete Beton*, Vol. 61, 1991b, pp. 13–18.

91. Alexander, M. G., Y. Ballim, and J. M. Mackechnie. *Concrete Durability Index Testing Manual*. Research Monograph No. 4, Department of Civil Engineering, University of Cape Town, Cape Town, South Africa, 1999.

92. Lawrence, C. D. Transport of Oxygen through Concrete. *Proceedings of the British Ceramic Society on the Chemistry and Chemical-Related Properties of Cement*, 1984, pp. 277–293.

93. Abbas, A., M. Carcasses, and J. -P. Ollivier. Gas Permeability of Concrete in Relation to its Degree of Saturation. *Materials and Structures*, Vol. 32, 1999, pp. 3–8.

94. ASTM C457/C457M-12. *Standard Test Method for Microscopical Determination of Parameters of the Air-Void System in Hardened Concrete*. ASTM International, West Conshohocken, Pennsylvania, 2012.

95. ASTM C666/C666M. *Standard Test Method for Resistance of Concrete to Rapid Freezing and Thawing*. ASTM International, West Conshohocken, Pennsylvania, 2008.

96. AASHTO T277. *Standard Method of Test for Rapid Determination of the Chloride Permeability of Concrete*. ASTM International, West Conshohocken, Pennsylvania, 2012.

97. Peterson, K. W., R. A. Swartz, L. L. Sutter, and T. J. Van Dam. Hardened Concrete Air Void Analysis with a Flatbed Scanner. In *Transportation Research Record: Journal of the Transportation Research Board*, No. 1775, Transportation Research Board of the National Academies, Washington, D. C., 2001, pp. 36–43.

98. ASTM E1876. *Standard Test Method for Dynamic Young's Modulus, Shear Modulus, and Poisson's Ratio by Impulse Excitation of Vibration*. ASTM International, West Conshohocken, Pennsylvania, 2009.

99. Newlon, H. Jr., and T. M. Mitchell. *Freezing and Thawing*. ASTM STP 169C, ASTM International, West Conshohocken, Pennsylvania, 1994, pp. 153–163.

100. Hover, K. C. *Air Content and Unit Weight of Hardened Concrete*. ASTM STP 169C, ASTM International, West Conshohocken, Pennsylvania, 1994, pp. 296–314.

101. Arribas-Colón, M. Investigation of Premature Distress around Joints in PCC Pavements. MSCE thesis, Purdue University, West Lafayette, Indiana, 2008.

102. Stark, J., and K. Bollmann. Delayed Ettringite Formation in Concrete. *Proceedings of the Nordic Concrete Research Meeting*, 1999, pp. 4–28.

103. ASTM C1260. *Standard Test Method for Potential Alkali Reactivity of Aggregates (Mortar-Bar Method)*. ASTM International, West Conshohocken, Pennsylvania, 2007.

104. Almanac. Weather History for West Lafayette, Indiana. *The Old Farmer's Almanac*, 2012. Web.

105. Pfeifer, D. W., and M .J. Scali. *Concrete Sealers for Protection of Bridge Structures*. Transportation Research Board. National Cooperative Highway Research Program Report 244, Washington, D.C., 1981.

106. Yang, Z., W. J. Weiss, and J. Olek. *Interaction Between Micro-Cracking, Cracking, and Reduced Durability of Concrete: Developing Methods for Considering Cumulative Damage in Life-Cycle Modeling*. Publication FHWA/IN/JTRP-2004/10. Joint Transportation Research Program, Indiana Department of Transportation and Purdue University, West Lafayette, Indiana, 2004. doi: 10.5703/1288284313255.

107. ASTM C172/C172M. *Standard Practice for Sampling Freshly Mixed Concrete*. ASTM International, West Conshohocken, Pennsylvania, 2014.

108. ASTM C143/C143M. *Standard Test Method for Slump of Hydraulic-Cement Concrete*. ASTM International, West Conshohocken, Pennsylvania, 2012.

109. ASTM C231/C231M. *Standard Test Method for Air Content of Freshly Mixed Concrete by the Pressure Method*. ASTM International, West Conshohocken, Pennsylvania, 2010.

110. ASTM C1556. *Standard Test Method for Determining the Apparent Chloride Diffusion Coefficient of Cementitious Mixtures by Bulk Diffusion*. ASTM International, West Conshohocken, Pennsylvania, 2011.

111. Rønning, T. F. Freeze-Thaw Resistance of Concrete Effect of Curing Conditions, Moisture Exchange and Materials. Dissertation. The Norwegian Institute of Technology, 2001.

112. Castro, J., D. Bentz, and J. Weiss. Effect of Sample Conditioning on the Water Absorption of Concrete. *Cement and Concrete Composites*, Vol. 33, No. 8, 2011, pp. 805–813.

113. Hearn, N., D. Hooton, and R. Mills. *Pore Structure and Permeability: Significance of Tests and Properties of Concrete and Concrete-Making Materials*. ASTM STP

169C, ASTM International, West Conshohocken, Pennsylvania, 1994, pp. 240–262.

114. Parrot, L. J. Water Absorption in Cover Concrete. *Materials and Structures*, Vol. 25, No. 5, 1992, pp. 284–292.

115. Fagerlund, G. Predicting the Service-Life of Concrete Exposed to Frost Action through a Modeling of the Water Absorption Process in the Air Pore System. In *The Modeling of Microstructure and its Potential for Studying Transport Properties and Durability*. The Netherlands, 1996, pp. 503–539.

116. Neithalath, N. Analysis of Moisture Transport in Mortars and Concrete Using Sorption-Diffusion Approach. *ACI Materials Journal*, Vol. 103, No. 3, 2006, pp. 209–217.

117. Wehrle, E. The Effects of Coatings and Sealers Used to Mitigate Alkali-Silica Reaction and/or Delayed Ettringite Formation in Hardened Concrete. MS thesis, University of Texas at Austin, Austin, Texas, 2010.

118. Ryell, J., and B. Chojnacki. Laboratory and Field Tests on Concrete Sealing Compounds. *Highway Research Record 328*, Highway Research Board, Washington, D.C., 1970, pp. 61–64.

119. Klieger, P., and W. F. Perenchio. Silicone Influence on Concrete Resistance to Freeze-Thaw and Deicer Damage. In *Highway Research Board Bulletin No. 169*, Portland Cement Association, Washington, D.C., 1963.

APPENDIX

Figure A.1 Mixture design for samples used in cold plate freeze-thaw testing.

53

ATS-100 LV

VOC Compliant   Alkyltrialkoxysilane

ADVANCED CHEMICAL TECHNOLOGIES, Inc.

"Protecting the World's Infrastructure"

LOW VOC CONTENT

Advanced Chemical Technologies has been at the forefront of developing environmentally friendly silane based protective products for concrete, masonry and natural stone structures. SIL-ACT™ ATS-100 LV is the latest development in this family of water repellent solutions. At less than 250 g/L, it is the lowest VOC content 100% silane product on the market, while maintaining the same water repellent characteristics our customers have come to expect. ATS-100 LV remains easy to apply and has almost no odor.

PERFORMANCE & DURABILITY

SIL-ACT™ ATS-100 LV is a clear, penetrating silane treatment which causes concrete, masonry and natural stone structures to become repellent to water, chloride, ions and waterborne contaminants, preventing their premature deterioration.

SIL-ACT™ ATS-100 LV forms a chemical bond which will last until the penetrated depth is abraded away. While the surface of the substrate is water repellent, it remains permeable, allowing harmful water vapor in the substrate to escape. This is the difference between SIL-ACT™ and film forming water proofing products.

BENEFITS

Low odor – making it an ideal water repellent for use in hospitals, retirement facilities, sports arenas, schools, parking structures; anywhere odor may be of concern.
**Flexible** – it is an effective treatment for new and existing concrete, masonry and many natural stones.
Does not change the appearance, skid resistance or permeability of the substrate (however, a test patch is always recommended).

ATS-100 LV is
LOW Odor & VOC Content

Easy to apply – it can be applied to the substrate surface by low-pressure spray, brush, roller or squeegee.
Easy to store – it can be stored on the job site at extreme temperatures, unlike emulsified silane products which can deteriorate under such conditions

STOPS
WATER
CHLORIDE
WATERBORNE
CONTAMINANTS

PERFORMANCE TESTED!

UNTREATED

SIL-ACT PENETRATED LAYER

SIL-ACT™ TREATED

SIL-ACT™'s penetrated silane treatment layer stops water and salt intrusion into concrete, brick, masonry and many types of stone without affecting natural vapor permeability.
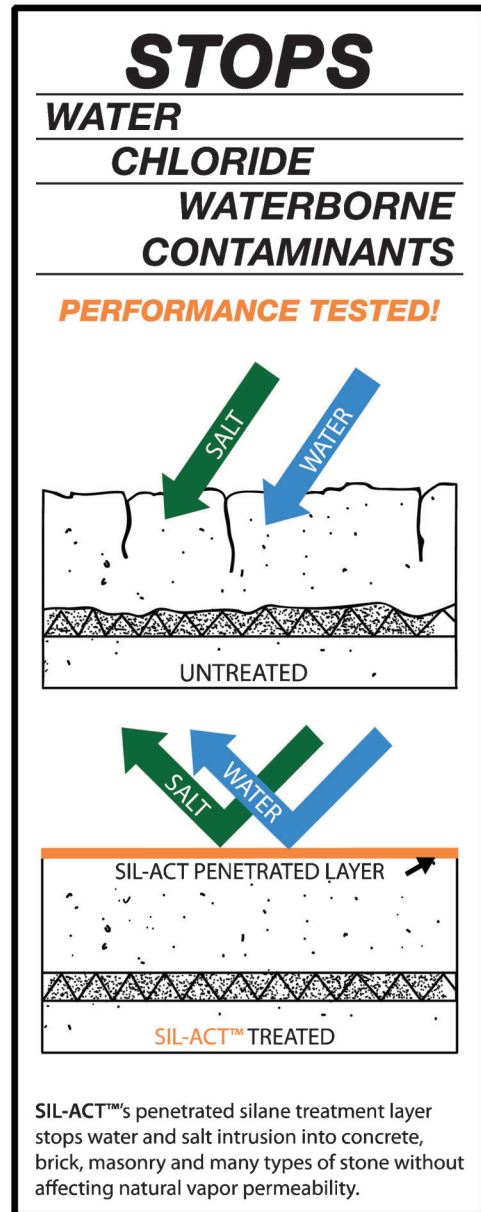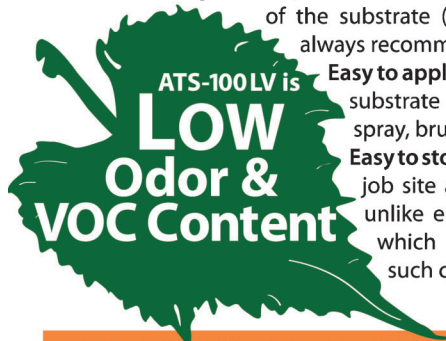
100 West Wilshire Blvd, Suite C-1   Oklahoma City, OK 73116   (405) 843-2585   Fax: (405)843-2596   www.advchemtech.com

Figure A.2   Data sheet for 100% silane sealant used in freeze-thaw testing.

TECHNICAL DATA		
PROPERTY	**TEST**	**ATS-100LV**
Active Ingredient		Alkyltrialkoxysilane
Specific Gravity	Method 24, ASTM D-5095	0.92
Density		7.68/ lb/gal
Solids Content		100% active
VOC Content		< 250 g/L
Appearance		Clear
Surface Appearance after Application		Unchanged
Drying time at 70°F		1 hour
Moisture Absorption Resistance	ASTM C-642	82%
Reduction in Absorbed Chloride	NCHRP 244 Series II	84%
	NCHRP 244 Series IV - Southern Climate	98%
Freeze-Thaw Scaling Resistance	ASTM C-672	0 at 50 cycles

INSTRUCTIONS

1. Test a small area prior to general application to ensure compatibility, desired results and coverage rates.

2. Treatment is most effective when the surface to be treated is clean and dry. Remove dirt, dust, oil, grease, curing compounds, coatings and other surface contaminants. Water blasting, sandblasting or shotblasting may be required.

3. Please refer to Advanced Chemical Technology's CleanACT line of concrete and masonry detergents and cleaners.

4. Do not proceed unless surface and air temperature is between 40°F and 110°F. Do not apply if frost, ice, or standing water are visible on the surface to be treated.

5. Windows, metals, etc. are not affected by SIL-ACT™. However avoid unnecessary overspray. If necessary, clean overspray areas with a clean dry cloth, soap and water or alcohol. Protect plants and vegetation from overspray. Prior to SIL-ACT™ installation check for preexisting contamination.

6. Spray, brush or roll SIL-ACT ATS-100 LV treatment on surface to be treated at the recommended application rate. See equipment section of this catalog or contact your Advanced Chemical Technologies rep for spray equipment options.

7. Apply to saturation. When spraying at low pressure, if necessary follow with broom or squeegee for even distribution.

8. Normal coverage rate is approximately 125 to 400 square feet per gallon. Coverage rates may vary depending on the porosity of the substrate to be treated.

9. Clean equipment with SIL-ACT™ Equipment Cleaner or 99.99% pure alcohol solvent.

10. Partially used containers should be properly sealed and protected from contamination by water or other foreign substances.

ADVANCED CHEMICAL TECHNOLOGIES, INC.

"Protecting the World's Infrastructure"
Technical Binder 2010

Figure A.2 *Continued.*

PRODUCT DATA

ENVIROSEAL® 20

Clear, water-based 20% silane penetrating sealer

Description

Enviroseal® 20 is a clear, water-based 20% alkylalkoxysilane penetrating sealer. It protects against moisture and chloride intrusion.

Yield

Concrete:
100 – 175 ft²/gal (2.4 – 4.3 m²/L)

Brick:
100 – 175 ft²/gal (2.4 – 4.3 m²/L)

Stucco:
60 – 100 ft²/gal (1.5 – 2.4 m²/L)

Always apply a test area to determine actual coverage rates. Coverage rates will vary greatly with the porosity of the substrate.

Packaging

5 gallon (19 L) pails

54 gallon (205 L) drums

Color

Milky white liquid; clear when dry

Shelf Life

18 months when properly stored

Storage

Store in unopened containers in a clean, dry area between 35 and 110° F (2 and 43° C).

Features

- Water based, VOC compliant
- USDA compliant (nonfood contact areas)
- Transparent, nonstaining
- Breathable
- One component
- Water repellent

Benefits

Environmentally friendly

Use in food manufacturing and service structures

Does not alter surface appearance

Allows interior moisture to escape without damaging sealer

Easy to apply; saves labor

Protects against damage from moisture intrusion and chloride ion penetration

Where to Use

LOCATION

- Horizontal and vertical
- Exterior or interior
- Above grade

SUBSTRATE

- Concrete
    Architectural
    Exposed aggregate
    Glass-fiber reinforced
    Precast
    Cast in place/precast
    Silica fume
- Hard burnt brick
- Stucco
    Troweled/smooth
    Integrally colored
- Brick pavers
- Tile (unglazed)

How to Apply

Surface Preparation

1. Verify substrate has properly cured. Concrete should obtain 80% of design strength, typically achieved within 14 – 28 days.

2. Clean all surfaces of all sand, surface dust and dirt, oil, grease, chemical films and coatings, and other contaminants prior to application. Use waterblast, sandblast, or shotblast as necessary to achieve the desired surface condition.

3. Air, material, and surface temperatures should be 40° F (4° C) or higher during application. Do not apply sealer when temperatures are expected to fall below 40° F (4° C) within 12 hours.

4. Surfaces to be treated can be slightly damp; however, a dry surface is suggested for maximum penetration of sealer. Do not apply Enviroseal® 20 if standing water is visible on the surface to be treated.

5. Crack control, caulking, patching, and expansion joint sealants can be installed before or after application of the sealer. Allow a minimum of 6 – 12 hours curing time for caulking and sealant materials (or until they have skinned over).

Figure A.3   Data sheet for 100% silane sealant used in freeze-thaw testing.

Technical Data

Composition

Enviroseal® 20 is a water-based alkylalkoxysilane sealer.

Compliances

- USDA acceptance on nonfood contact areas
- Alberta DOT, Type 1a

Typical Properties

PROPERTY	VALUE
Solids and active ingredients, % by weight	20
Specific gravity, kg/L	0.98
Density, lb/gal)	8.16
Penetration, in (mm), average depth, depending upon substrate	0.14 (3.6)

Test Data

PROPERTY	RESULTS	TEST METHODS
Flash point, ° F (° C)	> 200 (> 93)	ASTM D 3278, SETA
VOC content, lb/gal (g/L)	< 2.92 (< 350)	EPA Method 24
Moisture-vapor transmission rate, %	102	OHD-L-35
Water absorption, %, 48 hours	0.53	ASTM C 642
Scaling resistance rating, non-air-entrained concrete, 100 cycles treated concrete	0 – No Scaling	ASTM C 672
Resistance to chloride ion penetration, lb/yd^3 (kg/m^3) Criteria of 1.5 at 1/2" (13 mm) Criteria of 0.75 at 1" (25 mm)	< 0.27 (< 0.16) 0.00 (0.00)	AASHTO T 259 and T 260
Water weight gain, % reduction	86 – exceeds criteria	NCHRP 244 Series II-cube test
Absorbed chloride, % reduction	92 – exceeds criteria	NCHRP 244 Series II-cube test
Absorbed chloride, % reduction	99 – exceeds criteria	NCHRP 244 Series IV - Southern climate
Water repellent performance, %	85.6	Alberta Transportation and Utilities Procedures - Type 1a
Surface appearance after application	Unchanged	Federal Reflectance Test Method 6121

Test results are averages obtained at a coverage rate of 125 ft²/gal (3.12 m²/3.8 L) under laboratory conditions. Reasonable variations can be expected.

Figure A.3   *Continued.*

57

Application

1. Test a small area of the surface (generally a 5 by 5 ft [1.5 by 1.5 m] section) before starting general application of any clear, penetrating sealers to ensure desired results and coverage rates. Allow 5 – 7 days for the product to fully react before evaluating.

2. Stir material thoroughly before and during application.

3. Low-pressure non-atomizing spray application is recommended.

4 On vertical surfaces, apply from the bottom up. Flood surfaces using enough material to get a 8 – 12" (20 – 30 cm) material rundown.

5. For horizontal surfaces, apply to saturation. If necessary, follow by brooming for even distribution.

Drying Time

Typical drying time for Enviroseal® 20 is 4 hours at 70° F (21° C) and 50% relative humidity. Cooler temperatures or higher relative humidity can extend the drying time.

Clean Up

Clean equipment and tools with hot soapy water. Overspray can be cleaned immediately with hot soapy water. Dried residue can be cleaned with a mild citric acid or very hot water, then scrubbed with a plastic sponge.

For Best Performance

- Keep material from freezing.
- Do not dilute Enviroseal® 20.
- Do not apply during inclement weather or when inclement weather is anticipated within 12 hours.
- To prevent damage to nearby shrubbery and landscaping, cover or protect with drop cloth.
- Enviroseal® 20 may leave a temporary slippery surface for up to several hours after application. Therefore, do not reopen traffic-bearing surfaces until the treated surface is dry.
- Variations in the texture and porosity of the substrate will affect the coverage and performance of the product.
- Enviroseal® 20 will not inhibit water penetration through unsound or cracked surfaces, or surfaces with defective flashing, caulking, or structural waterproofing.
- Line striping can be done after application of the sealer.
- Make certain the most current versions of product data sheet and MSDS are being used; call Customer Service (1-800-433-9517) to verify the most current versions.
- Proper application is the responsibility of the user. Field visits by BASF personnel are for the purpose of making technical recommendations only and not for supervising or providing quality control on the jobsite.

Health and Safety

ENVIROSEAL® 20

Caution

Enviroseal® 20 contains alkoxysilane.

Risks

May cause skin, eye or respiratory irritation. Ingestion may cause irritation.

Precautions

KEEP OUT OF THE REACH OF CHILDREN. Avoid contact with skin, eyes, and clothing. Wash thoroughly after handling. Keep container closed when not in use. DO NOT take internally. Use only with adequate ventilation. Use impervious gloves, eye protection and if the TLV is exceeded or used in a poorly ventilated area, use NIOSH/MSHA approved respiratory protection in accordance with applicable federal, state and local regulations.

First Aid

In case of eye contact, flush thoroughly with water for at least 15 minutes. In case of skin contact, wash affected areas with soap and water. If irritation persists, SEEK MEDICAL ATTENTION. Remove and wash contaminated clothing. If inhalation causes physical discomfort, remove to fresh air. If discomfort persists or any breathing difficulty occurs or if swallowed, SEEK IMMEDIATE MEDICAL ATTENTION.

Refer to Material Safety Data Sheet (MSDS) for further information.

Proposition 65

This product contains material listed by the state of California to cause cancer, birth defects, or other reproductive harm.

VOC Content

Less than 2.92 lbs/gal or 350 g/L, less water and exempt solvents.

For medical emergencies only, call ChemTrec (1-800-424-9300).

Figure A.3 *Continued.*

Project Partners

Publication

This report was published in collaboration with the Joint Transportation Research Program and Purdue University. The full content of this technical report is available for download at http://dx.doi.org/10.5703/1288284315339. In addition, a print-on-demand bound version of this report can be purchased at that location.

Open Access and Collaboration with Purdue University

The Indiana legislature established the Joint Highway Research Project in 1937. In 1997, this collaborative venture between the Indiana Department of Transportation and Purdue University was renamed as the Joint Transportation Research Program (JTRP) to reflect state and national efforts to integrate the management and operation of various transportation modes. Since 1937, the JTRP program has published over 1500 technical reports. In 2010, the JTRP partnered with the Purdue University Libraries to incorporate these technical reports in the University's open access digital repository and to develop production processes for rapidly disseminating new research reports via this repository. Affiliated publications have also recently been added to the collection. As of 2014, the JTRP collection has over 750,000 downloads, with some particularly popular reports having over 20,000 downloads.